



**TECHNISCHE UNIVERSITÄT MÜNCHEN**

**Fakultät für Medizin**

## ***RNF43* mutations are drivers of pancreatic pathology and potential targets for T cell therapy**

**Anna Brutau Abia**

Vollständiger Abdruck der von der Fakultät für Medizin der Technischen Universität München zur Erlangung eines

**Doctor of Philosophy (Ph.D.)**

genehmigten Dissertation.

**Vorsitzender:** Prof. Dr. Marc Schmidt-Supprian

**Betreuer:** Prof. Dr. Markus Gerhard

**Prüfer der Dissertation:**

1. Prof. Dr. Dirk Busch
2. Prof. Dr. Radu Roland Rad

Die Dissertation wurde am 09.01.2023 bei der Fakultät für Medizin der Technischen Universität München eingereicht und durch die Fakultät für Medizin am 02.03.2023 angenommen.



## Table of content

<b>I. Summary .....</b>	<b>5</b>
<b>II. Zusammenfassung .....</b>	<b>6</b>
<b>1. Introduction .....</b>	<b>8</b>
<b>1.1 Anatomy of the pancreas .....</b>	<b>8</b>
<b>1.2 Chronic pancreatitis .....</b>	<b>9</b>
<b>1.3 Pancreatic cancer .....</b>	<b>11</b>
<b>1.4 PDAC progression.....</b>	<b>12</b>
<b>1.5 Wnt signaling pathway.....</b>	<b>14</b>
1.5.1 Canonical Wnt/ $\beta$ -catenin pathway.....	15
<b>1.6 RNF43 .....</b>	<b>18</b>
<b>1.7 Therapy for pancreatic cancer .....</b>	<b>20</b>
1.7.1 Adoptive T cell transfer in pancreatic cancer .....	22
<b>1.8 Aims of the thesis.....</b>	<b>23</b>
<b>2. Material and Methods .....</b>	<b>25</b>
<b>2.1 Materials.....</b>	<b>25</b>
2.1.1 Equipment .....	25
2.1.2 Consumables .....	25
2.1.3 Reagents and kits .....	26
2.1.4 Cell culture media components.....	27
2.1.5 Buffers .....	28
2.1.6 Oligo sequences .....	28
2.1.7 Antibodies .....	29
2.1.8 Cell lines .....	29
2.1.9 Mouse strains .....	30
<b>2.2 Cell characterization and assays .....</b>	<b>31</b>
2.2.1 Cell culture .....	31
2.2.2 HLA-typing of pancreatic cancer cell lines.....	31
2.2.3 Retroviral transduction of HLA-A*02 .....	32
2.2.4 Lentiviral knockdown of RNF43.....	32
2.2.5 Proliferation assay.....	33
2.2.6 Clonogenic assay .....	33
2.2.7 Soft agar colony formation assay .....	33
2.2.8 Wound healing assay.....	34
<b>2.3 Animal experiments .....</b>	<b>34</b>
2.3.1 Xenograft model.....	34
2.3.2 <i>Rnf43</i> mutant mouse models .....	35
2.3.2.1 Induction of pancreatitis.....	35
<b>2.4 Organoid culture .....</b>	<b>36</b>
2.4.1 Isolation and culture of pancreatic organoids.....	36
2.4.2 Viability assay .....	37
<b>2.5 Evaluation of RNF43 expression .....</b>	<b>37</b>
2.5.1 Quantification of RNF43 mRNA levels.....	37
2.5.1.1 RNA isolation from cell lines.....	37
2.5.1.2 Reverse transcription.....	37
2.5.1.3 Quantitative Real time PCR .....	38

2.5.2 Immunofluorescence.....	39
<b>2.6 Histological methods.....</b>	<b>39</b>
2.6.1 Embedding and sample preparation for staining.....	39
2.6.2 Hematoxylin and eosin staining.....	40
2.6.3 Sirius red staining.....	40
2.6.4 Immunohistochemistry.....	40
<b>2.7 SDS-PAGE and Western blot.....</b>	<b>41</b>
<b>2.8 TCR characterization assays.....</b>	<b>42</b>
2.8.1 Neo-epitope prediction.....	42
2.8.2 Real-time cytotoxicity assay.....	42
2.8.3 Reporter cell assay.....	43
<b>2.9 Statistical analysis.....</b>	<b>43</b>
<b>3. Results.....</b>	<b>44</b>
3.1 <i>RNF43</i> is frequently mutated in pancreatic cancer cell lines.....	44
3.2 Loss of <i>RNF43</i> function enhances the tumorigenic potential of pancreatic cancer cells <i>in vitro</i> .....	45
3.3 Loss of <i>RNF43</i> potentiates tumor growth <i>in vivo</i> .....	49
3.4 Mutations in <i>RNF43</i> drive pancreatic pathology during chronic pancreatitis.....	53
3.5 Neo-epitopes derived from the tumor suppressor gene <i>RNF43</i> as targets for T cell therapy	63
3.5.1 TCR R11 show cytotoxic activity in a peptide-pulsed setting.....	67
3.5.2 Engineered TCRs targeting the <i>RNF43</i> <i>VPSVWRSSL</i> peptide show cytotoxicity after peptide pulsing .....	72
<b>4. Discussion.....</b>	<b>74</b>
<b>5. Registers.....</b>	<b>82</b>
5.1 List of abbreviations.....	82
5.2 List of figures.....	86
5.3 List of tables.....	87
<b>6. References.....</b>	<b>88</b>
<b>7. Publications.....</b>	<b>99</b>
<b>8. Acknowledgments.....</b>	<b>100</b>

### I. Summary

Pancreatic cancer (PC) is one of the most aggressive cancer types, with a 5-year survival of 11%. This is attributable to numerous factors, including the lack of biomarkers and poor response to standard therapies. To gain a deeper understanding of the disease and improve outcome, it is essential to determine the molecular mechanisms that drive cancer onset and progression, to improve strategies to monitor patients at risk and to develop novel therapeutic means of intervention. The Ring finger E3-ubiquitin ligase (RNF43) is a tumor suppressor gene frequently mutated in the gastrointestinal tract, and loss of function of the protein mediates tumorigenesis in several cancers. Interestingly, *RNF43* exhibits a high prevalence of frame-shift mutations in PC, resulting in premature stop codons and protein truncation. These observations suggest that mutations in *RNF43* may be involved in PC development and could potentially be used as novel therapeutic targets.

Loss of RNF43 function in PC cells led to increased proliferation and tumor growth *in vitro* and *in vivo*, supporting a role of RNF43 as a tumor suppressor in the pancreas. Under inflammatory conditions, *Rnf43* mutant mice showed severe alterations in acinar structure, increased proliferation, acinar to ductal metaplasia, and increased fibrosis. However, long-term induction of inflammation did not induce progression to preneoplastic lesions or cancer, indicating that in the pancreas, mutations in *RNF43* alone are insufficient to initiate the development of PC. Given their high frequency and influence on pancreatic tumorigenesis, *RNF43* frame-shift mutations were explored as targets for T-cell therapy. Two RNF43 neo-peptides restricted to the HLA-A\*02:01 and HLA-B\*07:02 were selected, and TCRs specific for those peptides were isolated through a high-throughput platform and re-expressed in donor T cells through TCR orthotopic replacement. Engineered T cells recognized and killed target cells under peptide-pulsed conditions. However, no cytotoxic activity was seen in target cells with endogenous *RNF43* mutations, indicating that, although the approach was potentially promising, additional research is required.

In conclusion, mutations in RNF43 influence PC development and might be potential therapeutic targets in adoptive T cell transfer.

## II. Zusammenfassung

Bauchspeicheldrüsenkrebs (Pankreaskarzinom, PK) ist mit einer 5-Jahres-Überlebensrate von 11 % eine der aggressivsten Krebsarten. Dies ist auf zahlreiche Faktoren zurückzuführen, darunter auf das Fehlen von Biomarkern und das schlechte Ansprechen auf Standardtherapien. Um die Krankheit besser zu verstehen und die Überlebenschancen zu verbessern, müssen die molekularen Mechanismen bestimmt werden, die die Entstehung und das Fortschreiten dieses Krebses steuern. Die Ringfinger-E3-Ubiquitin-Ligase (RNF43) ist ein Tumorsuppressorgen, das häufig im Magen-Darm-Trakt mutiert ist, und der Funktionsverlust des Proteins vermittelt die Tumorentstehung bei verschiedenen Krebsarten. Interessanterweise weist *RNF43* eine hohe Prävalenz von Frame-Shift-Mutationen im PK auf, die zu vorzeitigen Stoppcodons und Proteinabbrüchen führen. Diese Beobachtungen deuten darauf hin, dass Mutationen in *RNF43* an der Entstehung des Pankreaskarzinoms beteiligt sind und möglicherweise als neue therapeutische Ziele genutzt werden könnten.

Der Verlust der Funktion von RNF43 in PK-Zellen führte zu erhöhter Proliferation und Tumorstadium *in vitro* und *in vivo*, was für eine Rolle von RNF43 als Tumorsuppressor in der Bauchspeicheldrüse spricht. Unter entzündlichen Bedingungen zeigten *Rnf43*-mutierte Mäuse schwere Veränderungen der Azinusstruktur, erhöhte Proliferation, azinär-duktales Metaplasie und verstärkte Fibrose. Die langfristige Induktion von Entzündung führte jedoch nicht zu präneoplastischen Läsionen oder Krebs, was darauf hindeutet, dass Mutationen in *RNF43* allein nicht ausreichen, um die Entwicklung von PC in der Bauchspeicheldrüse auszulösen. Angesichts ihrer hohen Häufigkeit und ihres Einflusses auf die Tumorentwicklung in der Bauchspeicheldrüse wurden Mutationen des RNF43-Leserahmens (sog. Frameshift Mutationen) als Ziele für eine T-Zell-Therapie untersucht. Zwei RNF43-Neo-Peptide, die auf HLA-A\*02:01 und HLA-B\*07:02 beschränkt sind, wurden ausgewählt, und TCRs, die für diese Peptide spezifisch sind, wurden mit Hilfe einer Hochdurchsatz-Plattform isoliert und in Spender-T-Zellen durch orthotopen TCR-Austausch re-exprimiert. Nach Beladung mit den RNF43 Neopeptiden erkannten die manipulierten T-Zellen die Zielzellen und töteten sie ab. Bei Zielzellen mit endogenen *RNF43*-Mutationen wurde jedoch keine zytotoxische Aktivität festgestellt, was darauf hindeutet, dass der Ansatz zwar vielversprechend ist, aber weitere Forschungsarbeiten erforderlich sind.

## Zusammenfassung

Zusammenfassend lässt sich sagen, dass Mutationen in *RNF43* die Entwicklung von Bauchspeicheldrüsenkrebs beeinflussen und potenzielle therapeutische Ziele für den adoptiven T-Zell-Transfer darstellen könnten.

## 1. Introduction

Cancer accounts for 21% of all deaths, making it a crucial public health problem worldwide. Among those, pancreatic cancer has the lowest survival [1]. Therefore, efforts in understanding the mechanisms and processes of the disease are crucial to improve the prognosis.

### 1.1 Anatomy of the pancreas

The pancreas is located in the upper abdomen behind the stomach. It is structurally divided into three parts: the head, body, and tail region. It is anatomically connected with other organs, including the spleen, stomach, and duodenum [2, 3]. It has both exocrine and endocrine functions; the endocrine pancreas is responsible for the secretion of hormones into the bloodstream to control energy metabolism and storage [4]. It comprises 1-2% of the pancreatic mass and is composed of the Islet of Langerhans [5], which contain a number of different endocrine cell types, including the alpha cells, responsible for glucagon production; beta cells that produce insulin in response to high blood glucose levels; pancreatic polypeptide (PP) cells, and delta cells responsible for somatostatin production [4, 6].

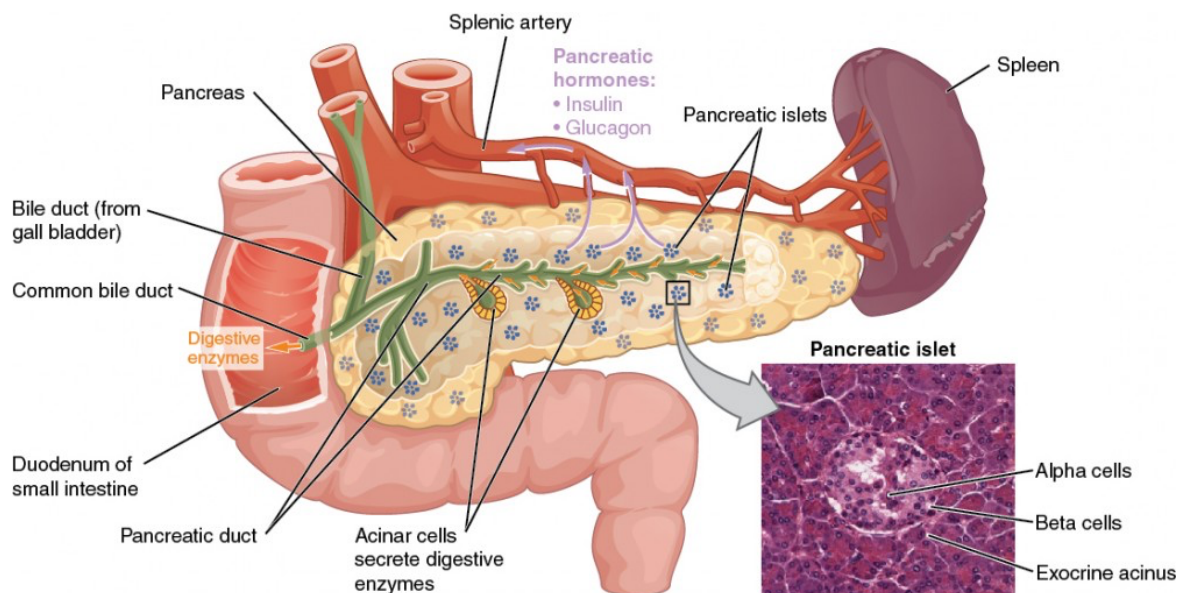


**Figure 1. Anatomy of the pancreas.**

The pancreas is composed by an endo- and exocrine part. The exocrine pancreas is responsible for the secretion of digesting enzymes into the duodenum, while the endocrine pancreas is responsible for the secretion of hormones such as insulin or glucagon into the bloodstream. Image extracted from Anatomy & Physiology. Provided by: OpenStax CNX. License: CC BY: Attribution. License Terms: Access for free at <https://openstax.org/books/anatomy-and-physiology/pages/1-introduction>

## Introduction

The exocrine pancreas is composed of acinar and ductal cells. Acinar cells constitute around 80% of the volume of the pancreas and secrete zymogens, the precursors of digestive enzymes, that are stored in granules. Those enzymes include amylases, lipases, and peptidases that will be secreted through the pancreatic duct into the duodenum's lumen for food digestion. Ductal cells are responsible for the secretion of sodium bicarbonate, providing the optimal pH for the pancreatic digestive enzymes to function and neutralizing the acidity coming into the small intestine from the stomach [5, 7].

Alterations in the pancreas can lead to several health problems. Those include diabetes, pancreatitis, and PC. However, the most common disorder of the pancreas is acute pancreatitis, which is caused by autodigestion; a process by which digestive enzymes damage the pancreas. This process is generally reversible, and the main triggers include alcohol abuse and gallstones. It is mild in around 80% of the cases, but in 20% of the cases, it can lead to severe disease with local and systemic complications [8].

### 1.2 Chronic pancreatitis

Repeated episodes of acute pancreatitis can lead to chronic pancreatitis (CP) [9]. CP is a persistent, chronic inflammation of the pancreas due to irreversible changes to the pancreatic structure, such as fibrosis, atrophy, and calcification [10, 11]. Globally, CP has an incidence of 20.6 per 100 000, making it a critical public health issue [12]. The main risk factor for CP is alcohol abuse, but it is also linked to smoking, elevated triglycerides, autoimmune diseases, some inherited or genetic conditions such as cystic fibrosis or hereditary pancreatitis and variants in several genes such as the serine protease 1 (*PRSS1*), the cystic fibrosis transmembrane conductance regulator (*CFTR*), The serine protease inhibitor Kazal type 1 (*SPINK1*) and the concerted actions of chymotrypsin C (*CTRC*) [13].

CP is a process that develops slowly, it typically begins with acinar cell injury, which prevents the normal secretion of the zymogens and causes tissue autodigestion. This process results in inflammation and the release of damage-associated molecular patterns (DAMPS), which activate the nuclear factor kappa-light-chain-enhancer of activated B cells (NF- $\kappa$ B) pathway

## Introduction

and initiates a pro-inflammatory cascade and the accumulation of oxygen reactive species (ROS) [14, 15].

Repeated bouts of acute pancreatitis may cause ductal dilation. Following the healing phase, pancreatic stellate cells generate fibrotic tissue [16]. This causes duct stenosis and further acinar atrophy [17]. Moreover, in particular situations, hypersecretion can lead to protein plug formation in the ducts, resulting in the accumulation of calcium deposits that cause ductal obstruction and atrophy of acinar cells [18, 19]. Acinar to ductal metaplasia (ADM, reviewed in the next section) is a major characteristic of CP, and 60% of precancerous lesions are associated with CP. Currently, patients diagnosed with CP, including those with hereditary pancreatitis, are not included in surveillance programs in spite of having a higher risk for PC [20].

Diagnosis of CP is normally assessed by contrast-enhanced computed tomographic (CT) scan, since it is able to identify early and small calcifications [21, 22]. Ducts can also be imaged with endoscopic retrograde cholangiopancreatography (ERCP) and, in some cases with magnetic resonance imaging (MRI). The clinical spectrum of CP is broad. Around 80% of the patients present with abdominal pain that may radiate to the back [23]. Damage to acinar cells diminishes the production of digestive enzymes, leading to pancreatic insufficiency. This results in difficulty absorbing food and fat, leading to weight loss, steatorrhea (fatty feces), and deficiency in fat-soluble vitamins (A, D, E, and K) [24, 25]. Long term consequences of CP are PC and the development of diabetes mellitus, as inflammation destroys alpha and beta cells [26, 27].

Most of the knowledge about the mechanism and outcome of CP derives from experiments using different animal models. Those include genetic mouse models, chemically induced models and mechanical models [28]. One of these models is cerulein-induced pancreatitis. This method was first established in 1977 [29] and is widely used due to its reproducibility and close mimicking of the human disease, since CP develops similarly after repeated bouts of acute pancreatitis, increasing the damage to the organ and eventually resulting in atrophy and fibrosis [30]. The effects of cerulein-induced pancreatitis regress when injections are

## Introduction

discontinued. Therefore, repeated injections of cerulein need to be administered over several weeks to induce and study CP [31].

### 1.3 Pancreatic cancer

PC is the 12th most common cause of cancer worldwide [32], but despite its relatively low incidence, it is a malignancy associated with poor prognosis. In 2022, the 5-year survival for PC was 11% [1]. And it is predicted that by 2030 PC will be the second leading cause of cancer-related death [33].

There are several contributing factors to this high mortality rate such as the asymptomatic early stages, the aggressive biology of the tumors, and the lack of biomarkers for early diagnosis. Therefore, PC is typically diagnosed at a late stage in most patients [34]. This poses an urgent need for new markers to create a screening program to diagnose the disease at an early stage. When symptoms do arise, these include weight loss, abdominal pain that might radiate to the back, jaundice, nausea, new-onset diabetes, and vomiting. In addition, pancreatic tumors are typically resistant to conventional treatments such as chemotherapy and radiotherapy and have a limited response to targeted therapies [35].

The two main risk factors for PC are age and cigarette smoking. In most cases, the disease occurs in patients between 60 and 80 years old, and smoking increases by 75% the risk of PC, with this risk persisting ten years after smoking cessation [36]. Additional risk factors include obesity [37], type 2 diabetes [38], a family history of PC [39], and CP [40].

Pancreatic ductal adenocarcinoma (PDAC), which accounts for more than 85% of all PC cases, is the most common pancreatic malignancy. From all PC types PDAC are associated with the poorest prognoses and survival. They are primarily solid tumors although they occasionally present cystic areas. There are additional tumor types that occur less frequently in PC and can coexist with PDAC lesions in tumors. These tumor forms include adeno-squamous carcinomas, which represent for 1% to 4% of PC, osteoclastic giant cell carcinoma, which accounts for 1.4% of all PC cases, and colloid carcinomas, found in 1% to 3% of all neoplasms and associated with a better 5-year overall survival rate of 55% [41-43].

### 1.4 PDAC progression

PDAC tumors are heterogeneous and contain an average of 60 to 70 mutations[44]. The Kirsten Rat Sarcoma (*KRAS*) oncogene, which is involved in tumor initiation and progression, is mutated in 90% of the tumors [45]. Moreover, PDAC frequently harbors mutations in the tumor suppressor genes *CDKN2A* (50%), *TP53* (60-70%), and *SMAD4* (40-50%) [44].

PDAC seems to originate from progressive dysplasia in precursor lesions derived resulting from the malignant transformation of normal cells [44]. Histological precursors of PDAC include pancreatic intraepithelial neoplasia (PanIN), intraductal papillary mucinous neoplasm (IPMN) and mucinous cystic neoplasm (MCN). PanINs are the most common precursor lesions of PC. They are microscopic papillary or flat non-invasive epithelial neoplasms, and they are graded based on the degree of cytological and architectural atypia [34, 46]. IPMNs are mucin-producing epithelial neoplasms. These lesions are larger than PanINs and harbor mutations in *GNAS*, *KRAS* and *RNF43*. MCNs are often found in women [47] and are associated with mutations in *KRAS* and *RNF43* [34]. Precursor lesions and their molecular alterations are depicted in Figure 2.

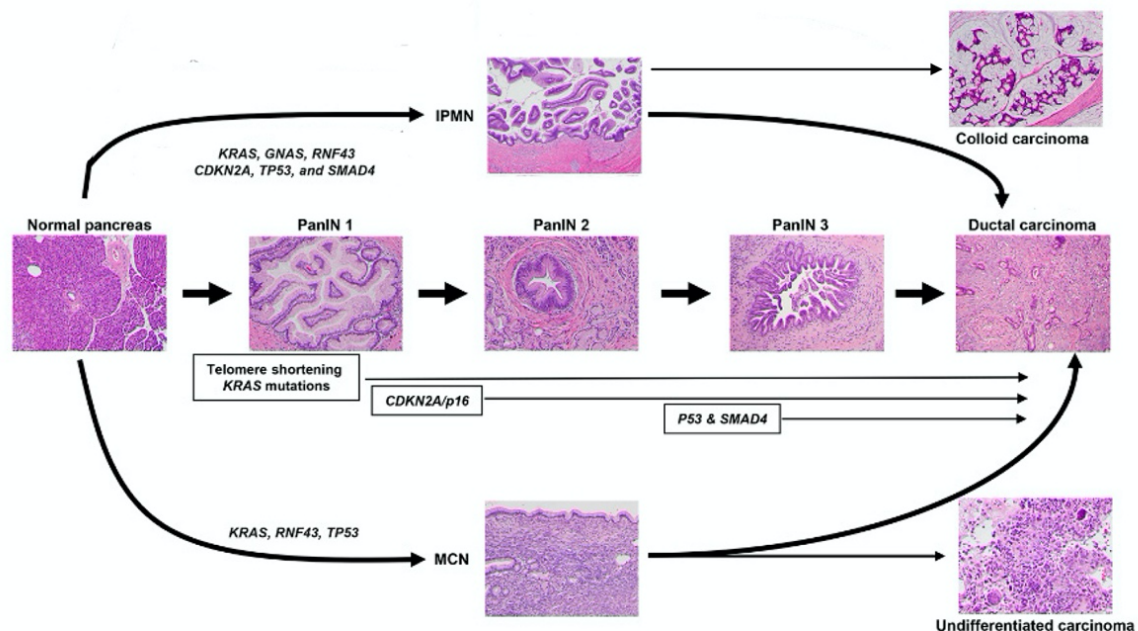


**Figure 2. Precursor lesions of PDAC and frequently mutated genes.**

Multiple precursors can give rise to pancreatic cancer, and several mutations are associated with these lesions and pancreatic cancer development. Precursor lesions include PanINs, IPMN and MCN. Figure adapted from Taherian, M.; Wang, H.; Wang, H. (2022) [34]. licensed under CC BY 4.0.

## Introduction

Despite recent advances, there is still disagreement regarding different aspects on PDAC tumor development, including how precursor lesions and PDAC evolve, and which cells can be implicated as the definitive origin of the disease.

Plasticity is a common feature of the normal pancreas. Different cell types can alter their cellular identity in response to injury, regeneration, and repair. In the endocrine pancreas, several studies reveal plasticity among differentiated cells. Removal of beta cell populations in a transgenic model showed through lineage tracing that alpha cells can go through trans-differentiation and restore the beta cell population [48]. A similar trend was observed in young mice when somatostatin-producing delta-cells could convert into beta cells via spontaneous reprogramming [49]. Furthermore, in adult mice with pancreatic duct ligation, beta cell progenitors located in the ductal lining can be activated and differentiated [50].

Similar results are observed in the exocrine pancreas. In a study where a transgenic mouse model was used to model the acinar and endocrine tissue ablation, cells from the remaining ductal compartment were able to regenerate both endocrine and acinar cells adopting the embryonic pancreatic developmental program. However, the authors claimed that regeneration probably occurred by reprogramming of ductal to acinar cells [51]. Asserting that plasticity is more evident in the acinar compartment [52, 53]. In acute pancreatitis models, acinar cells lose polarity and resemble ductal precursors in response to the injury. In this context, acinar cells acquire typical ductal features such as a mucinous cytoplasm and cytokeratin-19 (CK19) expression. Acinar cells lose some identity features, including the transcription factors *Ptf1a* and *Mist1* [44, 54]. This process is known as acinar to ductal metaplasia (ADM).

ADM is a reversible process that has been suggested to lead to precursor lesions of PC when associated with oncogenic genetic insults and/or sustained environmental stress [55]. This association is also evidenced by the frequent association of ADM I with PanIN lesions in PDAC patients [56, 57]. *KRAS* codon 12 mutations were found in 92.0% PanIN-1A, 92.3% PanIN-1B, 93.3% of 45 PanIN-2, and 21 PanIN-3 lesions [58], further suggesting that oncogenic *KRAS* hyperactivity is a key input for ADM progression [54, 59]. In a mouse model with conditional expression of an oncogenic *Kras* mutations, ADM becomes irreversible. However, deletion of

## Introduction

oncogenic *Kras* allows the reversal of ADM and PanIN [60]. Besides *Kras*, in transgenic mouse models persistent growth factor signaling also prevents redifferentiation and initiates further progression to low-grade precancerous lesions [54, 61-63]. In high-grade PanINs, biallelic inactivation of *CDKN2A*, and loss of *SMAD4* and *TP53* mutations are often observed (Figure 2) [34]. Understanding the intermediate states of ADM and key molecules that regulate the process may help in the development of preventive strategies with potential clinical translation that will benefit patients with risk of PC [55].

Several pathways are associated with the initiation and progression of PC due to dysregulation or mutations in the signaling components such as the TGF- $\beta$ /SMAD, Ras/MAPK, Notch or PI3K signaling pathway [64]. Among those, the Wnt signaling pathway has a crucial role in PC formation and therapeutic resistance [65].

### 1.5 Wnt signaling pathway

The Wnt signaling pathway is involved in regulating several processes of the cell, including morphogenesis during embryonic development, cell growth, migration, cell polarity and maintenance of somatic stem cells [66]. It is an evolutionarily conserved pathway and dysregulations can lead to tumorigenesis [67].

In humans, there are 19 Wnt proteins, each exhibiting distinct but frequently overlapping functions [68]. Wnt proteins can activate three pathways: the canonical Wnt/ $\beta$ -catenin pathway and the noncanonical wnt signaling pathway, which comprises two pathways: planar cell polarity (PCP) pathway that is involved in cell orientation during development and cytoskeleton organization, and the Wnt/Ca<sup>2+</sup> pathway, that controls intracellular influx of calcium, which can activate various downstream genes that control cell fate and migration [66, 69, 70].

## Introduction

### 1.5.1 Canonical Wnt/ $\beta$ -catenin pathway

The primary target of Wnt signaling is cytoplasmic  $\beta$ -catenin, a latent transcription regulator that is rapidly degraded in unstimulated cells but stabilized by Wnt signaling. In the absence of Wnt, cytoplasmic  $\beta$ -catenin is degraded by a large protein degradation complex that binds the protein, prevents it from entering the nucleus, and promotes its destruction. The  $\beta$ -catenin destruction complex consists of 4 proteins, including casein kinase 1 (CK1) and glycogen synthase kinase 3 (GSK3), and two scaffold proteins that hold the complex together: Axin and Adenomatous polyposis coli (APC) [71, 72]. Without Wnt ligands, CK1 phosphorylates  $\beta$ -catenin, priming it for further phosphorylation by GSK3 [73]. The E-3 ubiquitinating ligase  $\beta$ -Trcp recognizes phosphorylated  $\beta$ -catenin and adds a ubiquitin group, marking the protein for ubiquitylation and proteasomal degradation [74, 75]. This prevents its translocation to the nucleus and repressing the expression of downstream Wnt genes.

Wnt proteins regulate the proteolysis of  $\beta$ -catenin by interacting with two cell-surface co-factors; Frizzled and LDL-receptor-related protein receptors 5/6 (LRP5/6). The Frizzled receptor (Fzd) is a seven-pass transmembrane protein that contains an extracellular domain N-terminal cysteine-rich domain (CRD) that binds with high to the lipid domain of Wnt [76]. Wnt ligand proteins also bind to the LRP5/6 extracellular domain, dimerizing LRP and Fzd together and activating the signaling cascade [77, 78].

Receptor activation causes Dishevelled scaffold protein recruitment (Dvl). Dvl binds into the intracellular domain of the Fzd receptor to break down the  $\beta$ -cat destruction complex by binding to the Axin Ck1a and GSK3b complex [79-81]. This brings GSK3b close to the LRP5/6 and phosphorylates residues of the cytoplasmic tail [82]. This reaction acts as positive feedback. Consequently, Axin coupled with GSK3b can bind to the cytoplasmic tail of LRP5/6 and further sequester components of the  $\beta$ -catenin destruction complex [83]. Thus, phosphorylation and degradation of  $\beta$ -catenin are prevented, allowing  $\beta$ -catenin to accumulate in the cytoplasm and translocate into the nucleus, there inducing target gene expression.

## Introduction

In the absence of Wnt signaling, an inhibitory complex of transcription regulators silences Wnt-responsive genes. The complex consists of LEF1/TCF family proteins bound to a Groucho family co-repressor protein at the promoter region containing Wnt response elements (WRE) [84].  $\beta$ -catenin enters the nucleus in response to a Wnt signal and binds to the LEF1/TCF proteins, displacing Groucho [85].  $\beta$ -catenin now acts as a transcriptional coactivator, stimulating the transcription of Wnt target genes such as *Cyclin D1*, *MMP-7*, *c-myc* and *VEGF* [86, 87]. These genes are involved in several cancer hallmarks, including angiogenesis, epithelial to mesenchymal transition (EMT) and cell cycle progression [66].

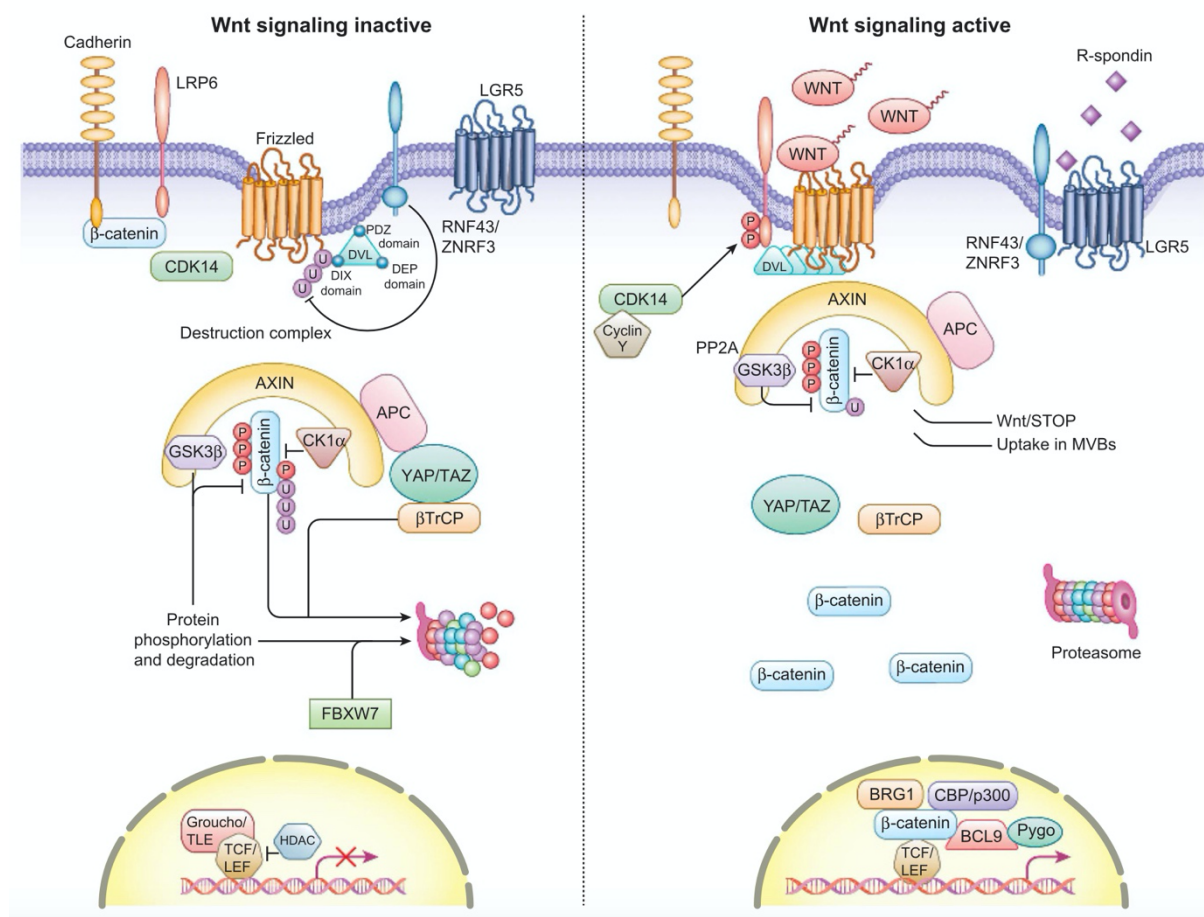


**Figure 3. Wnt/  $\beta$ -catenin signaling pathway.**

In absence of secreted Wnt binding to the receptor frizzled (Fzd),  $\beta$ -catenin binds to the destruction complex composed by CK1, GSK3 $\beta$ , Axin1 and APC. This results in phosphorylation of  $\beta$ -catenin by Gsk3 $\beta$  and CK1 and subsequently ubiquitination of  $\beta$ -catenin by  $\beta$ -Trcp and proteasomal degradation, preventing translocation of  $\beta$ -catenin in the nucleus. In an active state, Wnt ligands bind to Fzd and co-receptor LPR5/6. This recruits disheveled (Dvl), rendering the destruction complex inactive. Consequently,  $\beta$ -catenin is accumulated in the cytoplasm and translocated into the nucleus. This results in the displacement of the Groucho repressor and formation of a complex between  $\beta$ -catenin and TCF/LEF, causing transcriptional activation of Wnt target genes. Adapted from Zhan et al 2016 [88], with permission from Springer Nature.

## Introduction

Wnt signaling can be additionally regulated by agonists and antagonists. One factor that activates the canonical Wnt signaling pathway is R-spondins (RSPO). RSPO bind to the leucine-rich repeat containing G-protein-coupled (Lgr) family 4-6 with high affinity, and is essential for signal enhancement of low dose Wnt [89, 90]. This complex interacts with two highly homologous Wnt target genes: the E3 ubiquitin ligase Zinc and Ring finger 3 (*ZNRF3*) and the RING finger protein (*RNF43*) [91]. They are single trans-membrane E3 ubiquitin ligases known to ubiquitinate the lysine residues in the cytoplasmic loops of the 7TM domain of Fzd, causing endocytosis and lysosomal destruction of the Wnt receptors [70, 92], thus acting as negative regulators of the Wnt signaling pathway. This negative feedback is regulated by the presence of RSPO, which forms a complex with LGR4/5 and results in membrane clearance of the E3 ligases. This process leads to the accumulation and stabilization of the Fzd receptors in the cell's membrane, boosting Wnt signaling [93, 94]. Moreover, It has been shown that in the nucleus, RNF43 sequesters TCF4 to the nuclear membrane, hence reducing transcription of Wnt target genes [95].

The Wnt signaling pathway is highly involved in carcinogenesis. The first gene to be identified to have a role in cancer progression was APC in hereditary colon cancer [96]. Loss of the gene function leads to stabilization of  $\beta$ -catenin and aberrant activation of the pathway. Since then, mutations in several components of the pathway have been identified and its role on carcinogenesis have been studied. Including Axin2 in colorectal cancer,  $\beta$ -catenin in colorectal cancer and melanoma or RNF43 in ovary [97], colorectal cancer [98], PC [99], or gastric cancer [100, 101].

In the recent years several agonist and antagonists targeting the Wnt/  $\beta$ -catenin signaling pathway have been developed for solid tumors and hematological malignancies. Figure 4 shows an overview of those molecules targeting Wnt signaling components in cancer [102].

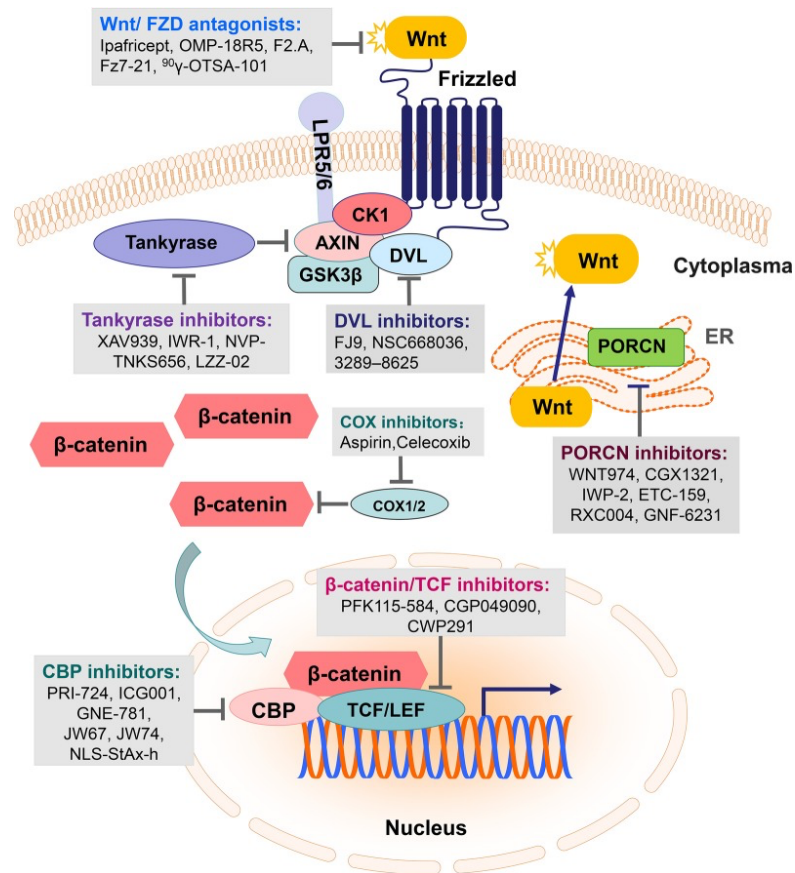


**Figure 4. Targeted therapies in Wnt signaling.**

Graphical representation of preclinical and clinical agonists and antagonist targeting Wnt signaling components. Zhang, Y. and X. Wang (2020) [102]; Figure licensed under CC BY 4.0.

### 1.6 RNF43

The RING finger protein 43 (RNF43) is an E3 ubiquitin ligase highly conserved in vertebrates. It belongs to the Goliath family of membrane-bound ubiquitin ligases. The gene is located at the minus strand of the long arm of chromosome 17, at position 22 (17q22) [98]. RNF43 has a regulatory region that contains two Wnt responsive elements (WRE) in intron 2, indicating that its expression is regulated by the Wnt/  $\beta$ -cat signaling pathway [103].

The protein consists of 783 amino acids and has a molecular mass of 85kDa. RNF43 is a transmembrane receptor; its N-terminal region consists of an extracellular domain with a variant of the protease-associated (PA) domain fold with a signal peptide. It is followed by a membrane-spanning and C-terminal regions, where the RING-type E3 ligase domain and the

## Introduction

cytoplasmic serine-rich region are found. This ring domain acts as a mediator for the direct transfer of ubiquitin between the ubiquitin-charged E2 ubiquitin-conjugating enzyme and the acceptor protein [92, 104].

RNF43 was first discovered together with the zinc and finger protein 3 (ZNF3). Both proteins downregulated the expression of Fzd in the nuclear membrane and are regulated by the presence of RSPO and the LGR4/5 complex. Based on their genetic redundancy and common function, it is believed that the two proteins are paralogs, despite having just 39% sequence identity [92]. It was observed that the PA domain, RING finger domain, and cytoplasmic serine-rich area displayed moderate conservation, indicating that these regions are crucial for Fzd control. However, in cancer, mutations in both genes are not frequently observed, and ZNF3 is not as frequently mutated in cancer as *RNF43*. This suggests that *RNF43* mutations function as dominant-negative mutations (DN) [105].

*RNF43* is frequently mutated in different cancer entities. Approximately 18% of colorectal cancer tumors contain a mutant *RNF43* gene, which is frequently detected in microsatellite-unstable tumors (MSI) [106]. In stomach and endometrial carcinomas, a similar pattern was observed where *RNF43* mutations were shown to be more prevalent in MSI tumors [106-108]. Most *RNF43* mutations are found in its RING domain and N-terminal region, causing an increase in Wnt activity [109]. This protein exhibits a high frequency of insertions and deletions, resulting in frame-shift mutations and protein truncation, with the most common mutations occurring at the amino acid positions G659fs and R177fs.

Inactivation mutations in *RNF43* were first reported in PC, *RNF43* is mutated 5-7% PDAC and 15-40% of premalignant IPMNs and MCNs and is associated with cancer progression [99] [110]. In an *in vivo* study using the *Kras*<sup>LSL.G12D/+</sup> *Pdx1*<sup>Cre</sup> model (KC), researchers used an inducible *in vivo* CRISPR/Cas9 approach (iCRISPR) to introduce large genomic deletions of *Rnf43*, which resulted in accelerated mutation-driven *Kras* carcinogenesis [111]. A 2022 study employing a mouse model with *Kras* mutations and RNF43 knockout (*Kras*<sup>G12D/+</sup> *Rnf43*<sup>-/-</sup>) showed that RNF43 promoted pancreatic preneoplasia initiation and development [112]. This suggests that targeting RNF43 in PC may have therapeutic potential.

## Introduction

### 1.7 Therapy for pancreatic cancer

Surgical resection is regarded as the only curative therapy for PC [113, 114]. However, 80% of the patients are diagnosed at an advanced stage of the disease and are not eligible for surgery [115]. Depending on the local extension of the tumor, PC without distant metastasis can be classified as resectable, borderline resectable and locally advanced (Figure 5) [116, 117].

Surgery followed by adjuvant chemotherapy is the standard of care for resectable tumors. Generally modified FOLFIRINOX (fluorouracil, oxaliplatin, irinotecan and leucovorin), a combination of gemcitabine and capecitabine or gemcitabine alone is given in individuals with good functional status. These regimes have been shown to delay recurrence and improve patients' overall survival [118-120].

Neoadjuvant therapy is an emerging strategy for borderline and locally advanced tumors [121, 122]. The role of this therapy is still controversial. In several studies, it has been shown that neoadjuvant therapy is associated with a higher R0 resection rate but not overall survival [123]. However, there are several clinical trials ongoing that will help determine the appropriate use of neoadjuvant therapy in PDAC.

Unresectable PC is treated with chemotherapy and local treatments to improve the symptoms. Generally, patients in good physical condition receive FOLFIRINOX, gemcitabine plus nanoparticle albumin-bound paclitaxel, and gemcitabine alone. However, the responses are usually low while the toxicity is significant [124]. Patients not responding to these therapies receive second-line therapies to prolong survival [121]. Patients not eligible for these therapies receive supportive care and palliative treatment to maximize the length of life, quality of life, and symptom control [125].

Despite all the therapy regimes, the median survival of patients in PC is very low (Figure 5), therefore there is a need for improved and more personalized therapies in PC. In recent years, immunotherapy has been a promising approach to treat cancer. Two immune checkpoint inhibitors targeting the cytotoxic T-lymphocyte-associated protein 4 (CTLA-4) and programmed cell death 1/programmed cell death ligand 1 (PD1/PD-L1) have recently been

## Introduction

developed. They demonstrated a significant effect on tumors with a high tumor burden and deficient mismatch repair [126]. In PC, however, they have limited success [127-129].

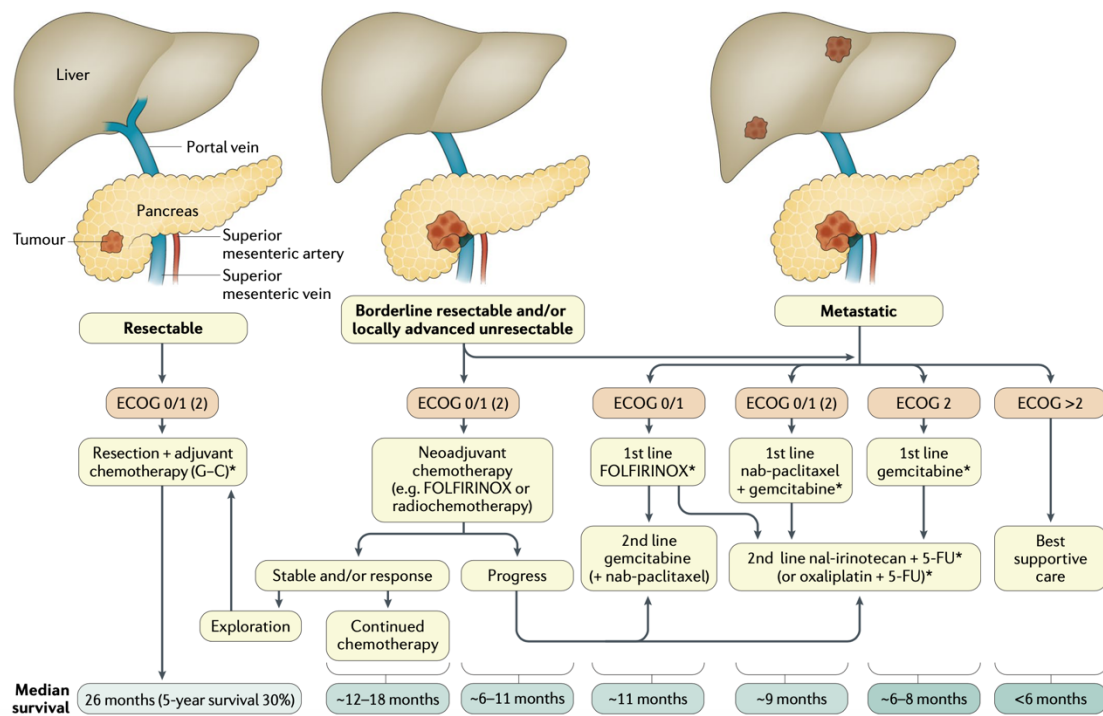


**Figure 5. Current treatments for pancreatic cancer patients.**

Treatment plans for PC patients are personalized based on the stage of the disease and general health of the patient (ECOG scale). Pancreatic cancers are classified as resectable, borderline resectable, or metastatic. Here is a representation of the patient's treatment and therapies, and the median survival for each condition. Figure by John P. Neoptolemos et al. (2018) [121] with permission from Springer Nature.

This limited success is attributed to PC's characteristic immunosuppressive tumor microenvironment (TME). It is characterized by abundant fibrosis and cancer-associated fibroblasts, which contribute to immune evasion and failure of immunotherapy [130, 131]. Currently, there are many efforts to develop therapies for remodeling the TME. A clinical trial treating patients with a combination of gemcitabine and nab-paclitaxel with PD-1/PDL-1 inhibitors showed activation of tumor-related fibroblast and increased tumor immunogenicity [124, 132, 133], giving hope for the implementation of target therapies alone or in combination with standard therapies or other immunotherapeutic agents for PC patients [134].

## Introduction

### 1.7.1 Adoptive T cell transfer in pancreatic cancer

Adoptive T cell therapy (ACT) is an emerging and promising cancer immunotherapy. It is based on harvesting T cells with a specific tumor antigen recognition, expanding them *ex vivo* and reinfused them into the patient, enhancing the immunological response. This personalized therapy is especially helpful for patients who are resistant to standard treatments [134, 135]. There are different types of T cell therapy approaches, infusion of tumor-infiltrating lymphocytes (TILs), and T-cell receptor (TCR)-engineered T cells. Those include CD19-directed chimeric antigen receptor (CAR-) T cells, and transfer of T cells with tumor-specific TCRs.

PDAC has traditionally been classified as a cold tumor due to the presence of myeloid-derived suppressor cells and scarcity of intratumoral CD8+ T cells [136, 137]. However, recent studies have revealed that PC tumors contain heterogeneous populations of TILs. The presence of those populations correlates with a better overall survival (OS) and slower disease progression [138-140], suggesting that ACT is a promising therapy in PDAC.

The most outstanding example of TCR-engineered T cells for ACT are CD19-directed chimeric antigen receptor CAR-T cells. Target-specific CAR-T cells can be modified to recognize antigens without being restricted by HLA molecules. Since 2017, the Food and drug administration (FDA) has approved six CAR-T cells therapies to treat specific lymphomas, multiple myeloma and leukemias [141]. However, CAR-T cells have the limitation that they are only able to recognize surface-expressed antigens and have low efficacy in treating solid tumors [124, 142, 143].

Adoptive transfer of T cells with tumor-specific TCR has the advantage of recognizing intracellular processed antigens, although they are restricted by the HLA context. One source of potential TCRs is the naive repertoires of healthy donors. The naive repertoire is a massive reservoir of reactive T cells that have already undergone central tolerance. This has numerous benefits, since it makes the application safer and they are easily accessible by apheresis [144].

Targeting of tumor mutation-derived neo-epitopes is an approach offering advantages in comparison to targeting tumor-associated antigens (TAA). Neo-antigens are tumor-specific

## Introduction

and not expressed in normal tissue, therefore, they do not underlie central tolerance. This minimizes the risk of autoimmunity, making this therapy less toxic than those targeting TAA [145-147]. In a recent study, a patient with metastatic PC was treated with an infusion of autologous T cells that had been engineered to target mutant *KRAS* G12D. The patient showed a 72% regression of the tumors and the engineered T cells could be found in circulation 6 months after the transfer [148].

Most mutations observed in PDAC do not accumulate in a specific mutation hotspot [149], reducing the likelihood of detecting neo-epitopes shared by patients. Nevertheless, some genes have high frequencies of insertions and deletions, which can generate frameshifts resulting in new open reading frames (neo-ORF). Targeting neo-epitopes derived from frameshift mutations has the advantage that these may be shared among patients [150, 151]. In this context, the tumor suppressor gene *RNF43* could be a potential target due to its high number of frame-shift mutations observed in PC patients (Figure 6).

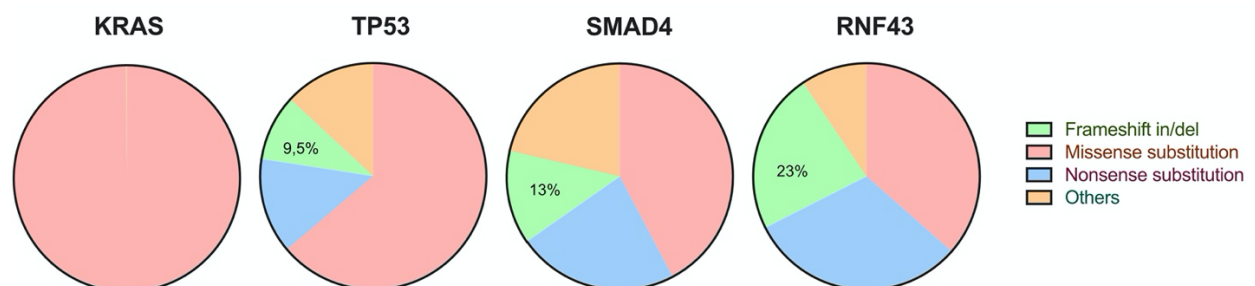


**Figure 6. *RNF43* presents a high number of frame-shift mutations in pancreatic cancer.**

Mutation distribution in frequently mutated genes *KRAS*, *TP53*, *SMAD4* and *RNF43* in pancreatic cancer. Data extracted from the COSMIC database in October 2022.

## 1.8 Aims of the thesis

*RNF43* is frequently mutated in PC. The focus of this thesis is to investigate the effects of these mutations on the development and progression of PC, as well as whether they can be used as therapeutic targets.

The effect of loss of *RNF43* function will be investigated through several *in vitro* assays and *in vivo* xenograft models to determine its carcinogenic potential. Previous *in vivo* studies showed more significant cancer progression in models with depletion of *RNF43* in

## Introduction

combination with oncogenic *KRAS* mutations. Here, the aim is to investigate whether *RNF43* mutations have a pathological effect under inflammatory conditions and whether they can also influence carcinogenesis in long-term pancreatitis.

In PC and its precursor lesions, *RNF43* typically accumulates insertions and deletions, resulting in the inactivation of its function by frame-shift mutations. Whether neo-epitopes derived from these frame-shift mutations can be used as therapeutic targets in adoptive T-cell therapy will be also assessed here.

## 2. Material and Methods

### 2.1 Materials

#### 2.1.1 Equipment

<b>Equipment</b>	<b>Company</b>
Aperio AT2 slide scanner	Leica Biosystems, Washington, USA
Bio-Rad CFX384 cycler	Bio-Rad, Hercules, USA
Biofuge fresco centrifuge	Heraeus, Hanau, Germany
Cell Counter	Corning, Corning, USA
ChemoCam Imager 3.2	Intas Science Imaging, Göttingen, USA
CytoFlex S	Beckman Coulter, Pasadena, USA
Evos cell imaging system	Invitrogen, Carlsbad, USA
Freezer – 20 °C	Liebherr, Bulle, Switzerland
Freezer – 80 °C	Thermo Fisher Scientific, Waltham, USA
Fridge	Liebherr, Bulle, Switzerland
Glomax plate reader	Promega, Madison, USA
Hera Safe Bio-Flow cell culture	Heraeus, Hanau, Germany
HeraCell 240 incubator	Heraeus, Hanau, Germany
Laminar airflow cabinet	Heraeus, Hanau, Germany
Maxwell RSC48 Instrument	Promega, Madison, USA
Megafuge 2.0 RS centrifuge	Heraeus, Hanau, Germany
Microtome RM2245	Leica Biosystems, Washington, USA
Mini Gel Tank	Invitrogen, Carlsbad, USA
Nikon eclipse TS-100 microscope	Nikon, Minato, Japan
pH-meter	Mettler-Toledo, Columbus, USA
Pipetboy	Corning, Corning, USA
precision scale	Sartorius, Göttingen, Germany
Rocker-Shaker MR-12	BioSan, Riga, Latvia
Sonovex Digitec ultrasound waterbath	Bandelin, Berlin, Germany
Spectrophotometer NanoDrop 1000	Thermo Fisher Scientific, Waltham, USA
Sunrise Microplate reader	Tecan, Männedorf, Switzerland
Thermal cycler C1000	Bio-Rad, Hercules, USA
Thermomixer compact	Eppendorf, Hamburg, Germany
Transblot SemiDry Transfer Cell	Bio-Rad, Hercules, USA
xCELLigence RTCA plate reader	Agilent technologies, Santa Clara, USA

#### 2.1.2 Consumables

<b>Consumables</b>	<b>Company</b>
100µm cell strainer	BD Biosciences, Franklin Lakes, NJ, USA
Blotting Paper	Whatman, Dassel, Germany
Cell culture flasks	Th.Geyer GmbH, Renningen, Germany

## Material and Methods

CellStar centrifuge tubes	Greiner Bio-one, Frickenhausen, Germany
Cryotubes	Th.Geyer GmbH, Renningen, Germany
FrameStar 384 plate	Azenta Life Sciences, Wotton, UK
FrameStar plate seal	Azenta Life Sciences, Wotton, UK
Glass coverslips	Menzel, Braunschweig, Germany
Nitrocellulose Transfer membrane	GE Healthcare, Chicago, USA
Non-tissue culture treated 24 well plates	Corning, Corning, USA
Novex gel cassettes	Invitrogen, Carlsbad, USA
Novex gel combs	Invitrogen, Carlsbad, USA
RCTA E-Plate 96	Agilent technologies, Santa Clara, USA
Reaction tubes	Th.Geyer GmbH, Renningen, Germany
Sequenza slide rack	Thermo Fisher Scientific, Waltham, USA
Serological pipettes	Greiner Bio-one, Frickenhausen, Germany
Superfrost plus microscope slides	Menzel, Braunschweig, Germany
TipOne Graduated Filter Tips	Starlab, Hamburg, Germany
Tissue culture plates	Corning, Corning, USA

### 2.1.3 Reagents and kits

#### Reagents

1% eosin  
Absolute ethanol  
Acetic acid  
Acetone  
Cell counting kit-8 (CCK-8)  
Cerulein  
  
Crystal violet  
Cultrex Basement Membrane Extract  
Difco Agar Noble  
DMSO  
dNTPs  
Glutaraldehyde  
Goat serum  
GoTaq qPCR system  
Hematoxylin solution  
Hexadimethrine bromide  
Ionomycin  
M-MLV  
M-MLV 5x reaction buffer  
Matrigel  
Maxwel RSC simply RNA Tissue Kit  
methanol

#### Company

Morphisto, Frankfurt am Main, Germany  
Carl Roth, Karlsruhe, Germany  
Carl Roth, Karlsruhe, Germany  
Merck, Darmstadt, Germany  
Sigma-Aldrich, Saint Luis, USA  
R&D Systems, Minneaoplis, USA and Sigma-Aldrich, Saint Luis, USA  
Merck, Darmstadt, Germany  
R&D Systems (Trevigen), Minneaoplis, USA  
BD, East Rutherford, USA  
AppliChem, Darmstadt, Germany  
Promega, Madison, USA  
AppliChem, Darmstadt, Germany  
Abcam, Cambridge, UK  
Promega, Madison, USA  
Carl Roth, Karlsruhe, Germany  
Sigma-Aldrich, Saint Luis, USA  
Merck, Darmstadt, Germany  
Promega, Madison, USA  
Promega, Madison, USA  
Corning, Corning, USA  
Promega, Madison, USA  
Merck, Darmstadt, Germany

## Material and Methods

Mitomycin C	Merck, Darmstadt, Germany
MTT	Sigma-Aldrich, Saint Luis, USA
Nuclease-free water	Promega, Madison, USA
Picric acid	Sigma-Aldrich, Saint Luis, USA
Pierce ECL solution	Thermo Fisher Scientific, Waltham, USA
PMA	Merck, Darmstadt, Germany
Puromycin	Merck, Darmstadt, Germany
Random primers	Promega, Madison, USA
RealTime-Glo MT Cell Viability Assay	Promega, Madison, USA
Retronectin	Takara Bio, Shiga, Japan
Roti-mount	Carl Roth, Karlsruhe, Germany
Roticlear	Carl Roth, Karlsruhe, Germany
SignalStain Antibody Diluent	Cell signaling, Danvers, USA
Signalstain DAB Substrate kit	Cell signaling, Danvers, USA
Sirius Red	Sigma-Aldrich, Saint Luis, USA
Sodium citrate	Carl Roth, Karlsruhe, Germany
Triton X-100	Carl Roth, Karlsruhe, Germany
Vectashield DAPI-containing mounting medium	Vector Laboratories, Burlingame, USA

### 2.1.4 Cell culture media components

<b>Component</b>	<b>Company</b>
3,3,5-Triiodo-L-thyronine	Sigma-Aldrich, Saint Luis, USA
Dexamethasone	
Bovine Pituitary extract	Corning, Corning, USA
Cell Recovery Solution	Corning, Corning, USA
Cholera toxin	Sigma-Aldrich, Saint Luis, USA
collagenase type II	Sigma-Aldrich, Saint Luis, USA
Cryo-SFM	PromoCell, Heidelberg, Germany
D-glucose	Invitrogen, Carlsbad, USA
Dexamethasone	Sigma-Aldrich, Saint Luis, USA
EGF	Thermo Fisher Scientific, Waltham, USA
Fetal bovine serum (FBS)	Sigma-Aldrich, Saint Luis, USA
Gibco Advanced DMEM F12	Invitrogen, Carlsbad, USA
Gibco DMEM	Invitrogen, Carlsbad, USA
Gibco OptiMEM	Invitrogen, Carlsbad, USA
Gibco Penicillin/Streptomycin	Invitrogen, Carlsbad, USA
Gibco RPMI	Invitrogen, Carlsbad, USA
Gibco Trypan blue	Invitrogen, Carlsbad, USA
Gibco Trypsin/EDTA	Invitrogen, Carlsbad, USA
Gibco™ IMDM no phenol red	Invitrogen, Carlsbad, USA

## Material and Methods

ITS+ premix	Corning, Corning, USA
Nicotinamide	Sigma-Aldrich, Saint Luis, USA
Nu-Serum IV	Corning, Corning, USA
ROCKi	Sigma-Aldrich, Saint Luis, USA

### 2.1.5 Buffers

Buffers/Solutions	Composition
PBS	137 mM NaCl 2.7 mM KCl 100 mM Na <sub>2</sub> HPO <sub>4</sub> *2H <sub>2</sub> O 2 mM KH <sub>2</sub> PO <sub>4</sub> 800mL of dH <sub>2</sub> O and adjusted to pH 7.4
FACS buffer	1xPBS FBS 2% (v/v)
SDS 1X	62.5 mM TRIS pH 6.8 2% w/v SDS 10% Glycerol 0.01% Bromophenol blue 50mM DTT (add before use)
TBS with Tween-20 (TBS-T)	TRIS 50 mM NaCl 150 mM Tween20 0.1 % pH 7.6
WB Blocking buffer	5% milk TBS-T
SDS running buffer	TRIS 25 mM Glycine 0.2 M SDS 0.1 %
IF Wash solution 1	3 % (w/v) BSA 1 % (w/v) Saponin in PBS
IF Wash solution 2	1 % (w/v) Saponin In PBS
IF blocking buffer	3 % (w/v) BSA 1 % (w/v) Saponin 1 % (v/v) Triton X-100

### 2.1.6 Oligo sequences

Oligo	Forward sequence	Reverse sequence
<b>Short hairpin DNA sequences</b>		
ShCtrl	GCAACTTCAGCTATATCATT	AAATGATATAGCTGAAGTTGC
ShRNF43	ATGAATCTCCCTCTGTGATT	AAATCACAGAGGGAGATTCAT
<b>Human primer sequences for RT-qPCR</b>		
GAPDH	GAAGGTGAAGGTCGGAGT	GAAGATGGTGATGGGATTTC
RNF43	CCTGTGTGTGCCATCTGTCT	GCAAGTCCGATGCTGATGTA

## Material and Methods

### 2.1.7 Antibodies

<b>Antibody</b>	<b>Dilution</b>	<b>Company</b>
<b>Primary antibodies for IHC</b>		
Ki67 (D3B5)	1:400	Cell signaling, Danvers, USA
CD3 (MAK1477)	1:200	Linaris, Eching, Germany
$\beta$ -catenin (19807)	1:1000	Cell signaling, Danvers, USA
E-cadherin (24E10)	1:400	Cell signaling, Danvers, USA
IBA1 (19741)	1:100	Sigma-Aldrich (Wako), Saint Luis, USA
NF- $\kappa$ B p65 (8242)	1:800	Cell signaling, Danvers, USA
RNF43 (HPA008079)	1:1000	(ATLAS) Invitrogen, Carlsbad, USA
<b>Primary antibodies for WB</b>		
GAPDH (14C10)	1:1000	Cell signaling, Danvers, USA
PD-L1 (E1L3N)	1:1000	Cell signaling, Danvers, USA
<b>Secondary antibodies for IHC/WB</b>		
Rabbit IgG (W4021)	1:3000	Promega, Madison, USA
Anti-Rabbit IgG (H+L), HRP Conjugate	1:200	Promega, Madison, USA
<b>Antibodies for IF</b>		
RNF43	1:200	Bioss Antibodies, Wobum, USA
chicken anti-rabbit IgG Alexa Fluor 488	1:300	Invitrogen, Carlsbad, USA
<b>Conjugated antibodies for flow cytometry</b>		
PE anti-human HLA-B7	1:200	BioLegend, San Diego, USA
Alexa Fluor 700 anti-human HLA-A2 Antibody	1:200	BioLegend, San Diego, USA

### 2.1.8 Cell lines

<b>Cell line</b>	<b>Media</b>	<b>Reference</b>
<b>AGS</b>	DMEM	ATCC, CRL-1739
<b>AsPC-1</b>	RPMI	ATCC, CRL-1682
<b>BxPC-3</b>	RPMI	ATCC, CRL-1687
<b>Capan 1</b>	RPMI	ATCC, HTB-79 <sup>1</sup>
<b>Capan2</b>	RPMI	ATCC, HTB-80 <sup>1</sup>
<b>CFPAC1</b>	DMEM	ATCC, CRL-1918
<b>DAN-G</b>	RPMI	CVCL_0243
<b>HPAC</b>	DMEM	ATCC, CRL-2119
<b>HPAF-II</b>	RPMI	ATCC, CRL-1997
<b>Huck</b>	RPMI	Patient-derived line <sup>2</sup>

## Material and Methods

<b>HuP-T4</b>	RPMI	CVCL_1300 <sup>2</sup>
<b>HupT3</b>	RPMI	CVCL_1299
<b>IMIMPC2</b>	DMEM	Vilá MR et al. [152] <sup>1</sup>
<b>MIA-PaCa-2</b>	DMEM	ATCC, CRL-1420
<b>MZ1-PC</b>	DMEM	CVCL_1434 <sup>3</sup>
<b>MZPCX-1</b>	DMEM	Heike M et al.[153] <sup>1</sup>
<b>MZPCX-2</b>	DMEM	Wölfel T et al.[154] <sup>1</sup>
<b>PA-TU-8988T</b>	DMEM	CVCL_1847
<b>PANC-10-05</b>	RPMI	ATCC, CRL-2547
<b>Panc02.03</b>	RPMI	ATCC, CRL-2553
<b>Panc05.04</b>	DMEM	ATCC, CRL-2557 <sup>2</sup>
<b>Panc08.13</b>	RPMI	ATCC, CRL-2551
<b>Panc28</b>	DMEM	CVCL_3917 <sup>1</sup>
<b>Panc3</b>	DMEM	CVCL_3921 <sup>1</sup>
<b>Panc1</b>	DMEM	ATCC, CRL-1469 <sup>3</sup>
<b>Patu8889S</b>	DMEM	CVCL_1846
<b>PSN1</b>	RPMI	ATCC, CRL-3211
<b>RWP1</b>	DMEM	CVCL_4373
<b>SK-PC1</b>	DMEM	Vilá MR et al. [152] <sup>1</sup>
<b>SK-PC2</b>	DMEM	Vilá MR et al.[152] <sup>1</sup>
<b>SK-PC3</b>	DMEM	Vilá MR et al.[152] <sup>1</sup>
<b>SMJ31</b>	RPMI	Patient-derived line <sup>2</sup>
<b>SU8686</b>	RPMI	ATCC, CRL-1837
<b>SW1990</b>	RPMI	ATCC, CRL-2172
<b>T3M4</b>	RPMI	CVCL_4056

Kindly provided by <sup>1</sup>the Cell Culture Maintenance Unit (IMIM Core Facilities, Hospital del Mar Medical Research Institute, Barcelona), <sup>2</sup>PD.Dr Günter Schneider and <sup>3</sup>Prof. Dr. Roland Rad.

### 2.1.9 Mouse strains

<b>Mouse strains</b>	<b>Source</b>
CrI:NU(NCr)-Foxn1 <sup>nu</sup>	Charles rivers laboratories, Wilmington, USA
C57BL/6JolaHsd	Envigo, Indianapolis, USA
C57BL/6 Rnf43 <sup>ΔExon8</sup>	In house breeding
C57BL/6 Rnf43 <sup>H292R/H295R</sup>	In house breeding

## Material and Methods

### 2.2 Cell characterization and assays

#### 2.2.1 Cell culture

Depending on their specifications (Section 2.1.8), human pancreatic cell lines were maintained in either Dulbecco's modified Eagle's medium (DMEM, Gibco) or Roswell Park Memorial Institute medium (RPMI, Gibco) supplemented with 10% fetal bovine serum (FBS, Sigma) and 1% Penicillin/Streptomycin (Gibco). Flasks were incubated at 37°C and 5% CO<sub>2</sub>.

Cells were passaged at 70-80% confluency; the medium was aspirated, and the flasks were rinsed with 5mL of Phosphate Buffer Saline (PBS). To dissociate and detach the cells from the surface, 2mL of Trypsin/EDTA (Gibco) were added into the flasks and incubated for 5-10 minutes at 37°C to achieve optimum trypsin activity. To stop the protease activity, 5mL of medium was added into the flasks, and the cell suspension was transferred into a 15mL falcon tube. Cells were centrifuged at 1000g for 5min, and the supernatant was discarded. Cell pellets were resuspended in 1mL of media, divided in a 1:10 ratio and transferred into a new 75cm<sup>2</sup> flask.

For long-term storage, 1x10<sup>6</sup> cells were resuspended in a solution containing 900µl of Media and 100µl of Dimethyl sulfoxide (DMSO). The cell suspension was placed in cryotubes and stored at -80°C or in liquid nitrogen.

To determine the cell number for assays, the automated Corning Cell Counter (Corning) was used following the manufacturer's instructions.

#### 2.2.2 HLA-typing of pancreatic cancer cell lines

Expression of HLA-A\*02:01 and HLA-B\*07:02 in PC cell lines was determined by flow cytometry. 1x10<sup>5</sup> cells were seeded in a 96-well plate (U-bottom), centrifuged at 1500rpm for five minutes, and washed two times with PBS and FACS buffer (Section 2.1.5). Cells were stained with the primary antibody diluted in 50µl of FACS buffer and incubated in the dark for 30 minutes at 4°C. After incubation, the plate was washed three times with 200 µl of FACS buffer. Prior to flow cytometry analysis, cells were resuspended in 150µl of FACS buffer, and HLA expression was analyzed using the CytoFlex S. (Beckman Coulter). The software FlowJo was used to analyze the data.

## Material and Methods

### 2.2.3 Retroviral transduction of HLA-A\*02

Viral particles containing the HLA-A\*02 construct were provided by the group of Prof. Dr. Busch. Non-tissue culture treated 24-well plates were coated with Retronectin (1:100 with PBS) at RT for 3 hours and washed twice with PBS. 1mL of filtered virus supernatant was added to each well and the plate was centrifuged at 2000g and 32°C for 1 hour. After centrifugation,  $1 \times 10^5$  Capan-1 cells were resuspended in 50µl of medium and added on top of the well. The plate was centrifuged at 1000g and 32°C for 10min, and cells were incubated for three days at 37°C and 5% CO<sub>2</sub>.

Cells were stained with anti-HLA-A\*02 (Section 2.2.2) and sorted in the Core Facility CyTUM of the Institute for Medical Microbiology, Immunology, and Hygiene (MIH) by HLA-A\*02 expression.

### 2.2.4 Lentiviral knockdown of RNF43

Knockdown of RNF43 was performed by employing short hairpin RNAs (shRNA) through lentiviral vector delivery. This method enables stable integration of the shRNA and long-term down-modulation of the target gene [155]. Two shRNAs were used in this study, a specific shRNA targeting the RNF43 mRNA (shRNF43) and a control nonsense shRNA, with no target gene (shCtrl). Lentivirus bearing the plasmids pCLV-U6-sh\_hRNF43-J-007004-11-EF1a-Puro (shRNF43) and pCLV-U6-sh\_mRNF43-4886-EF1a-Puro (shCtrl) were acquired from Sirion Biotech and stored at -80°C. shRNA sequences can be found in section 2.1.6.

Lentiviral knockdown of RNF43 was performed in the ASPC1, T3M4 and BxPC3 cell lines.  $3 \times 10^5$  cells/well were seeded in a 6-well plate 24h before transduction. Lentiviral particles were used at an MOI of 10 and adjusted with Opti-MEM media (Gibco) to a final volume of 1mL per transduced well. Hexadimethrine bromide was added to the lentiviral suspension at a concentration of 8 µg/ml. The media was aspirated from the wells and cells were washed with PBS. 1mL of the lentiviral suspension was added to each well and incubated at 37°C for two hours, gently swirling the plate every 30 minutes. After the incubation, 4mL of complete media was added to the wells and the media was exchanged after 24 hours.

## Material and Methods

Successfully transduced cells were selected by adding puromycin at a concentration of 200 µg/ml into the culture, and RNF43 knockdown was assessed by quantification of RNF43 mRNA levels and immunofluorescence.

### 2.2.5 Proliferation assay

Cell proliferation in knockdown cells was assessed with the cell counting kit-8 (CCK-8, Sigma) by measuring dehydrogenase activity in viable cells.  $5 \times 10^3$  T3M4 and BxPC3 shCtrl/shRNF43 cells were seeded in triplicates in 96-well plate 24 hours prior to cell measurement. 10 µl of the CCK-8 solution was added per well, and the plate was incubated at 37°C and 5% CO<sub>2</sub> for one hour. The absorbance of the wells was measured using a microplate reader (Tecan) at 450nm and 670nm as a reference value.

### 2.2.6 Clonogenic assay

Clonogenic assay was performed in knockdown cells to determine the ability of single cells to grow into colonies [156]. For that purpose,  $1 \times 10^3$  cells were seeded in a 2.5cm plate and incubated for two weeks at 37°C and 5% CO<sub>2</sub>. The medium was aspirated from the plates and cells were washed with PBS. Cells were fixed and stained with 6% glutaraldehyde/crystal violet solution at room temperature (RT) for 30 minutes. Plates were washed with tap water, and the number of colonies was determined by manual counting.

### 2.2.7 Soft agar colony formation assay

The soft agar assay was performed to determine the ability of RNF43 knockdown cells to grow in an anchorage-independent manner. For the test, two distinct agar layers were prepared at different concentrations. The bottom layer was composed of 0.6% agar in Iscove's Modified Dulbecco's Medium (IMDM), and the top agar layer of 0.3% agar in IMDM supplemented with 20% FBS. The agar solutions were kept liquid by placing them in a thermocycler at 42°C while shaking. 50 µl of the bottom layer was added to each well of a 96-well plate and allowed to solidify at room temperature.  $1 \times 10^3$  and  $1.5 \times 10^3$  cells per well were counted and resuspended in 25 µl of IMDM. The cell suspension was mixed with the top layer of agar and plated on top of the bottom layer of agar. After the layer had solidified, IMDM containing 10% FBS was

## Material and Methods

added to the top of the well as a feeding layer. Plates were sealed with paraffin and incubated for one week at 37°C and 5% CO<sub>2</sub>.

Colony formation was determined by microscopy, and the cell viability was quantified by adding 40µl of 3-(4,5-dimethylthiazol-2-yl)-2,5-diphenyltetrazolium bromide (MTT) at a concentration of 5 mg/ml. The plate was incubated at 37°C and 5% CO<sub>2</sub> for three hours before the absorption values were measured at a 570nm wavelength using a plate reader (Tecan).

### 2.2.8 Wound healing assay

The migration capacity of RNF43 knockdown cells was evaluated through the wound healing assay. Cells were seeded at high confluency (1x10<sup>4</sup> cells/well) in a 96 well plate 24 hours prior to performing the assay. To avoid interference of cell proliferation in the migration assay, wells were treated with mitomycin C, a DNA synthesis inhibitor at a concentration of 5µg/ml [157]. A wound was produced by scratching the center of the well with a pipette tip. For 48 hours, images of the wells were taken every hour using the EVOS cell imaging system (Invitrogen) to monitor cell migration. The area of the wound was quantified over time using the ImageJ software.

## 2.3 Animal experiments

### 2.3.1 Xenograft model

A xenograft model was implemented to study the effect of RNF43 knockdown *in vivo*. For that aim, the immunodeficient athymic nude mouse line Crl:NU(NCr)-Foxn1<sup>nu</sup> was used. 6-week-old female mice were obtained from Charles River Laboratories and housed in the S2 area at the MIH animal facility. 24 hours prior to cell engraftment, whole body irradiation at 4.5Gy was performed to improve transplantability. For each injection, 5x10<sup>6</sup> BxPC3 or T3M4 shCtrl/shRNF43 cells were resuspended in OptimMEM and mixed with Cultrex Basement Membrane Extract (Trevigen) to a final concentration of 7mg/mL. 200µl of the control and RNF43 knockdown cell suspension cells were injected subcutaneously on each flank of the mouse. After one week, mice were monitored daily and sacrificed at day 42 or when the tumors had a diameter greater than 1.5 cm (Figure 9B). At the endpoint, mice were sacrificed by cervical dislocation and the tumors were resected from the mouse flanks. Tumors were

## Material and Methods

weighed and fixed in paraformaldehyde (PFA) for histopathological analysis. Tissue samples were processed and stained at the TUM Institute of Pathology.

### 2.3.2 *Rnf43* mutant mouse models

Two mouse models bearing endogenous mutations in the *Rnf43* locus were used in this study to determine the impact of *Rnf43* mutations in the pancreas. C57BL/6 *Rnf43*<sup>ΔExon8</sup> mice have a 57 base pair deletion in the RNF43 RING domain, leading to inactivation of *Rnf43*. While in C57BL/6 *Rnf43*<sup>H292R/H295R</sup> mice, a histidine residue has been replaced by an arginine at positions 292 and 295 of the amino acid sequence. This resulted in hyperactivity of the Wnt signaling pathway *in vitro* [95]. More information about the mouse generation can be found in Neumeyer et al. 2019 [158]. Control wild type C57BL/6JolaHsd mice were purchased from Envigo. Animals were housed in the S2 area at the MIH animal facility.

Mice were sacrificed by cervical dislocation and the pancreas of *Rnf43* mutant mice were collected at four weeks, twelve weeks, twenty-four weeks, thirty-two weeks, and forty weeks of age. The organs were fixed in PFA and prepared for histopathological analysis.

#### 2.3.2.1 Induction of pancreatitis

To investigate the effect of *Rnf43* mutations on the progression of chronic pancreatitis, a risk factor for PC, intraperitoneal cerulein was administered to mice according to a protocol previously described by Neuschwander-Tetri et al. [159]. Injections were carried every 3 to 4 days for 10 weeks, thereby inducing repeated episodes of acute pancreatitis. On the injection day, mice were weighed and received six injections at intervals of one hour of 50μg/kg of body weight of cerulein dissolved in sterile PBS. Control mice received intraperitoneal injections of PBS at the same frequency (Figure 14A).

After analysis of the first group, *Rnf43* mutant mice developed a more severe pathology, with development of ADM. To verify whether the induced ADM persisted in our model and developed into PanIN or even to PC, additional groups were analyzed up to 3 months after the last cerulein treatment. Mice received the same treatment described above until day 70. Group 1 was analyzed 10 days after the last cerulein treatment (day 77). Group 2, 3 and 4 received re-administration of cerulein 2 weeks after the last injection (at days 84, 87 and 90).

## Material and Methods

Group 2 was analyzed at day 91, group 3 at day 98 and group 4 at day 188, 3 months after the last cerulein injection (Figure 16A).

At the endpoint, mice were euthanized with carbon dioxide (CO<sub>2</sub>). The abdomen of the mice was cut open and examined for macroscopic pathological findings. The pancreas and the spleen of the mice were removed and fixed with PFA for histopathological analysis. Tissue samples were processed and stained at the TUM Institute of Pathology.

### 2.4 Organoid culture

#### 2.4.1 Isolation and culture of pancreatic organoids

Ductal cell isolation was performed in wt and *Rnf43* mutant mice. A piece of pancreas of around 5 mm was collected and placed in cold PBS. The tissue was chopped into small pieces and introduced in a 50mL falcon tube with 2mL of collagenase type II solution (2mg/mL, Sigma). Samples were incubated in a shaker at 500rpm and 37°C for 30 minutes. After the incubation, 20mL of cold PBS were added into the tube and centrifuged at 350g and 4°C for 5 minutes. The supernatant was discarded, and pellet was resuspended in 5mL of PBS. The cell suspension was strained through a 100µm cell strainer and centrifuged at 350g and 4°C for 5 minutes. The supernatant was discarded and the samples were resuspended in a 500µL PBS, transferred into a 1.5mL reaction tube and centrifuged at 350g and 4°C for 5 minutes. The pellet was resuspended and embedded in Matrigel (Corning). 50µL of suspension was pipetted in each well of a 24-well plate and let for 15 minutes to polymerized. 500µL of organoid media (Table 1) supplemented with 10µM of ROCKi. Organoids were incubated at 37°C and 5% CO<sub>2</sub>.

For organoid culture maintenance, media was exchanged every two days. Organoids were passaged once a week at a 1:3 ratio and monitored using the EVOS cell imaging system (Invitrogen). For long term storage, organoid pellets were resuspended in 1mL of freezing media (cryo-SFM, PromoCell), placed in cryotubes and stored in liquid nitrogen.

Component	Stock concentration	Final concentration
Advanced DMEM F12	-	-
Nu-Serum IV	100%	5%
D-Glucose	200mg/mL	5mg/mL
Nicotamide	1M	10mM
Bovine Pituitary extract	15.6mg/mL	25µg/mL

## Material and Methods

ITS+ premix	100%	0.5%
3,3,5-Triiodo-L-thyronine	50 $\mu$ M	5nM
Dexamethasone	10mM	1 $\mu$ M
Cholera toxin	1mg/mL	100ng/mL
EGF	500 $\mu$ g/mL	20ng/mL

**Table 1. Components for pancreatic organoid cell culture media.**

### 2.4.2 Viability assay

Proliferation capacities of murine-derived pancreatic organoids was assessed through the RealTime-Glo™ MT Cell Viability Assay (Promega). 10 organoids were seeded per well in Matrigel on a white glass bottom 96-well plate. Per well, 100 $\mu$ L of media supplemented with 2 $\mu$ L/mL of NanoLuc® luciferase and MT Cell Viability Substrate was added and the luminescence values were measured using the Glomax® plate reader (Promega). After the first measurement, the remaining 100 $\mu$ L of media were added into the wells and measurements were performed daily. Values were normalized to the first measurement.

## 2.5 Evaluation of RNF43 expression

### 2.5.1 Quantification of RNF43 mRNA levels

#### 2.5.1.1 RNA isolation from cell lines

RNA isolation was performed to determine RNF43 mRNA levels by quantitative PCR. RNA was extracted using the automated Maxwell system (Promega) and the Maxwell RSC simply RNA Tissue Kit (Promega) was used following the manufacturer's instructions. Samples were eluted in 60  $\mu$ l of nuclease-free water and RNA concentration was determined by Nanodrop (Thermo Fisher) measurement. Samples were stored at -80°C.

#### 2.5.1.2 Reverse transcription

Complementary DNA (cDNA) was synthesized from the isolated RNA samples using the Moloney murine leukemia virus transcriptase (M-MLV, Promega). RNA samples were prepared in duplicates, since one of the samples was used as a control without retrotranscription to identify potential DNA contamination. For each reaction, 1 $\mu$ g of RNA was mixed with 150ng random primers (Promega) and nuclease free water was added to a

## Material and Methods

final volume of 14 $\mu$ l. Samples were incubated in a thermocycler at 70°C for five minutes, and five minutes on ice. Afterwards, 1.25 $\mu$ l of 10 mM deoxyribonucleotide triphosphates (dNTP, Promega), 5 $\mu$ l M-MLV 5x reaction buffer (Promega) and 1 $\mu$ l of M-MLV reverse transcriptase (Promega) were added to each sample, and the reaction was incubated for 10 minutes at room temperature. The retrotranscription control was incubated without transcriptase. The tubes were then loaded into a thermocycler (BioRad) and incubated 50 minutes at 50°C and 15 minutes at 70 °C. cDNA samples were stored at -20°C.

### 2.5.1.3 Quantitative Real time PCR

Quantitative Realtime PCR (RT-qPCR) was used to determine mRNA levels of RNF43 in cell lines. Previous generated cDNA samples were dilute 1:10 in nuclease-free water, and each sample was prepared in triplicates. 4 $\mu$ l of sample were pipetted in the bottom of a 384-well plate (4titude Framestar). Per reaction, 5 $\mu$ l GoTaq qPCR system (Promega) and 0.5 $\mu$ l Primer (forward and reverse) were pipetted on top of the well. Primer sequences can be found in section 2.1.6. The RT-qPCR plate was sealed and centrifuged before loading into the CFX Real-Time System thermocycler (Biorad). Program conditions are depicted in Table 2. Data were processed using the CFX manager software (Biorad) and analyzed in Excel. Gene expression values were normalized to the housekeeping gene *GAPDH*, and the relative expression level of each sample was calculated as  $2^{\Delta Ct}$ .

Step	Temperature (°C)	Time (min)
1.Pre-incubation	95	5:00
2.Amplification (40 cycles)	95	0:10
	60	0:30
	Plate read	
3.Melting curve	60	0:31
4. Melting curves (70 cycles)	60	0:05
	+ 0.5 °C/ cycle Ramp 0.5 °C/s Plate read	
5.Hold	12	$\infty$

**Table 2. Cycling conditions for RT-qPCR**

## Material and Methods

### 2.5.2 Immunofluorescence

RNF43 expression in cells with an RNF43 knockdown was assessed using immunofluorescence.  $1.5 \times 10^6$  cells were seeded onto glass coverslips in a 12-well plate and incubated overnight at 37°C and 5% CO<sub>2</sub>. On the next day, media was removed, and the slides were washed with cold PBS. Cells were fixed in 500µl of a 1:1 mixture of methanol and acetone for 15 minutes on ice and then washed three times with PBS at RT. Cells were permeabilized and blocked by adding 500µl IF blocking buffer for 10 min at RT. Slides were washed twice with the IF wash solution 1 (Section 2.1.5). Slides were inserted in a wet chamber, 50µl of the primary antibody was then diluted in IF wash solution 1 was added to the slide and incubated overnight at 4°C.

On the next day, slides were washed three times in IF wash solution 1 at room temperature and then 50µl of the secondary antibody diluted in IF wash solution 1 was added. Slides were incubated at room temperature for 1h and washed three times using IF wash solution 2, then three times with PBS. For mounting, one drop of DAPI-containing mounting medium (Vectashield) was added to the slide. Cells were imaged with the confocal microscope FluoView FV3000 (Olympus), and images were composed with the software ImageJ.

### 2.6 Histological methods

#### 2.6.1 Embedding and sample preparation for staining

The pellet of murine pancreatic organoids was fixed in for 30 minutes in PFA. Samples were dehydrated by incubation in at increasing ethanol concentrations. Pellets were incubated for 10 minutes with 30% 50%, 70%, 90%, absolute ethanol (Roth) and Roticlear (Roth) solution concentrations. To exchange the solution, samples centrifuged for 5 minutes at 2.500rpm. Afterwards, samples were embedded in paraffin using metal cuvettes. Using a microtome (Leica), paraffin blocks were cut into 2µm sections and place in superfrost microscope slides (Menzel).

For mouse pancreas, tissue fragments were placed in cassettes and fixed in PFA for 48hours. Dehydration and paraffin inclusion was performed at the TUM Institute of Pathology. 4µm

## Material and Methods

paraffin sections were cut using a microtome (Leica) and placed on superfrost microscope slides (Menzel) for further processing.

### 2.6.2 Hematoxylin and eosin staining

Hematoxylin and eosin staining (H&E) is the gold standard stain for pathology diagnosis, with the hematoxylin solution used to stain cell nuclei and eosin used to stain the cytoplasm [160]. To deparaffinize the slides, the samples were placed in an oven and incubated at 60°C for 20 to 30 minutes, until the paraffin melted. Slides were incubated three times for 10 minutes in Roticlear (Xylene), twice for 10 minutes in absolute ethanol, five minutes in 90% ethanol, five minutes in 70% ethanol, and five minutes in 30% ethanol to rehydrate the samples. Slides were transported in distilled water and stained in Hematoxylin solution (Mayer) for six minutes. Samples were washed in tap water and further stained with 1% eosin (Morphisto) for six minutes. The slides were washed in tap water and dehydrated by incubating them for 5 minutes in 50% Ethanol followed by a 5-minute incubation in 70% Ethanol, 5 minutes in 90% Ethanol, twice in absolute Ethanol for 10 minutes and three times in Xylene for 10 minutes. The slides were mounted with a drop of Roti-mount (Roth) mounting medium, and the cover slide was immediately placed over the sample. Microscopy slides were scanned with the Aperio AT2 slide scanner (Leica) and visualized with Aperio ImageScope software.

### 2.6.3 Sirius red staining

The levels of fibrosis in pancreatic samples were evaluated using the Sirius red stain. The above-described protocol was used to deparaffinize and rehydrate slides (Section 2.6.2). Pico-Sirius red, a solution composed of 0.5g Sirius Red (Sigma-Aldrich) diluted in 500mL of saturated aqueous solution of picric acid, was then applied to the slides for one hour (Sigma-Aldrich). After incubation, the slides were twice washed in acidic water (5mL acetic acid in 1L of tap water). Samples were further dehydrated and mounted as described in section 2.6.2.

### 2.6.4 Immunohistochemistry

Immunohistochemistry (IHC) was used to further describe and analyze organoids and murine pancreatic slides. Samples were deparaffinized and rehydrated using the protocol described in section 2.6.2. For antigen retrieval, the slides were boiled for 8 minutes in 0.01M sodium

## Material and Methods

citrate buffer with pH 6 in a pressure cooker. After boiling, samples were let to cool down for 30 minutes. The slides were rinsed in distilled water before being placed in cover plates (Thermo Scientific) and into a Sequenza slide rack (Thermo Scientific). To inhibit the endogenous peroxidase, slides were incubated 10 minutes at room temperature with 3% hydrogen peroxide. Afterwards, samples were washed for 5 minutes in water and 5 minutes with Tris-buffered saline containing 0.1% Tween 20 (TBS-T). Blocking of the slides was performed using 5% goat serum diluted in TBS-T for 1 hour at RT. The slides were then incubated with the primary antibody diluted with SignalStain Antibody Diluent (Cell Signaling) and incubated overnight at 4°C.

On the following day, slides were washed four times with TBS-T, and the secondary antibody in SignalStain Antibody Diluent (Cell Signaling) was added and incubated at RT for one hour. Samples were further washed four times in TBS-T. For developing, one drop of the chromogen (Signalstain DAB Substrate kit, Cell signaling) was added per milliliter of substrate and incubated at RT for 7 minutes. The slides were washed in distilled water and counterstained with Hematoxylin for 3 minutes. The slides were washed in tap water, dehydrated and mounted as described in section 2.6.2. The primary and secondary antibodies are listed in section 2.1.7.

### 2.7 SDS-PAGE and Western blot

PD-L1 expression was analyzed in PC cell lines models to test T cell toxicity. For that,  $4 \times 10^4$  cells were centrifuged and washed twice with PBS. Pellets were resuspended in 1x SDS buffer, sonicated for 10 minutes, and boiled for 5 minutes at 95°C using a Thermoblock. XX% acrylamide gels were cast, and samples were run in an SDS-PAGE gel (Table 3).

Stacking gel	
Component	Amounts
0,5M TRIS pH 6,5 0,4% SDS	0,5mL
10% Ammonium persulfate (APS)	10 µl
Tetramethylethylenediamine (TEMED)	2 µl
40% Acrylamide	0,2mL
Distilled water (dH2O)	1,28mL

Separating gel (8%)	
Component	Amounts
1.5M TRIS pH 8,8 0,4% SDS	1,5mL
10% Ammonium persulfate (APS)	30 µl
Tetramethylethylenediamine (TEMED)	6 µl
40% Acrylamide	1,2mL
Distilled water (dH2O)	3,26mL

**Table 3. SDS polyacrylamide gel preparation**

After running the SDS-PAGE, the gels were used in a Western blot to transfer the proteins to a nitrocellulose membrane, using a Transblot SD (Bio-Rad) following the manufacturer's instructions. The membrane was then incubated in blocking buffer (section 2.1.5) for 1 hour at RT and washed in TBS with Tween-20 (TBS-T). The membrane was then incubated with the primary antibody diluted in 5% bovine serum albumin (BSA)/TBS-T overnight at 4°C. After that, the membrane was washed three times in TBS-T for ten minutes before adding the secondary antibody in 5% milk with TBS-T for 1 hour at RT. The membrane was then washed six times in TBS-T for ten minutes and developed in Pierce (Thermo) ECL solution. The developed membrane was visualized with the Chemostar ECL imager (Intas Science Imaging).

## 2.8 TCR characterization assays

### 2.8.1 Neo-epitope prediction

Using the netMHC4.0 software, all possible neo-ORFs of *RNF43* were evaluated to determine potential T cell therapy targets. The search was restricted to HLA-A\*02:01 and HLA-B\*07:01 alleles and customize to a minimum peptide length of 8 amino acids. From all the results, peptides with a predicted MHC binding affinity of less than 20 nM were chosen.

### 2.8.2 Real-time cytotoxicity assay

The cytotoxicity potential of engineered T cells was measured with the quantitative real-time xCELLigence RTCA system (Agilent). In the peptide-pulsed setting,  $3 \times 10^6$  target cells were incubated with the *VSVWRSSL* or *SLLPTCWAL* peptide at a concentration of  $10^{-5}$ M at RT while rotating for two hours. 100µl of culture medium was added to 96-well RCTA E-plates (Agilent)

## Material and Methods

and inserted into the RTCA device in order to measure the background and normalize the cell index.  $2 \times 10^4$  target cells in 100  $\mu$ l of media were seeded into the plate, and triplicates were performed for each condition group. Impedance measurements were performed every 15 minutes. After 24 hours of culture, the target cells were added at different effector-to-target ratios (1:1, 10:1, 20:1). 100  $\mu$ l of the medium was removed from the plate, and the engineered T cells were added to the wells. As a negative control, RPMI medium was added to the wells, whereas 2% Triton X-100, which causes cell lysis, was added as a positive killing control. The cell index was measured over the course of three days, and data was visualized using the RTCA software and processed with GraphPad prism.

### 2.8.3 Reporter cell assay

Jurkat T cells equipped to express TCR R11, R13 and R15 were provided by the group of Prof. Busch. These Jurkat cells contain a reporter gene (GFP) under the control of the *NFAT* gene, therefore T cell activation upon peptide stimulation was measured through GFP expression. Target cells were pulsed with the *SLLPTCWAL* peptide at concentrations ranging from  $1 \times 10^{-4}$  to  $1 \times 10^{-12}$  M at RT while rotating for two hours. Engineered Jurkat cells were co-cultured for 24 hours with the target cells, and GFP expression was measured using flow cytometry. As a positive activation control, Jurkat T cells were incubated with 25 ng/mL phorbol myristate acetate (PMA) and 25 ng/mL ionomycin. As negative control, Jurkat cells were incubated with normal media. As a reference, two highly functional Jurkat lines targeting severe acute respiratory syndrome coronavirus 2 (SARS-CoV-2) peptides were included (sCoV5 and sCoV76). Data was processed with the FlowJo software. Using the software GraphPad Prism, dose response curves and EC50 values were determined.

### 2.9 Statistical analysis

All experiments were conducted with at least three biological replicates. The standard deviation is depicted with error bars. Unless otherwise indicated, statistical analysis of normally distributed data was performed using Student's and two-way ANOVA tests, or the Mann-Whitney U-Test if the data was not normally distributed and calculated with the software GraphPad Prism9 (GraphPad Software, California, USA). Statistical significance was determined at a p value  $\leq 0.05$ .

### 3. Results

#### 3.1 *RNF43* is frequently mutated in pancreatic cancer cell lines

*RNF43* mutations have been frequently observed in precursor lesions and in approximately 7% of PDAC tumors. In this study, a panel of established PC cell lines was evaluated for their relevance as tools for investigating the effects of *RNF43* mutations. The mutational status of the cells was assessed by whole-exon sequencing and by searching in the cell lines project from the COSMIC database. From the twenty-one cell lines analyzed, ten had mutations in the *RNF43* gene (Table 4). From those, the cell lines MZ1, Panc-10-05 and Capan2 presented frame-shift mutations that resulted in an early stop codon affecting the RING domain of the protein, and thus causing a loss of function (LOF) of *RNF43*.

One limitation when studying *RNF43* is the lack of validated anti-*RNF43* antibodies. Currently, there are no established antibodies for western blot application, for this reason, expression of *RNF43* in the cells was examined by measuring mRNA through qPCR. *RNF43* expression was classified as “low”, “moderate” and “high” (Table 4).

This data was compiled in a collaboration within the SFB1321 with the Gastroenterology department ‘Innere Medizin II’ of the Klinikum rechts der Isar.

Cell line	<i>RNF43</i> mutational status			RNF43 mRNA expression levels
	cDNA	AA	Classification	
AsPC-1	c.2159C>G	p.S720*	nonsense	high
BxPC-3	c.1484C>A	p.S495Y	missense	high
MZ1-PC	c.727delC	p.L243fs*176	frameshift	n.d.
HPAF-II	c.520G>T	p.E174*	nonsense	high
PA-TU-8988T	c.206T>G	p.F69C	missense	low
PANC-10-05	c.53_54insATCA	p.M18fs*23	frameshift	low
Capan 1		wt		high
DAN-G		wt		low
HPAC		wt		high
HuP-T4		wt		low
MIA-PaCa-2		wt		low

### 3. Results

<b>Patu 8889S</b>		wt		high
<b>Panc1</b>		p.P231L	missense	low
<b>SU8686</b>		p.P591P	synonymous substitution	low
<b>T3M4</b>		wt		moderate
<b>Patu111</b>		p.P758P	synonymous substitution	low
<b>PSN1</b>		wt		low
<b>Panc05.04</b>		wt		low
<b>Panc3</b>		n.d.		high
<b>Panc28</b>		n.d.		high
<b>Capan2</b>	c.989delG	p.R330fs	frameshift	n.d.

**Table 4. Characterization of pancreatic cancer cell lines.**

The *RNF43* mutational status of cells was assessed by sequencing. mRNA levels of *RNF43* were quantified using real-time PCR. 'n.d.' denotes not determined.

In summary, mutations in *RNF43* were found with high frequency in PC cancer cell lines. The majority of mutations found in the tumor suppressor were classified as frameshift or nonsense mutations, resulting in a truncation of the functional RING domain of *RNF43* and causing LOF.

#### 3.2 Loss of *RNF43* function enhances the tumorigenic potential of pancreatic cancer cells *in vitro*

To evaluate the impact of *RNF43* loss on PC, cellular models were established. Thus, the protein expression was knocked down in multiple PC cell lines. For that purpose, short harpin RNA (shRNA) delivered by a lentiviral vector was used. Cells were transduced with a specific probe targeting the mRNA of *RNF43* (sh*RNF43*) and as a control, a shRNA with a nonsense sequence (shCtrl) was used (see Material and Methods 2.2.4).

Based on the screening results shown in Table 4, three cell lines were selected to knock-down *RNF43* expression. ASPC1, BxPC3, and T3M4 cells showing high/moderate mRNA expression levels and carrying either wild-type (wt) *RNF43* or mutations not affecting functionality were chosen. ASPC1 harbors a mutation at position 2159 of the cDNA, which results in a premature stop codon at position 720 of the amino acid sequence. This mutation is found in exon 9 of the protein, after the functional RING domain of *RNF43*. BxPC3 cells carry a mutation in the

### 3. Results

position 1484 of the cDNA sequence that leads to a change of a serine to a tyrosine in position 495 of the protein sequence. This mutation is classified as missense, and several studies have reported that it has no effect on the protein function. Therefore, BxPC3 cells have been employed as a wt control in different RNF43 studies [161, 162].

Since concomitant mutations could also affect the behavior of these cells, the mutation status of other genes described to drive PC, namely *KRAS*, *TP53*, *SMAD4* and *CDKN2A*, was explored using the databases COSMIC cell lines projects and cellosaurus.org. The T3M4 cell line has mutations in the *KRAS* and *TP53* genes, while the mutation status of *SMAD4* and *CDKN2A* was unknown. BxPC3 cells express wild type *KRAS* but have mutations in *TP53* and deletion of *SMAD4* and *CDKN2A*. ASPC1 cells carry mutations in the *KRAS*, *TP53*, and *SMAD4* genes.

Cell lines	<i>KRAS</i>	<i>TP53</i>	<i>SMAD4</i>	<i>CDKN2A</i>
<b>T3M4</b>	p.G61H (c.183A>C)	p.T220C (c.659A>G)	-	-
<b>BxPC3</b>	wt	T220C (c.659A>G)	Gene deletion	Gene deletion
<b>ASPC1</b>	p.G12D (c.35G>A)	p.C135A (c.403delC)	p.R100T (c.299G>C)	-

**Table 5. Sequence variations of frequently mutated genes in pancreatic cancer cell lines.**

'p.' denotes the *amino acid* position where the mutation occurs and 'c.' the *nucleotide* position where the mutation occurs according to the cell lines project from the COSMIC database. '-' denotes that no information about the mutational status of the gene was available.

After lentiviral transduction, levels of *RNF43* mRNA expression were determined by qPCR. T3M4 shRNF43 cells showed an 85% reduction in *RNF43* mRNA levels, while a reduction of 60% was observed in BxPC3 shRNF43 cells. Transduction of ASPC1 cells did not result in a significant reduction of *RNF43* mRNA expression (Figure 7A). Therefore, these cells were excluded from further experiments. Changes in protein expression were analyzed by immunofluorescence. Consistent with the mRNA levels observed, a reduction in protein expression was observed, which was more pronounced in T3M4 shRNF43 cells compared to BxPC3 shRNF43 cells (Figure 7B).

### 3. Results

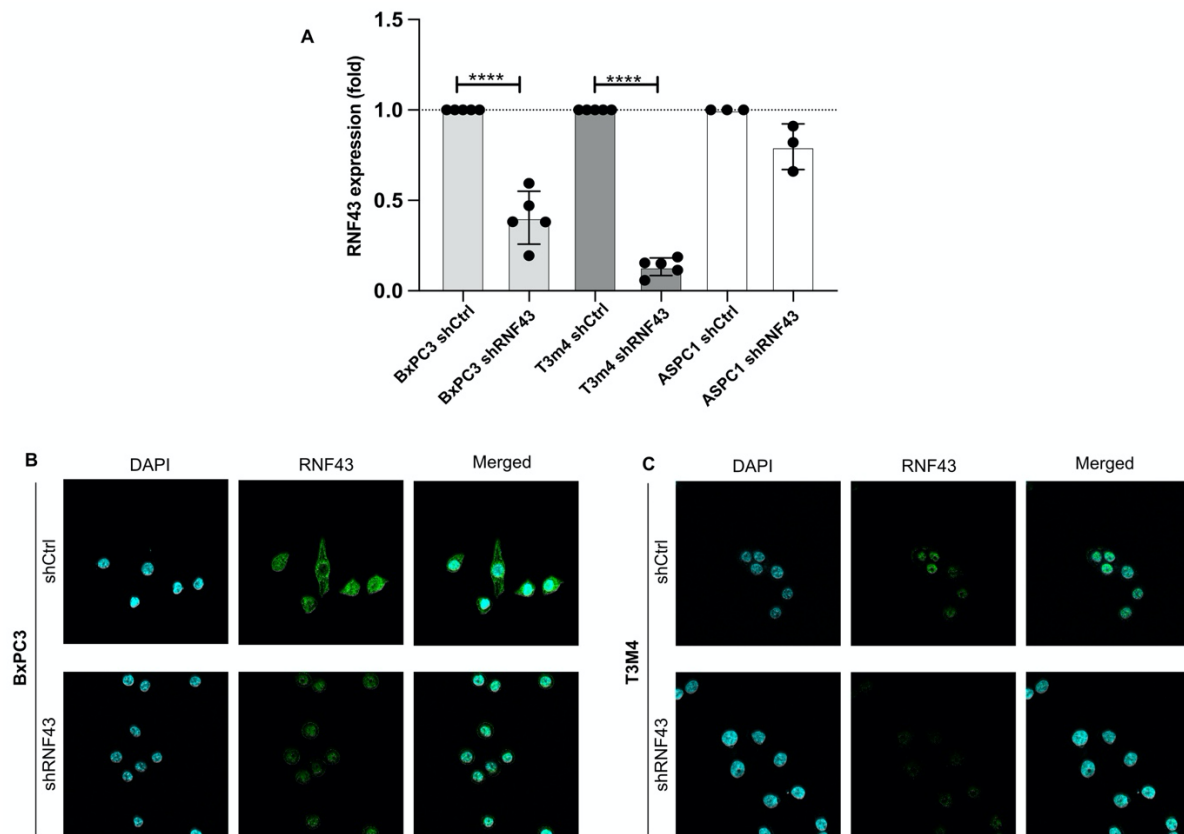


**Figure 7. RNF43 expression in pancreatic cancer cell lines.**

(A) mRNA levels of RNF43 after shRNA lentiviral transduction of BxPC3, T3M4 and ASPC1 cells. Values were normalized to the housekeeping gene GAPDH, and the expression levels observed in ShCtrl transduced cells. The graph shows the mean  $\pm$  SD of at least three independent experiments. Unpaired t-test. \*\*\*\*  $p \leq 0.0001$  (B) Confocal immunofluorescence imaging of endogenous RNF43 expression (green) in BxPC3 and T3M4 shCtrl/shRNF cells. Nuclei are stained with DAPI (blue).

Once the cellular models had been characterized, the impact of loss of RNF43 expression on the tumorigenic potential of the cells was investigated *in vitro* using different assays. First, the proliferative capacity of the cells was evaluated using the CCK-8 assay. Cells with a knock-down of the protein showed a higher proliferative capacity compared to controls (Figure 8A). This observation was confirmed in clonogenicity assays showing a similar trend of higher proliferation capacity of shRNF43 cells (Figure 8B).

In a next step, the ability of the cells to grow independently of a solid surface was measured in soft agar-based assays. Knock-down of RNF43 led to an enhanced anchorage-dependent growth of T3M4 cells, while no significant changes were observed between BxPC3shRNF43 and BxPC3 shCtrl cells (Figure 8C).

### 3. Results

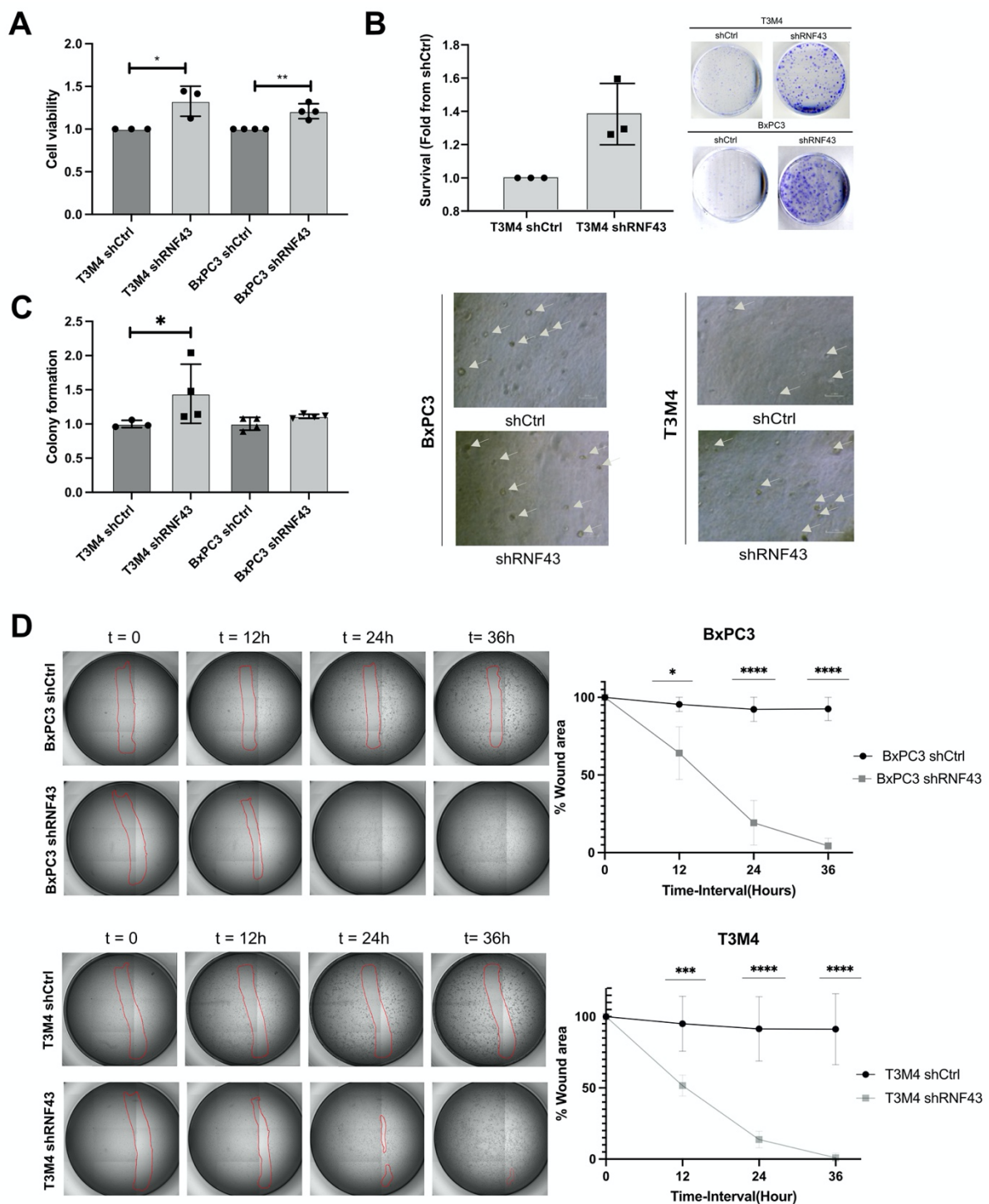


**Figure 8. Knockdown of RNF43 increases the tumorigenic potential of pancreatic cancer cell lines.** (A) Cell viability measured by adding CCK-8 into the cells and measuring the OD at 450nm. Values were normalized by the shCtrl and the graph depicts mean  $\pm$  SD (B) Clonogenicity assay showing the ability of single cells to survive and divide from single colonies. T3M4 shCtrl and shRNF43 cells were seeded at a low density and cultured for two weeks and then fixed and stained with crystal violet. The graph displays cell counts of three independent experiments. Values were normalized to the shCtrl and the graph depicts mean  $\pm$  SD (C) Anchor-independent growth measured by growing single cells between two agar layers and measuring the ability of those cells to form colonies. White arrows mark colony

### 3. Results

formation. Quantification was performed by adding MTT into the wells and measuring the absorbance at 570nm with a plate reader. Values were normalized by the shCtrl, and the graph depicts mean  $\pm$  SD (D) Wound healing assay assessing cell migration. Cells were seeded at high confluency and scratched to make a wound. Pictures of the plate were taken for 36 hours, and the wound size was measured over time. Wound area was measured with ImageJ and values were normalized to t=0. Representative images with the wound size are shown and the percentage of wound area is plotted in the graph. All graphs depict at least three independent experiments. \*\*  $p \leq 0,01$ , \*\*\*  $p \leq 0,001$ , \*\*\*\*  $p \leq 0,0001$ .

Finally, the tumorigenic potential of the cells was measured by assessing their migration capacity in wound healing assays. Since the wound could also close merely due to proliferation of the cells, mitomycin C was added to the wells to inhibit cell proliferation. Knock-down of RNF43 enhanced the migration of both BxPC3 and T3M4 cells, confirming that loss of RNF43 function enhances the tumorigenic potential of PC cells *in vitro* (Figure 8D).

#### 3.3 Loss of RNF43 potentiates tumor growth *in vivo*

After observing that loss of RNF43 increased the tumorigenic potential of pancreatic cells *in vitro*, the effects of knocking down RNF43 were evaluated *in vivo*. To this end, an athymic mouse model to engraft shCtrl and shRNF43 BxPC3 and T3M4 cells was established. Injection of the cells into each flank of the mice allowed a direct comparison of shCtrl and shRNF43 cells. When injecting BxPC3 cells, out of 12 mice, 11 developed tumors in the shRNF43 flank and 5 in the shCtrl flank (Figure 9B). Apart from an outlier, tumors in the shRNF43 flank grew larger over time, and the tumor weight at the endpoint was significantly increased compared to the tumors derived from shCtrl cells (Figure 9C). A similar trend was observed in the mice grafted with the T3M4 cell line. In this case, 8 out of 12 mice developed tumors in the shRNF43 flank, and interestingly, only 2 mice in the shCtrl flank (Figure 9B). Tumors derived from shRNF43 cells were significantly bigger than tumors grown from shCtrl cells. (Figure 9D).

### 3. Results

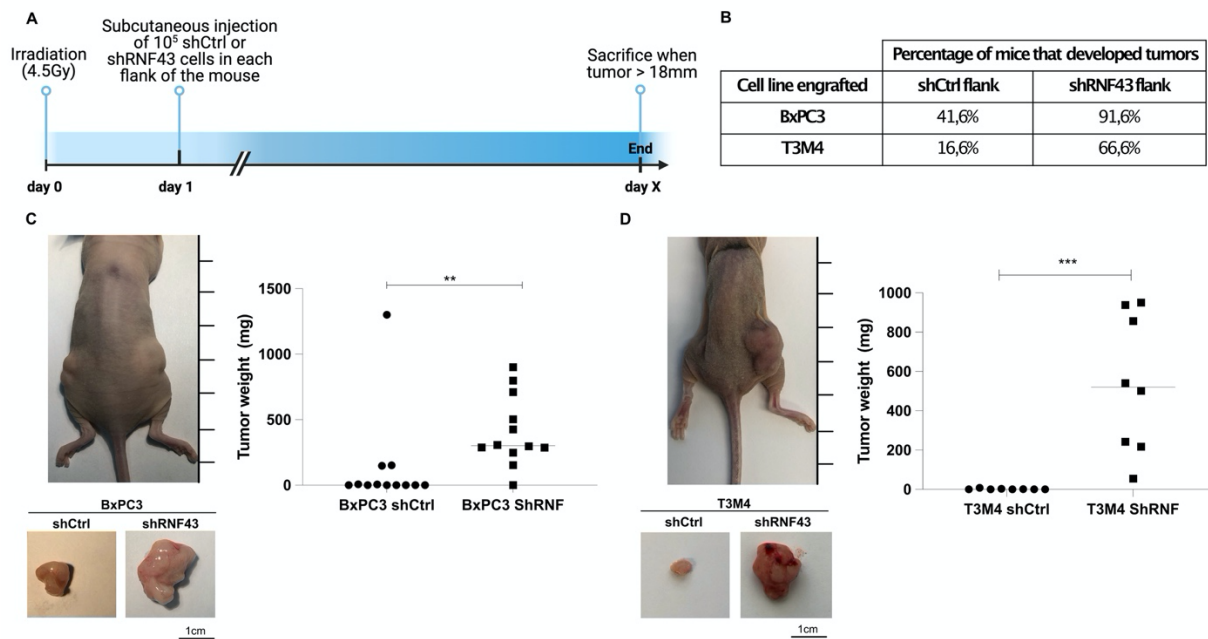


**Figure 9. RNF43 knockdown potentiates tumor growth *in vivo*.**

Immunodeficient mice  $Foxn1^{nu}$  were subcutaneously injected with either shCtrl (left flank) and shRNF43 cells (right flank). (A) Graphic timeline of the experiment. Created with BioRender.com (B) Percentage of mice that developed tumors in the shCtrl and shRNF43 flank of the mice for the cell line T3M4 and BxPC3. Macroscopic images of the mice flanks and the resected tumors derived from (C) BxPC3 shCtrl/shRNF43 and (D) T3M4 shCtrl/shRNF cells are shown. Tumor weight (mg) was measured at the end of the experiment. Each point represents a mouse, and the horizontal line depicts median. Mann-Whitney test. \*\*  $p \leq 0,01$ , \*\*\*  $p \leq 0,001$ . Scale bar, 1cm.

To further characterize the xenograft tumors and explore mechanisms that could explain the differences in tumor formation between shCtrl and shRNF43 tumor cells, histological sections were stained with hematoxylin and eosin (H&E) for pathological scoring.

BxPC3 tumors showed a squamous growth pattern, with high number of mitosis and necrosis. A variable degree of infiltration with different inflammatory cells (neutrophils, lymphocytes, plasma cells and macrophages), mostly at the margins of the tumors, was also observed. Tumors derived from the shCtrl cells were smaller than the generated from shRNF43 cells. They also showed a more undifferentiated/solid growth pattern and were highly infiltrated with inflammatory cells namely polymorphonuclear cells (Figure 10). The shRNF43 tumors showed more compact margins were better differentiated, were more cohesive, and showed a glandular pattern with less infiltration of immune cells (Figure 10).

### 3. Results

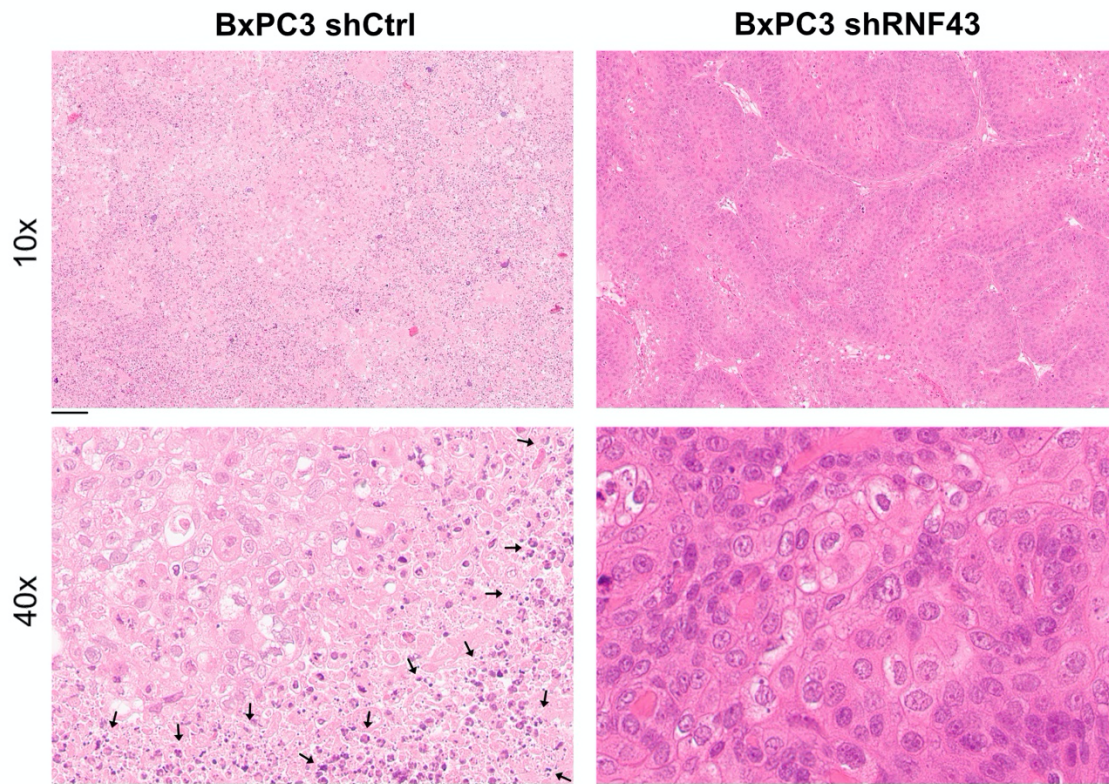


**Figure 10. Xenografts derived from shRNF43 cells present low immune cell infiltration.**

Hematoxylin and Eosin staining of representative BxPC3 shCtrl and shRNF43 tumors at 10x and 40x magnification. Black arrows indicate areas with high immune infiltration. Scale bar is 100 $\mu$ m.

Tumors derived from T3M4 cells showed a more undifferentiated/solid growth pattern compared to the tumors generated from BxPC3 cells. In addition, no glandular formations were observed. (Figure 11). Tumors from shCtrl cells were encapsulated and presented more inflammation and immune infiltration, similarly to what was observed for tumors derived from BxPC3 shCtrl cells. shRNF43 tumors presented a more solid growth pattern, with necrotic cells and less immune infiltration.

To confirm loss of RNF43 expression in the tumors derived from shRNF43 cells, tumors were stained for RNF43 by IHC. As expected, tumors derived from shCtrl cells expressed relatively high expression levels of RNF43, while reduced expression was detected in tumors from both BxPC3 and T3M4 shRNF43 cells (Figure 11).

Knock down of RNF43 induced changes in the proliferative capacity of the PC cells *in vitro*. Therefore, to investigate whether the same effect was observed *in vivo*, tumors were stained

### 3. Results

with the proliferation marker ki67. Tumors derived from BxPC3 and T3M4 cells were highly proliferative (Figure 11). However, shRNF43 tumors showed a higher proliferation trend compared to tumors derived from shCtrl cells. Interestingly, in the shCtrl tumors, highly proliferating ki67 positive cells corresponded to immune infiltrates.

RNF43 was suggested to regulate epithelial-mesenchymal transition (EMT) through E-cadherin ubiquitination and degradation [163]. Therefore, the expression pattern of E-cadherin was evaluated, and shRNF43 tumors showed higher E-cadherin positivity compared to the shCtrls.

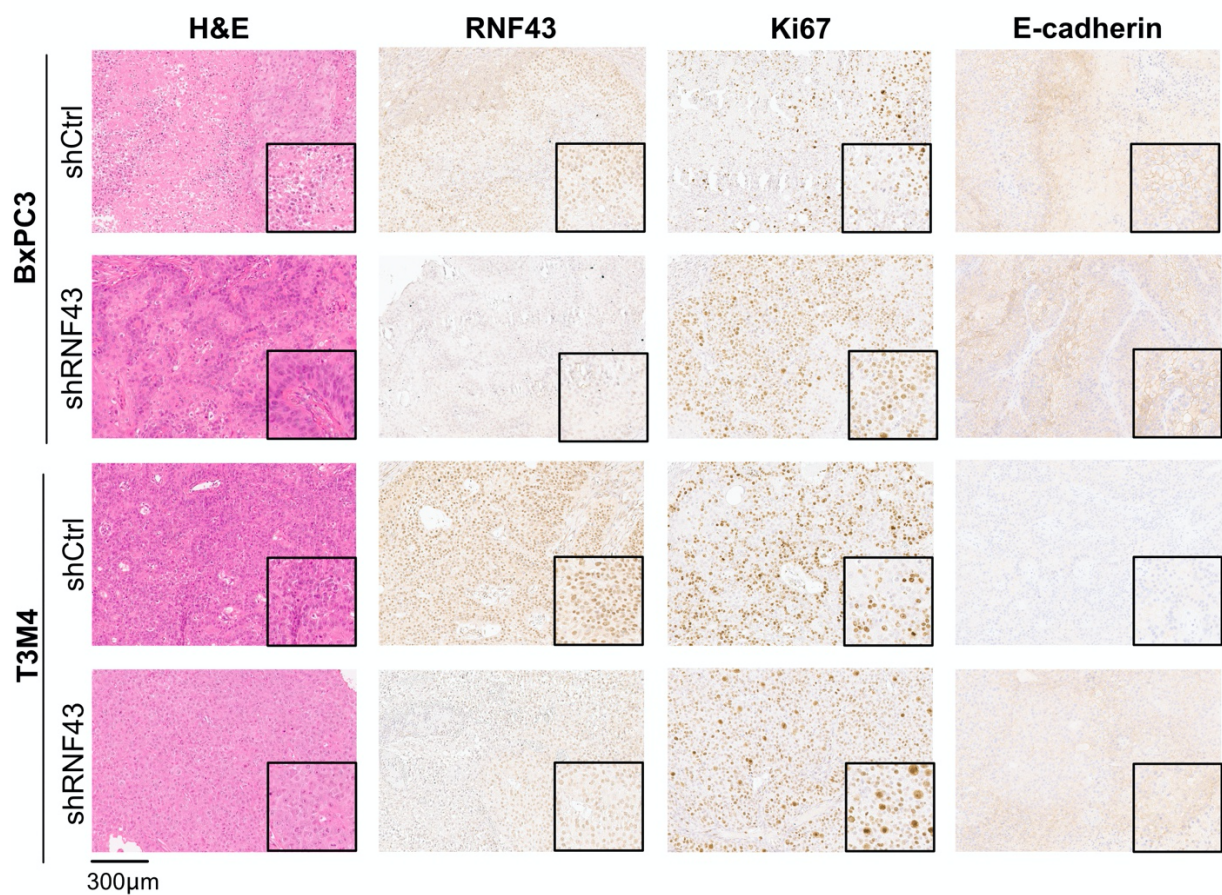


**Figure 11. Tumors derived from shRNF43 pancreatic cancer cells are highly proliferative.**

Representative images of xenograft tumors derived from BxPC3 shCtrl/shRNF43 and T3M4 shCtrl/shRNF43 cell lines. Tumor sections were stained with H&E. Expression of RNF43, Ki67 and E-cadherin was analyzed by IHC. Scale bar, 300µm.

Together, these results indicate that knock-down of RNF43 potentiates proliferation and tumor growth *in vivo*.

### 3. Results

#### 3.4 Mutations in *RNF43* drive pancreatic pathology during chronic pancreatitis

*In vitro* data and xenograft models suggested that alterations in RNF43 supports tumorigenesis. In humans, loss of RNF43 function is induced by mutations in the protein, mainly frame-shift mutations that induce an early stop codon, causing premature translation termination. Therefore, the effect of mutated *RNF43* in pancreas physiology and response to inflammatory triggers was studied using two mouse models carrying mutations in *Rnf43*. C57BL/6 *Rnf43*<sup>ΔExon8</sup> mice have a 57 base pair deletion in the RING domain of the RNF43 protein, leading to inactivation of Rnf43. C57BL/6 RNF43<sup>H292R/H295R</sup> mice show a genetic alteration in the RING domain of the *Rnf43* gene. Here, two histidines were replaced by arginine at positions 292 and 295, leading to hyperactivation of the Wnt signaling pathway *in vitro*. As control, wt C57BL/6JolaHsd mice were used.

Effects of *Rnf43* mutation in pancreatic physiology was first explored using pancreatic organoids established from both animal models. Pancreatic organoids were generated by isolating pancreatic ductal cells from 8 weeks old wt and *Rnf43* mutant mice. Organoids were cultured and monitored for five weeks. Representative pictures from each genotype were taken twice a week and are depicted in Figure 12A. A high variation in differentiation and growth pattern of the pancreatic organoids between genotypes was observed. Thus, *Rnf43* mutant organoids grew more rapidly in size than organoids derived from the pancreas of wt mice. This growth advantage was supported by ki67 stainings showing a higher ratio of Ki67-positive cells in organoids derived from the mutant mice (Figure 12B). Proliferation was also assessed by a cell viability assay (Figure 12C). In line with the previous data, organoids from mutant mice exhibited higher proliferation than wt pancreatic organoids. This difference was more pronounced when comparing the organoids derived from RNF43<sup>H292R/H295R</sup> mice to wt, suggesting that hyperactivation of the Wnt signaling pathway might have a more oncogenic effect *in vivo*.

### 3. Results

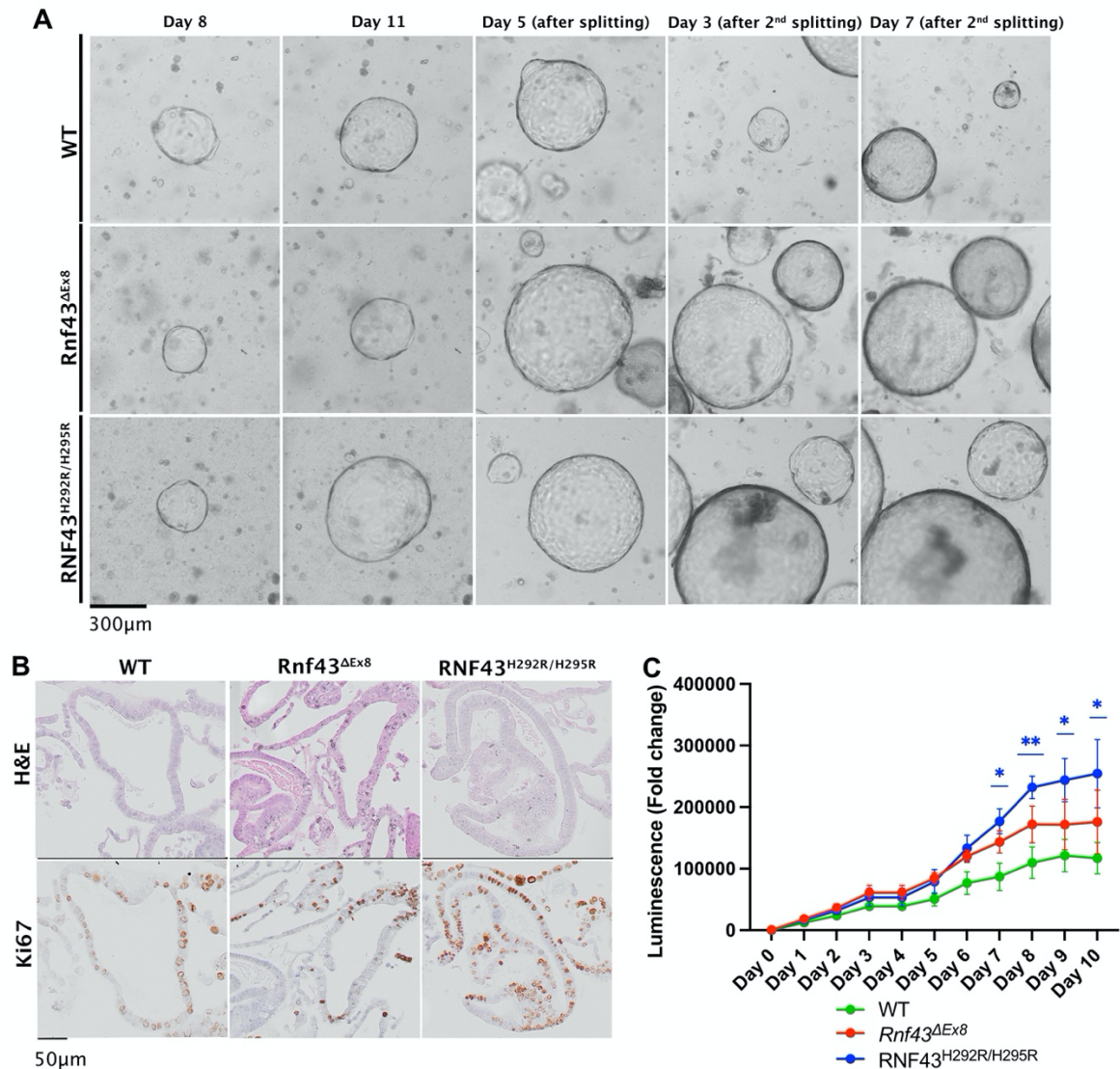


**Figure 12. Pancreatic organoids derived from Rnf43 mutant mice increase proliferation *in vitro*.**

Organoids were isolated from the pancreas of 8-week-old wt, RNF43<sup>H292R/H295R</sup> and Rnf43<sup>ΔEx8</sup> (A) Representative images of the organoids over five weeks after isolation and passaging. Scale bar 300 μm. (B) Organoids were embedded and stained for H&E and Ki67. Representative pictures of each genotype are shown. Scale bar is 50 μm. (C) Growth curve of murine wt and RNF43 mutated organoids. Ten organoids were seeded in each well on a 96-well plate. Cell viability was measured for ten days and determined with the CellTiter-Glo assay. Data was normalized by the first measurement, and it depicts mean ± SD of 3 independent wells. One-way ANOVA test were performed for each day between the genotypes. Blue asterisks indicate the significant differences between wt and RNF43<sup>H292R/H295R</sup>. \* p ≤ 0,05, \*\* p ≤ 0,01.

In a next step, the pancreas of the two Rnf43 mutant mice strains was examined at different time points (four weeks, twelve weeks, twenty-four weeks, thirty-two weeks, and forty weeks (w) of age) under basal conditions. The overall structure of the pancreas was analyzed macroscopically, and in tissue sections stained with Hematoxylin & Eosin. For all age groups, there were no significant differences between the wild-type and Rnf43 mutant mice were

### 3. Results

observed. Representative stained sections from mice at the oldest time point collected (40w) are shown in Figure 13. Both wild-type and *Rnf43* mutant mice displayed normal acinar structure, also no differences in the islets of Langerhans between the genotypes were observed, indicating normal pancreatic tissue architecture.

Fibrosis is a hallmark of pancreatitis and PC. To investigate the levels of fibrosis in *Rnf43* mutant mice, tissue sections were stained with Sirius Red. In Figure 13, fibrotic structures such as blood vessels, are visible. However, no sign of increased pancreatic fibrosis was observed.

Considering the changes in proliferation observed in the pancreatic organoids derived from *Rnf43* mutant mice, tissue samples were stained with Ki67. However, only few Ki67-positive cells were observed in the pancreas independently of the genotype of the mice.

Previous observations of other organs of these mouse models suggested changes in immunity [158]. Therefore, anti-CD3 IHC staining was used to investigate lymphocyte infiltration in the pancreas, but almost no positive cells were observed (Figure 13).

Finally, and considering the important role of RNF43 in regulating Wnt signaling, the expression of  $\beta$ -catenin, a key component of this pathway, was evaluated. The protein was detected at the plasma membrane of both acinar and islet cells, but there were no differences in expression between wild-type and *Rnf43* mutant mice (Figure 13).

In summary, mutant mice displayed typical pancreatic characteristics, including low proliferative ratios, low immune cell infiltration, and low levels of fibrosis that were not changed over time, indicating that *Rnf43* mutations alone do not induce changes in the pancreas under basal conditions.

### 3. Results

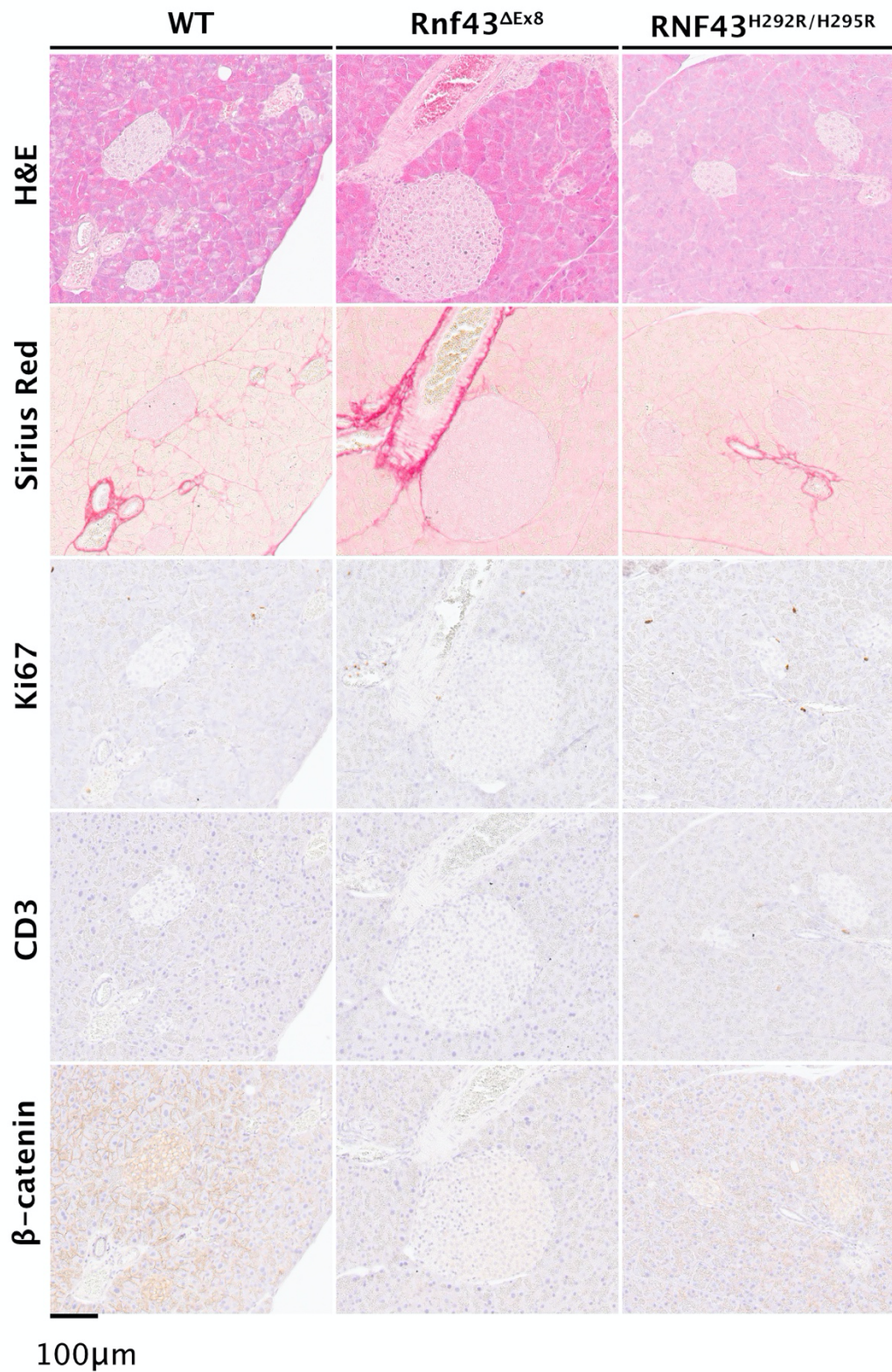


**Figure 13. *Rnf43* mutant mice display a normal pancreatic tissue architecture under basal conditions.** Representative images of hematoxylin-eosin, Sirius red and Ki67, CD3 and β-catenin staining of pancreas tissue samples from of 40-week-old wt, *RNF43*<sup>H292R/H295R</sup>, *Rnf43*<sup>ΔEx8</sup> mice. Scale bar, 100 μm.

### 3. Results

Chronic pancreatitis is a malignancy that predisposes to the development of PC. Many factors can contribute to the progression of cancer, including oncogenic insults. To investigate the influence of *RNF43* mutations during chronic pancreatitis, *Rnf43* mutant mice were treated with cerulein. Cerulein induces inflammation by dysregulating exocrine pancreatic secretion, causing acinar cell damage, vacuolization, and infiltration of immune cells. Mice were injected with cerulein or PBS for ten weeks following the schedule shown in Figure 14A.

Mice were sacrificed after 10 weeks, and the pancreas was examined macroscopically (Figure 14B). The pancreas of mice treated with cerulein was enlarged and whiter compared to PBS-treated mice. In addition, the organ of mice injected with cerulein exhibited a gelatinous consistency with high water content.

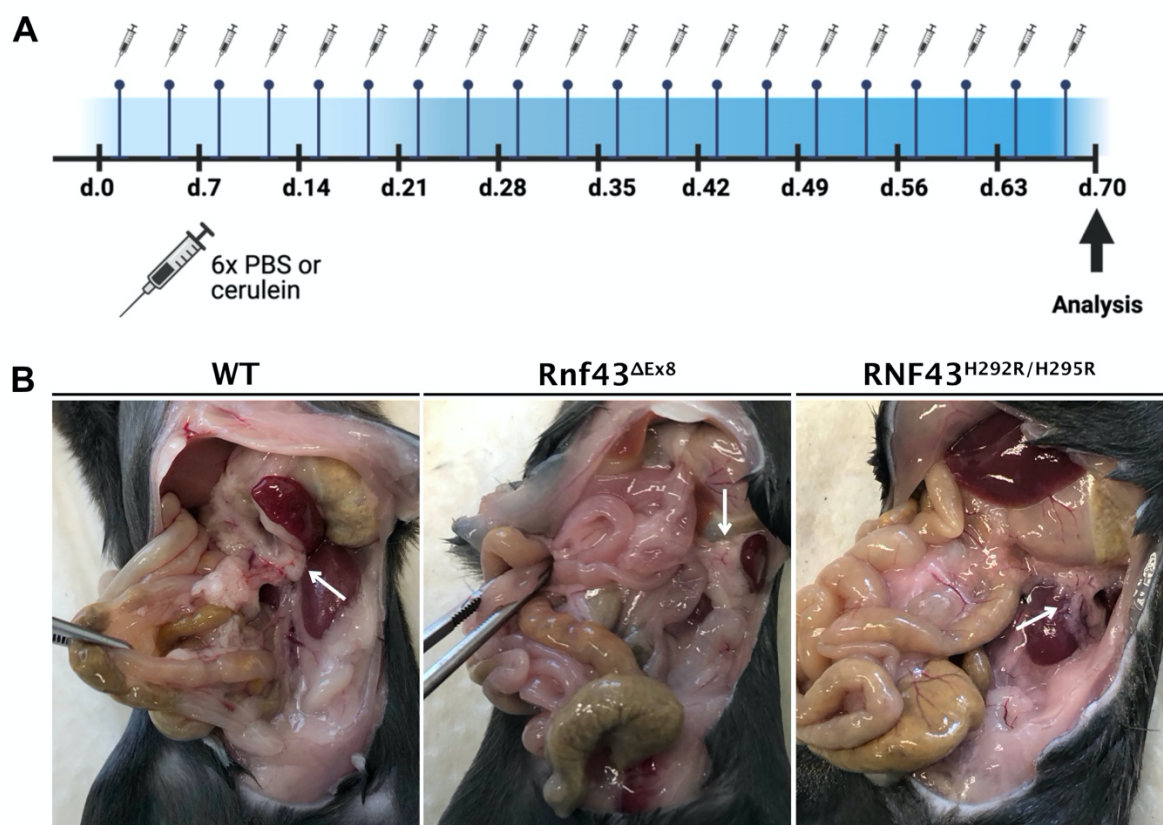


**Figure 14. Cerulein-treated mice present morphological changes in the pancreas.**

(A) Graphic timeline of the experiment. Created with BioRender.com (B) Representative images of the macroscopic appearance of pancreas after 10 weeks of cerulein treatment. White arrows mark the pancreas.

### 3. Results

To evaluate the degree of tissue damage induced by the treatment, the pancreas of the mice was embedded in paraffin and stained with H&E and Sirius red. As observed for *Rnf43* mutant untreated mice before, PBS-treated mice exhibited a normal pancreatic tissue architecture (Figure 15A). In contrast, the pancreas of wt and *Rnf43* mutant mice treated with cerulein exhibited edema and inflammation, with significant structural changes, such as alterations in the acinar structure and increased collagen surrounding the acini and islets of Langerhans.

When comparing the genotypes, we observed that  $RNF43^{H292R/H295R}$  mice presented more vacuolization in the acinar cells and larger islets of Langerhans compared to wt cerulein-treated mice. These observations pointed towards an islet hyperplasia. More striking differences were found in the *Rnf43*<sup>ΔEx8</sup> mice. Cerulein treatment induced a completely disrupted acinar architecture with severe acinar to ductal metaplasia (ADM) (Figure 15A). In addition, increased fibrosis in both *Rnf43* mutant mice was observed compared to wt (Figure 15A), with more overall collagen deposits in the *Rnf43*<sup>ΔEx8</sup> mice (Figure 15B).

Few proliferative cells were found in the PBS control wt and *Rnf43* mutant mice, whereas cerulein-treated mice exhibited a higher number of Ki67-positive cells, primarily acinar cells, regardless of the genotype. When comparing wt to *Rnf43* mutant mice, more positive Ki67 cells were observed in *Rnf43* mutant mice corresponding to immune infiltrating cells and in cells the acinar compartment. Although increased proliferation was found in both *Rnf43* mutant mice compared to wt animals, *Rnf43*<sup>ΔEx8</sup> mice showed the most significant changes in proliferation (Figure 15B).

Immune cell infiltrates were observed in the cerulein-treated mice, mainly macrophages, consistent with their role in tissue remodeling after injury. Lymphocyte infiltration was evaluated. As expected, CD3 positive cells were barely detected in the pancreas of wt and *Rnf43* mutant PBS-treated mice (Figure 15A). In contrast, mice treated with cerulein showed a weak infiltration of CD3 positive cells in their altered acini. However, the total number of CD3+ cells was very low. When comparing the genotypes, *Rnf43* mutant mice showed a slightly but not significant higher number of CD3 positive cells (Figure 15B).

### 3. Results

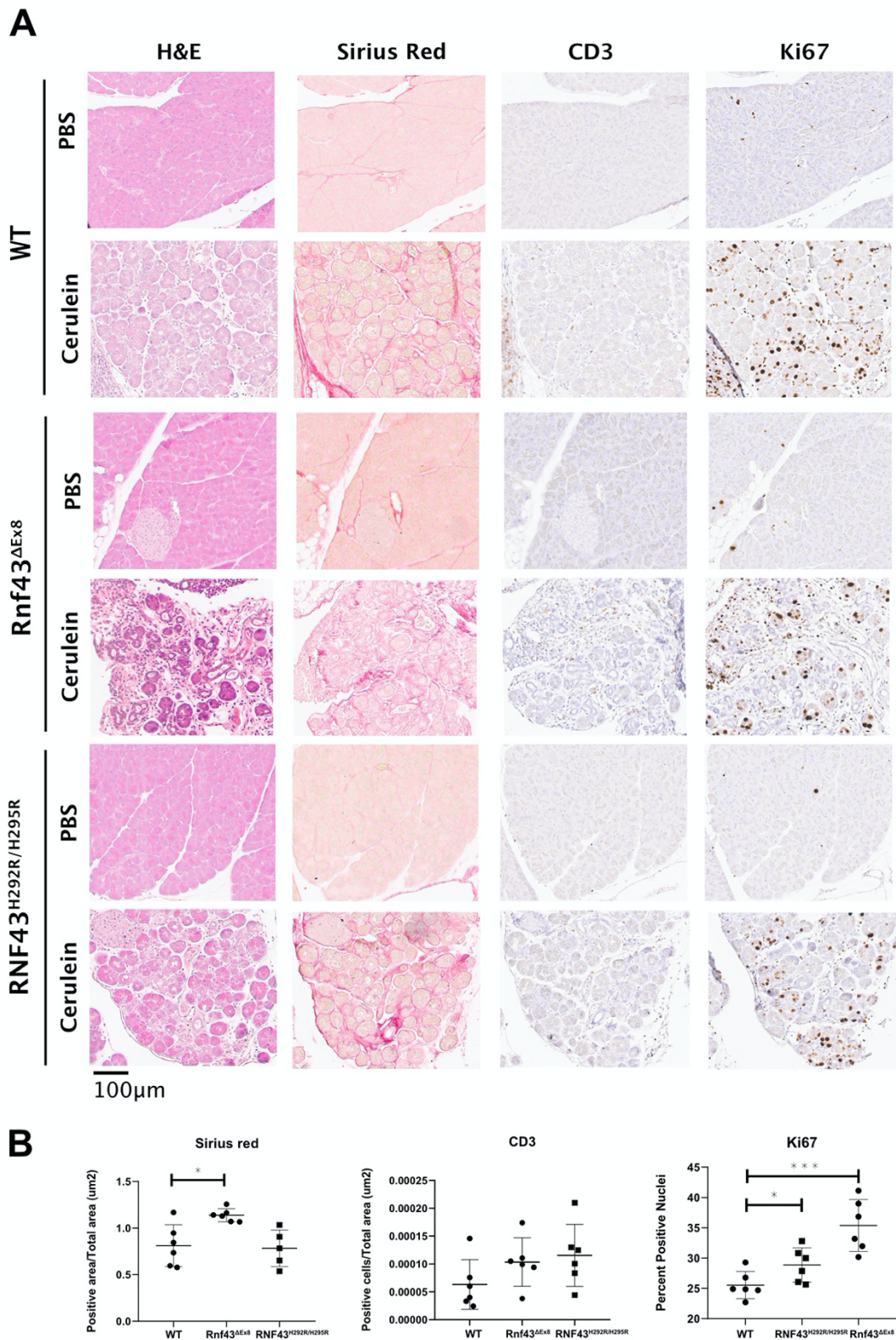


**Figure 15. Rnf43 mutant mice exhibit more severe cerulein-induced pancreatitis than the wt.**

Tissue sections of wt and *Rnf43* mutant mice receiving either PBS or cerulein were stained with H&E, Sirius Red, and IHC antibodies against Ki67 and CD3. (A) Representative images from each genotype. Scale bar is 100μm. (B) quantification of Sirius red, Ki67 and CD3 stainings. Each point represents a mouse, and the horizontal line depicts median± SD. T-test \*  $p \leq 0,05$ , \*\*  $p \leq 0,01$ . \*\*\*  $p \leq 0,001$

### 3. Results

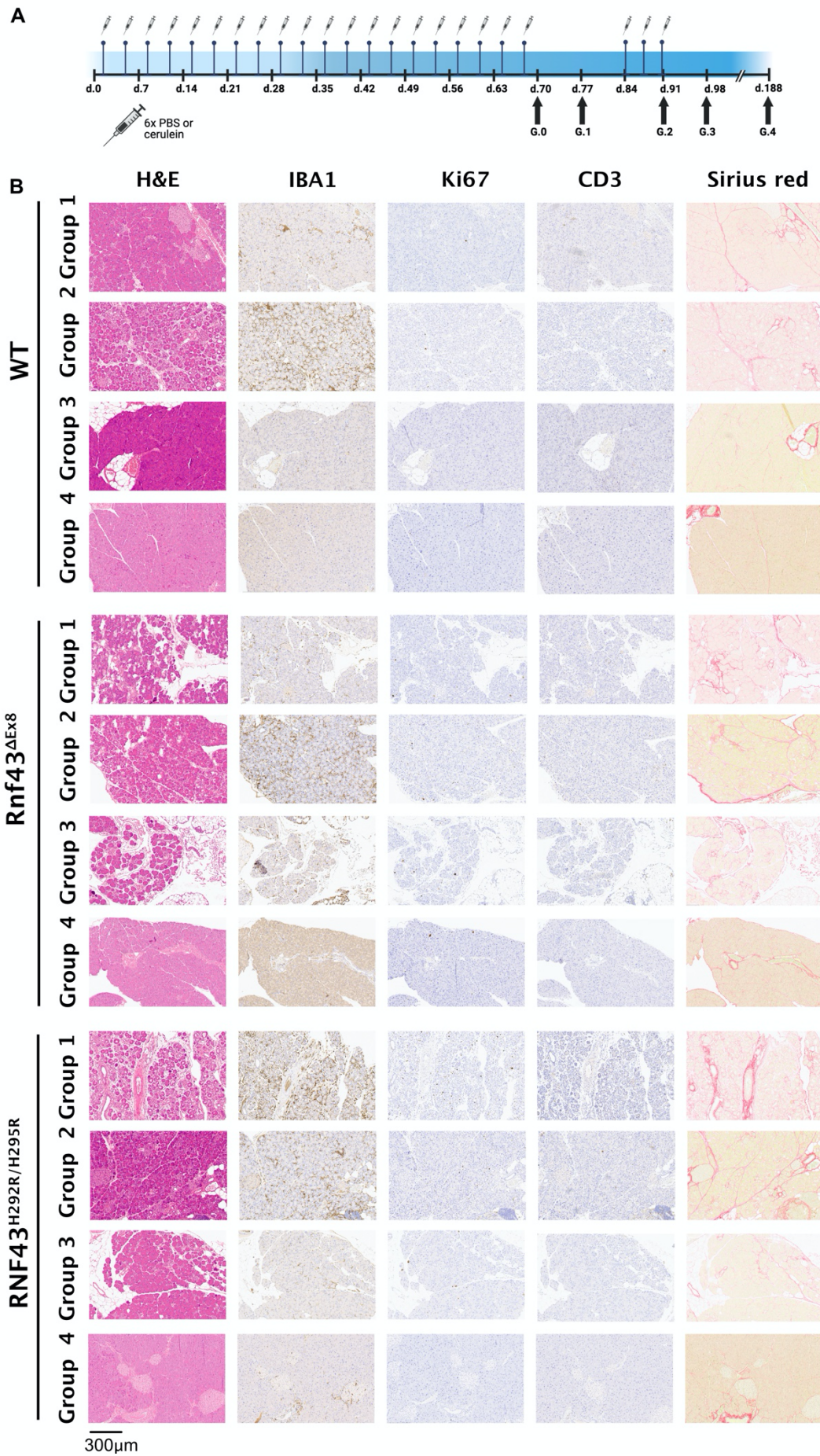
Altogether, after cerulein treatment, the pancreas of *Rnf43* mutant mice undergoes more severe structural changes compared to wt mice. Those include a completely disrupted acinar architecture, with presence of ADM progression, more fibrosis and increased proliferation.

To determine whether ADM, which is a precursor lesion for PC development [55, 164] could progress to other preneoplastic lesions such as PanINs or eventually to cancer, long-term time treatment experiments were carried out. To this end, mice were divided in different groups and treated with cerulein following different schedules depicted in Figure 16A.

Group one (G.1) received cerulein injections for ten weeks and mice were sacrificed ten days after the last injection. In this group, inflammation and ADM was lower compared to the group described before (sacrificed at day 70, right after the last cerulein injection), as the pancreas was already regenerating. A high number of Ki67 positive cells was observed in this group, as acinar cells proliferate during regeneration. Slight interstitial fibrosis was detected by Sirius red staining (Figure 16B), however, no major alterations in pancreas architecture were detected that could indicate progression of ADM to pre-neoplastic lesions.

Group two (G.2) mice received cerulein injections for ten weeks and re-administration of cerulein two weeks after the last injection (at day 84, 87 and 90). The cerulein-treated mice showed the expected increase in ADM, inflammation, and edema (Figure 16B). Compared to group one, the inflammation was more prominent, but still moderate. Comparing the groups, wt mice showed more remodeling and edema compared to the *Rnf43* mutant mice. In addition, less macrophage infiltration was observed in *RNF43<sup>H292R/H295R</sup>* mice genotype. However, ADM progression or more advanced pre-neoplastic lesions were not detected.

### 3. Results



### 3. Results

#### **Figure 16. Long term pancreatitis in *Rnf43* mutant mice does not progress to PanIN lesions.**

(A) Graphic timeline of the experiment. Created with BioRender.com (B) Tissue sections of wt and *Rnf43* mutant mice receiving either PBS or cerulein were stained with H&E, Sirius Red, and IHC antibodies against IBA1, Ki67 and CD3. Representative images from each group and genotype. Scale bar is 300µm.

Group 3 (G.3) mice received cerulein or PBS injections for ten weeks and re-administration of cerulein/PBS two weeks after the last injection (days 84, 87 and 90, Figure 16A). The analysis was performed on day 98 (1 week after the last injection). All PBS controls appeared normal, one pancreas showed a small focus of infiltration, but that was a minor and unspecific finding. The cerulein mice showed regeneration of the pancreas with less ADM, edema and inflammation and some slight fibrosis. In the more peripherally located lobules of the pancreas, the exocrine parenchyma was mildly replaced by fat cells (fatty replacement). This is an expected finding after the induced alteration/atrophy of the acinar cells by cerulein. Comparing the groups, the wt mice showed less fatty replacement compared to the *Rnf43* mutant mice. Additionally, less macrophage infiltration was observed in the  $RNF43^{H292R/H295R}$  mice genotype.

Group four (G.4). mice received cerulein or PBS (control) injections for ten weeks and re-administration of cerulein/PBS two weeks after the last injection (days 84, 87 and 90). The analysis was performed on day 188 (three months after the last injection). At this time point the pancreata of the cerulein mice was also nearly back to normal appearance after the induced inflammation. Each had small remaining foci of remodeling and (periductal) inflammation, but most of the parenchyma was regenerated. In general, the  $RNF43^{H292R/H295R}$  mice showed less of those remnants compared to the other two groups and they also presented less macrophage infiltration. When assessing the CD3 staining, more residues of periductal T-cell infiltration were observed in the *Rnf43*<sup>ΔEx8</sup> group compared to the wt.

In summary, subtle differences in proliferation, immune cell infiltration and tissue regeneration in *Rnf43* mutant mice over the course of the experiment. However, long-term pancreatitis in *Rnf43* mutant mice did not progress to PanIN lesions and cancer.

### 3. Results

#### 3.5 Neo-epitopes derived from the tumor suppressor gene *RNF43* as targets for T cell therapy

The identification of novel treatment options for PC patients is extremely important. As mentioned before, immunotherapy represents an interesting strategy, and the targeting of neo-epitopes derived from frame-shift mutations in frequently mutated genes might have good potential for PC patients. Functional analysis of TCRs targeting RNF43 neo-epitopes were done in collaboration with the group of Prof. Dirk H. Busch. Parts of the results in this section, including TCR isolation and characterization were conducted by Karolin Isabel Wagner, and can be found in her doctoral thesis "*Identification, isolation and characterization of T cell receptors for adoptive T cell therapy in tumor and viral infections*". For this reason, these results are excluded from this dissertation and only schematic representations of the workflow are shown.

The tumor suppressor *RNF43* is frequently mutated in the gastrointestinal tract with a high frequency of frame-shift mutations. These mutations lead to the generation of new open reading frames (neo-ORFs) that result in neo-epitopes. To identify potential T cell therapy targets, all possible neo-ORFs of *RNF43* were analyzed and peptide affinities were predicted *in silico* for the two most common HLA class I molecules, HLA-A\*02:01 and HLA-B\*07:02, using the online software netMHC 4.0. This resulted in the prediction of over 4000 peptides with varying lengths and MHC binding affinities. To narrow the search down, only peptides of at least 8 amino acids in length and with a predicted MHC binding affinity of less than 20 nM were selected. Seven of these peptides were tested for *in vitro* proteasomal processing and HLA loading for surface presentation by Prof. Dr. Peter Kloetzel. The chosen peptides are displayed in Table 6.

*RNF43* mutations found in PC patients were researched in publicly available databases (COSMIC, cbioportal). Mutations in the protein that led to insertions or deletions in the DNA sequence were screened, and the neo-ORF caused by the frameshift was analyzed for the amino acid sequences of the candidate peptides. Patient derived mutations that gave rise to the chosen peptides are listed in Table 6. G659fs is the most prevalent mutation in *RNF43*. Consequently, finding TCRs that target this mutation could benefit a large number of patients.

### 3. Results

In this instance, the mutated neo-ORF was analyzed using the netMHC 4.0 tool with the same parameters described previously. However, no peptides with a predicted affinity of at least 20 nM were discovered. For this reason, the affinity threshold was increased, and the HLA-A\*02:01-restricted peptide *TQLARFFPI* was identified. The predicted affinity of this peptide was lower (50 nM), but still within the range for immunogenicity and therefore was included in the study (Table 6).

Peptide	HLA type	Predicted affinity (Kd, nM)	Patient mutations leading to neoORF with epitope	<i>in vitro</i> processed
<b>VPSVWRSSL</b>	HLA-B*07:02	6	R27fs, K145fs, R40fs, S41fs, E43fs, L65fs, A115fs, C119fs, P192fs, P195fs, R225fs, Q254fs, S264fs, A269fs	epitope, 10mer, 11mer
<b>SLLPTCWAL</b>	HLA-A*02:01	6,8	R27fs, K145fs, R40fs, S41fs, E43fs, L65fs, A115fs, C119fs, P192fs, P195fs, R225fs, Q254fs, S264fs, A269fs, C275fs, E318fs, C309fs	epitope
<b>APGRSPAPL</b>	HLA-B*07:02	15	A33fs, K54fs, L88fs, R119fs, L311fs, R363fs, K45fs, L61fs, F69fs, P195fs,	epitope
<b>HPRSQAWAL</b>	HLA-B*07:02	5	R27fs, K145fs, R40fs, S41fs, E43fs, L65fs, A115fs, R117fs, C119fs, P192fs, R225fs, Q254fs, S264fs, C275fs	11mer, 12mer, 14mer
<b>IPAMPTTSL</b>	HLA-B*07:02	6,5	R27fs, K145fs, R40fs, S41fs, E43fs, L65fs, A115fs, R117fs, C119fs, P192fs, P195fs, R225fs, Q254fs, S264fs, C275fs	13mer, 14mer
<b>RPAAGRPGV</b>	HLA-B*07:02	13,2	R27fs, K145fs, R40fs, S41fs, E43fs, L65fs, A115fs, R117fs, C119fs, P195fs, R225fs,	12mer, 14mer
<b>TQLARFFPI</b>	HLA-A*02:01	50	R657fs, I680fs, A604fs, K559fs, G659fs	epitope

**Table 6. RNF43 candidate peptides for T cell therapy**

Two peptides were selected to start with the characterization: *SLLPTCWAL* a HLA-A\*02:01 restricted peptide, and the HLA-B\*07:02-restricted peptide *VPSVWRSSL*. T cells were isolated from the naïve repertoire of HLA-matched healthy donors via pHLA multimer-guided cell sorting (Figure 17). Since naïve CD8+ T cells recognizing the neo-epitopes are found in extremely low frequencies, they were purified from CD8+ apheresis. Antigen-specific T cells were enriched firstly by speed enrichment on single multimer staining, and then purity sorted through a double multimer staining.

### 3. Results

Single cells were expanded for two weeks, and their TCR sequences were amplified by PCR and sequenced in order to determine their alpha-beta chains. This enabled to reconstitute in silico the TCR expressed by the original sorted cells, and the transgenic TCRs were introduced using guide RNAs targeting the T-cell receptor  $\alpha$  constant (TRAC) locus of donor T cells via CRISPR/Cas9-mediated knock-in. To prevent TCR mispairing, the endogenous TCR on donor cells was knocked out [165, 166]. The engineered T cells went through additional testing and functional characterization to determine their target avidity and killing potential.

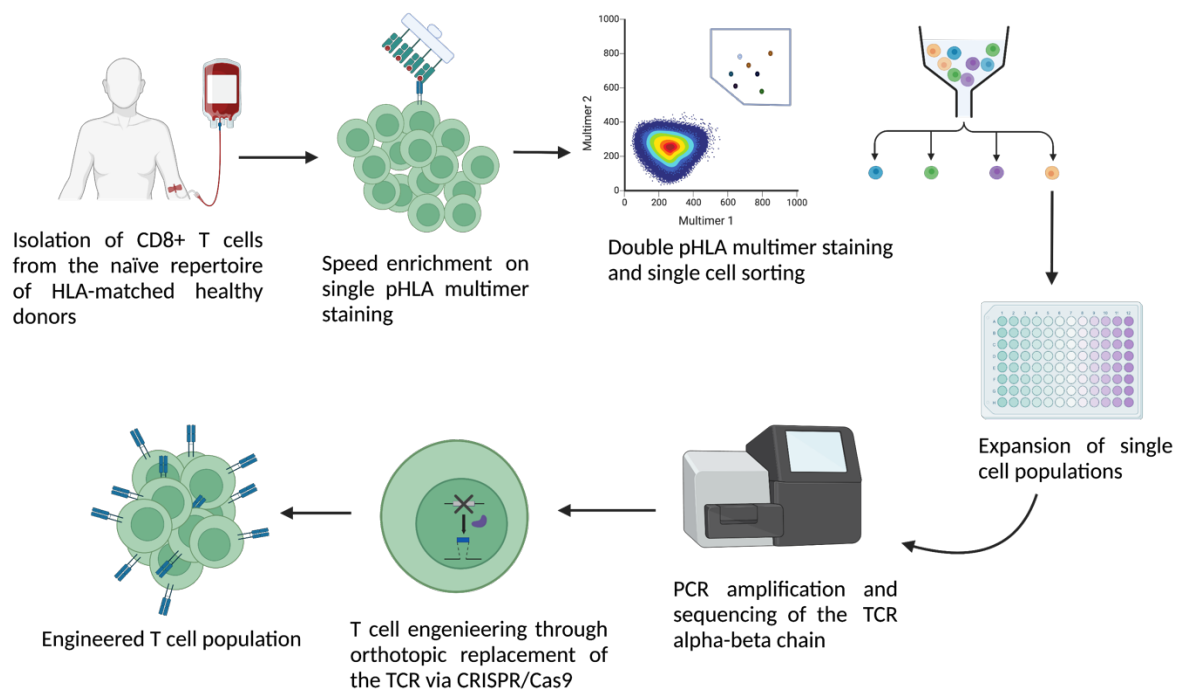


**Figure 17. Graphical representation of the isolation of RNF43 neo-epitope specific TCRs from the naïve repertoire of a healthy donor.**

Created with BioRender.com

Once the TCR-engineered T cells were produced, they were functionally characterized. Cells were evaluated for the antigen specificity through pHLA multimer staining and peptide-TCR avidity through TCR:pHLA koff-rate assay [167]. Activation of the cells upon peptide recognition was analyzed through the measurement of levels of interferon gamma (IFN- $\gamma$ ) production. For that, target cells were pulsed with candidate peptides at a concentration range of ( $10^{-12}$  to  $10^{-4}$  M) and TCR-transgenic T cells were added into the wells and co-cultured. After several hours, the levels of interferon IFN- $\gamma$  production were measured via intracellular

### 3. Results

staining and flow cytometry. Half maximal effective concentration ( $EC_{50}$ ) of IFN- $\gamma$  production upon peptide stimulation for each candidate TCR is shown in Figure 18.

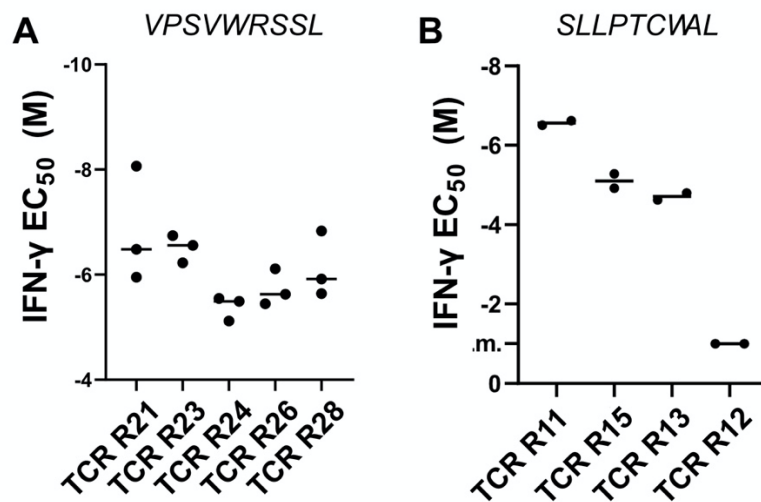


**Figure 18. VPSVWRSSL and SLLPTCWAL specific TCR repertoires contain functional TCRs.**  $EC_{50}$  values of IFN- $\gamma$  production upon peptide stimulation for the TCRs candidate targeting (A) the HLA-B\*07:02 restricted peptide VPSVWRSSL and (B) the HLA-A\*02:01 restricted SLLPTCWAL peptide.

For the HLA-B\*07:02 restricted peptide *VPSVWRSSL*, five potential TCR candidates were produced: TCR R21, TCR R23, TCR R24, TCR R26 and TCR R28. They all led to IFN- $\gamma$  production after peptide stimulation. For the HLA-A\*02:01 restricted peptide *SLLPTCWAL*, four TCRs were analyzed: TCR R11, TCR R12, TCR R13 and TCR R15. Overall, engineered T cells carrying those TCRs show IFN- $\gamma$  production at higher concentrations of peptide stimulation compared to cells with TCRs targeting the *VPSVWRSSL* peptide, indicating that they might have lower affinity, with the exception of TCR R12, that shows no activation. Among all the *SLLPTCWAL*-targeting TCRs, TCR R11, showed response at lower peptide concentrations ( $10^{-8}$ M) and better overall responses in all the other assays. For further details, refer to Karolin Isabel Wagner doctoral thesis.

The HLA-A\*02:01 restricted peptide *SLLPTCWAL* and the HLA-B\*07:02 restricted *VPSVWRSSL* were further evaluated for cytotoxicity effects. To establish proper cellular models to test this, a panel of 35 cell lines derived from pancreatic tumors was firstly screened for the expression of HLA\*A201 and HLA\*B702 via flow cytometry (Table 7). From those, eleven cell lines were HLA\*A201 positive and only two were positive for HLA\*B702 (Panc3 and Panc28).

### 3. Results

Cell line	HLA-type		Cell line	HLA-type	
	HLA-A*02	HLA-B*07		HLA-A*02	HLA-B*07
<b>AsPC-1</b>	positive	negative	<b>Panc28</b>	positive	positive
<b>BxPC-3</b>	positive	negative	<b>Capan2</b>	negative	negative
<b>MZ1-PC</b>	positive	negative	<b>SK-PC1</b>	negative	negative
<b>HPAF-II</b>	negative	negative	<b>SK-PC2</b>	negative	negative
<b>PA-TU-8988T</b>	negative	negative	<b>SK-PC3</b>	negative	negative
<b>PANC-10-05</b>	negative	negative	<b>MZPCX-1</b>	positive	negative
<b>Capan 1</b>	negative	negative	<b>MZPCX-2</b>	positive	negative
<b>DAN-G</b>	positive	negative	<b>RWP1</b>	negative	negative
<b>HPAC</b>	negative	negative	<b>MZ-2</b>	negative	negative
<b>HuP-T4</b>	positive	negative	<b>MZ-4</b>	negative	negative
<b>MIA-PaCa-2</b>	negative	negative	<b>M220- IMIMPC2</b>	negative	negative
<b>Patu 8889S</b>	negative	negative	<b>Huck</b>	negative	negative
<b>Pancl</b>	positive	negative	<b>SMJ31</b>	negative	negative
<b>SU8686</b>	negative	negative	<b>Panc02.03</b>	negative	negative
<b>T3M4</b>	positive	negative	<b>Panc08.13</b>	negative	negative
<b>PatuIII</b>	positive	negative	<b>SW1990</b>	negative	negative
<b>PSN1</b>	negative	negative	<b>HupT3</b>	negative	negative
<b>Panc05.04</b>	positive	negative	<b>CFPAC1</b>	negative	negative
<b>Panc3</b>	positive	positive			

**Table 7. HLA-typing of pancreatic cancer cell lines.**

The expression of HLA-A\*02:01 and HLA-B\*07:02 was measured by flow cytometry in a panel of PC cell lines.

#### 3.5.1 TCR R11 show cytotoxic activity in a peptide-pulsed setting

Based on the HLA and the *RNF43* mutational status, PC cell lines were used as models to perform cytotoxicity assays with engineered T cells targeting the *SLLPTCWAL* peptide. Thus, Capan2 and MZ-1 (Table 4 and 7) cells were selected. MZ-1 presented a one base pair deletion in the position 727 of the coding sequence of *RNF43*. This leads to the frame-shift mutation R330fs, giving rise to the *SLLPTCWAL* peptide. Flow cytometry staining for HLA-A\*02:01 showed that the cell line was positive. Capan2 presented a one base pair deletion in the position 989 of the coding sequence of *RNF43*, leading to the frame-shift mutation R330fs which should give rise to the *SLLPTCWAL* peptide. However, Capan-2 was found to be HLA-A\*02:01 negative (Table 7). To overcome this problem, cells were retrovirally transduced with

### 3. Results

HLA-A\*02:01 (Capan2-A2+) and sorted based on HLA-A\*02:01 expression. Cells were expanded after the sort and re-stained for HLA-A\*02:01 (Figure 19B), showing that around 93% of the population was positive for HLA-A\*02.

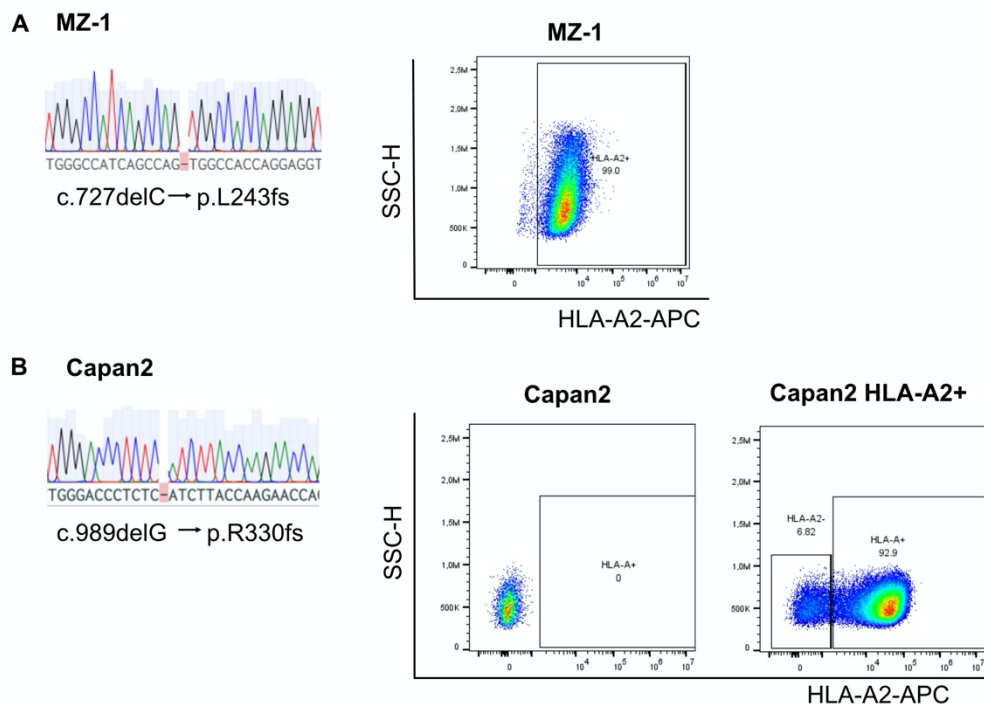


**Figure 19. MZ1 and Capan2 cells carry mutations in RNF43 leading to the *SLLP*TCWAL peptide.**

(A) Base pair deletion leading to a frame-shift mutation of RNF43 in the MZ-1 cell line and flow cytometry analysis for HLA-A\*02:01 expression. (B) Base pair deletion leading to a frame-shift mutation of RNF43 in the Capan2 cell line. FACs plots for the staining of HLA-A\*02:01 before and after retroviral transduction of HLA-A\*02:01 and sorting. Both cells were pre-gated on singlets.

The TCR R11 was chosen for cytotoxic testing since it demonstrated activity upon stimulation at lower peptide concentrations and thus possessed the greatest potential among all engineered TCRs. Cell proliferation was assessed through impedance measurements over time using an xCELLigence real time analyzer (Figure 20). The *SLLP*TCWAL peptide was pulsed overnight into the Capan2 HLA-A\*02+ cell line. As a control, the Capan2 cell line without pulsing was used. Cells were seeded and monitored for their cell index (impedance), and 24 hours later TCR R11 T cells were added into the well at an effector to target ratio of 10:1 and 20:1. RPMI media was added to the wells as a negative control, while Triton-X 100, which causes cell lysis, was added as a positive control.

In the peptide pulsing setting, the TCR R11 T cells at a 20:1 ratio recognized and killed the target cells almost immediately after their addition. There was cytotoxicity also in the 10:1

### 3. Results

ratio, but the slope of the curve was not as steep. In the absence of T cells, target cells continued to proliferate over time. In the Capan2 cell line unpulsed setting, no cytotoxicity was observed. The addition of T cells inhibited per se the growth of target cells in a T cell dose-dependent manner, most likely due to competition between cells for resources and well saturation. In the 10:1 ratio, cells continued to grow, but not at the same rate as in the control media, whereas in the 20:1 ratio, the well was likely to be saturated. Still, an accelerated drop of impedance in the pulsed setting was observed. Together these results indicate that TCR R11 T cells specifically recognized the target peptide.

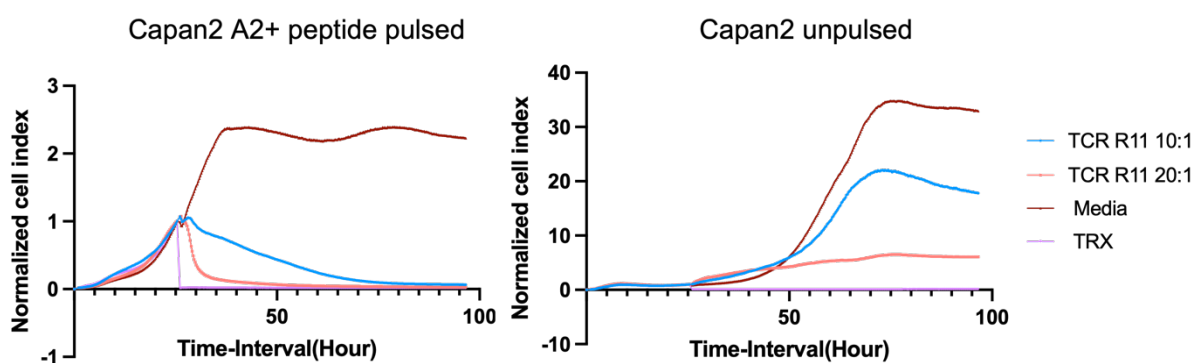


**Figure 20. TCR R11 shows recognition in a peptide-pulsed setting.**

Engineered T cells expressing the TCR R11 were co-cultured in an effector to target ratio 10:1 and 20:1. Media and triton X-100 (TRX) were added as controls. Capan2 HLA-A\*02+ cells were pulsed with the *SLLPTCWAL* peptide. Non pulsed Capan2 cells were used as control. Cell index was normalized to the point of treatment addition.

As specific cytotoxicity in the peptide pulsed setting was demonstrated, it was assessed whether the killing potential of the TCRs could be also observed in cells bearing endogenous *RNF43* mutations (MZ-1 and Capan2 HLA-A\*02+). Panc1, a cell line that does not express frame-shift mutations in *RNF43*, and Capan2, a cell line that expresses the R330 fs-mutation but is HLA-A\*02:01 negative, were used as controls. Besides TCR R11, TCR R13 and TCR R15, which showed good activation potential, were also included for evaluation. As a control to test for specificity, engineered T cells targeting the MART-1 antigen were added (Figure 21).

TCRs 11 and 13 were tested at a 10:1 and 20:1 effector to target ratio, while TCR R15 was tested at a 10:1 ratio. However, no killing effect was observed in any of the cell lines after addition of the T cells.

### 3. Results

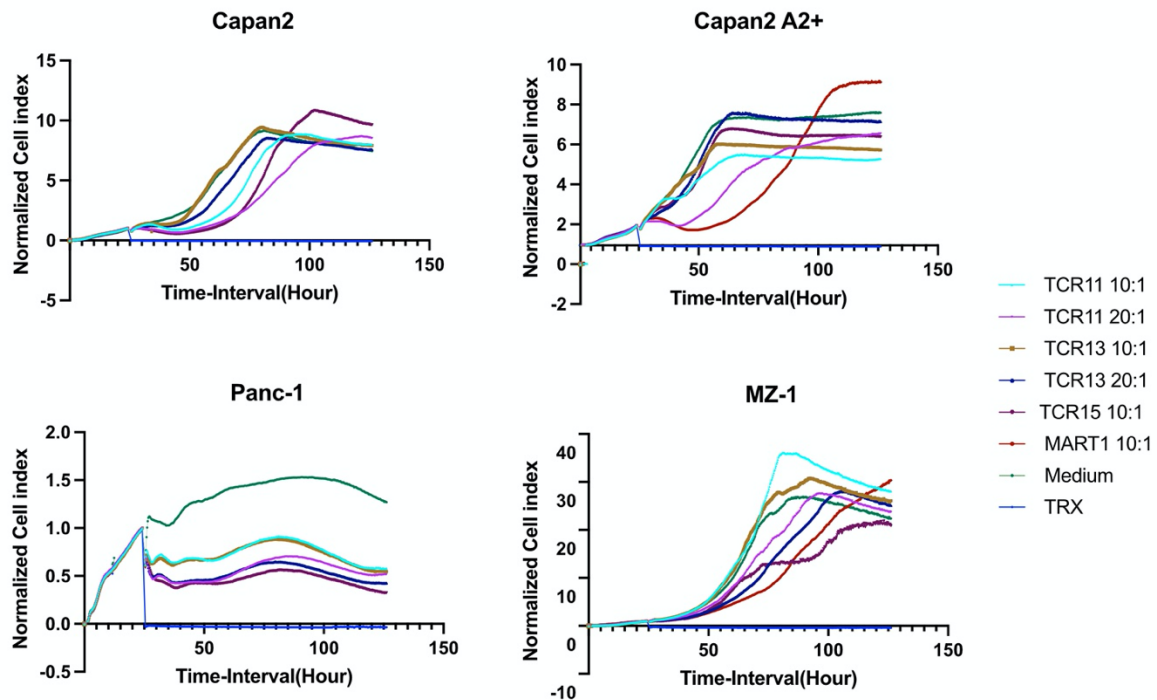


**Figure 21. TCRs targeting the SLLPTCWAL peptide show no cytotoxicity effect in cell lines expressing endogenous RNF43 fs-mutations.**

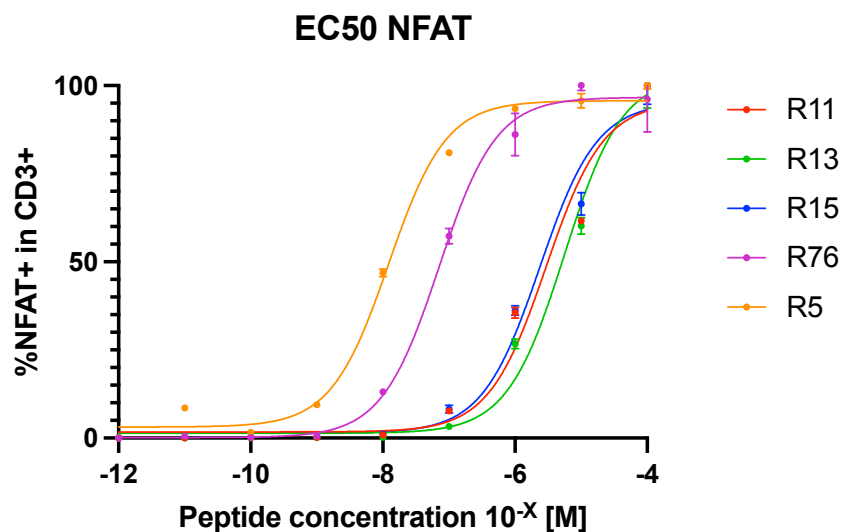
Engineered T cells expressing the TCR R11, TCR R13 and TCR R15 were co-cultured with the cell lines MZ-1 and Capan2 HLA-A\*02+ bearing endogenous *RNF43* mutations leading to the *SLLPTCWAL* peptide in an effector to target ratio 10:1 and 20:1. Media and triton X-100 (TRX) were added as controls. Capan2 and Panc-1 cell lines were used as negative controls. Cell index was normalized to the point of treatment addition.

Lack of cytotoxicity of the TCR-engineered T cells under endogenous expression of *RNF43* fs-mutations could be explained by a low potency of the TCRs, especially since T cells targeting the *SLLPTCWAL* peptide showed IFN- $\gamma$  production only at higher concentrations of peptide stimulation (Figure 18). To test this hypothesis, Jurkat cells were employed, since they are immortalized T lymphocyte cells and thus represent a faster model for TCR characterization. Jurkat T cells equipped to express the previously tested TCR R11, R13 and R15 were provided by the group of Prof. Busch. T cell activation could be measured since engineered Jurkat cell lines contain a reporter gene (*GFP*) under the control of the nuclear factor of activated T-cells (*NFAT*) gene.

Target cells were pulsed with the *SLLPTCWAL* peptide at a concentration gradient ( $10^{-12}$  to  $10^{-4}$  M) and NFAT activation via GFP expression was assessed by flow cytometry. This allowed the creation of a dose-response curve. In this case, TCR R11, R13 and R15 showed similar

### 3. Results

responses (Figure 22). To contextualize the potency of the *SLLPTCWAL*-specific TCRs at a quantitative level, two Jurkat cell lines expressing highly functional TCRs targeting severe acute respiratory syndrome coronavirus 2 (SARS-CoV-2) peptides were also included (sCoV5 and sCoV76) (Figure 22).



	R11	R12	R13	R15	SCoV5	SCoV76
LogEC50	-5.529	-1.416	-5.250	-5.627	-7.913	-7.151

**Figure 22. RNF43 TCRs are activated at higher peptide concentrations than SarsCov-2 TCRs.**

Dose-response curve and EC<sub>50</sub> values for NFAT expression in TCR R11, R15 and R17 upon *SLLPTCWAL* peptide stimulation compared to the highly functional TCRs R76 and R25 upon SARS-CoV-2 peptide stimulation.

The R5 and R76 TCRs showed better overall responses than the RNF43 TCRs. *NFAT* activation in RNF43 Jurkat cells upon peptide stimulation was observed at a peptide concentration of 10<sup>-7</sup> M, and the EC<sub>50</sub> values were approximately two logarithmic orders of magnitude lower than the TCRs targeting SARSCoV2 peptides. Together, these results indicate that the RNF43 *SLLPTCWAL* TCRs are of intermediate/low potency.

Cancer cells are known to employ multiple strategies to evade immune responses such as the upregulation of programmed death ligand-1 expression (PDL-1). PD-L1 binds to the immune checkpoint receptor programmed cell death-1 (PD-1), which is expressed on macrophages, monocytes, natural killer cells, and T cells. Under basal conditions, cells express PD-L1 to inhibit T cell response and maintain homeostasis; however, cancer cells exploit this

### 3. Results

mechanism to evade the immune response [168]. This could be another explanation for the lack of killing activity in the engineered T cells. Therefore, the expression of PD-L1 was analyzed in the PC cell lines employed for the T cell cytotoxicity assays by western blot. Panc1 and AGS, a gastric cancer cell line with wild-type *RNF43*, expressed less PD-L1 than the *RNF43*-mutant cell lines Capan2 and MZ-1, indicating that mutations in the protein may be associated with immune evasion and, consequently, T cell inhibition (Figure 23).

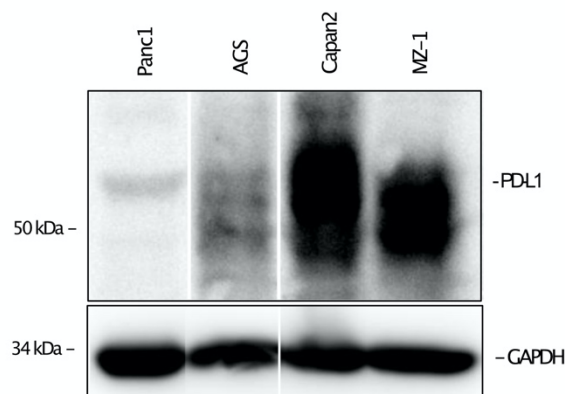


**Figure 23. Cells with endogenous *RNF43* fs-mutations show high expression of PDL-1.**

Western blot showing expression of PDL-1 in the cell lines with wt *RNF43* Panc1, AGS and in cell lines with *RNF43* fs-mutations Capan2 and MZ-1. GAPDH is used as a loading control.

In summary, TCR R11 engineered T cells only recognized the target peptide under peptide-pulsing conditions, while target cells bearing endogenous *RNF43* mutations were insufficient for T cell activation. This could be explained by a too low potency of the engineered TCRs, which may not be sufficient to induce a cytotoxic response, or the increased expression of PD-L1 in cells with mutations in *RNF43* inducing inhibitory signals for T cell activation.

#### 3.5.2 Engineered TCRs targeting the *RNF43* *VPSVWRSSL* peptide show cytotoxicity after peptide pulsing

Five functional TCRs were obtained for the targeting of the *VPSVWRSSL* peptide. As a first approach, the Panc-28 cell line was selected to test the cytotoxic effect of the engineered T cells in a peptide-pulsed setting due to its endogenous HLA-B\*07:02 expression. Cells were pulsed and seeded in a xCELLigence plate, where impedance was measured over time. After 24 hours the engineered T cells were added into the culture.

### 3. Results

T cells engineered with the TCR R21, R23, R24 and R26 recognized the target peptide and killed the cells thus lowering the impedance measurement in a 1:1 target-effector ratio (Figure 24). Triton X-100 was added as a positive killing control. Media control showed undisturbed growth of the cells. As a control for unspecific cytotoxicity, unedited T cells were added, and no killing effect was observed. However, engineered T cells expressing the TCR R28 showed a very limited effect on the target cells despite having good IFN- $\gamma$  production (Figure 18).

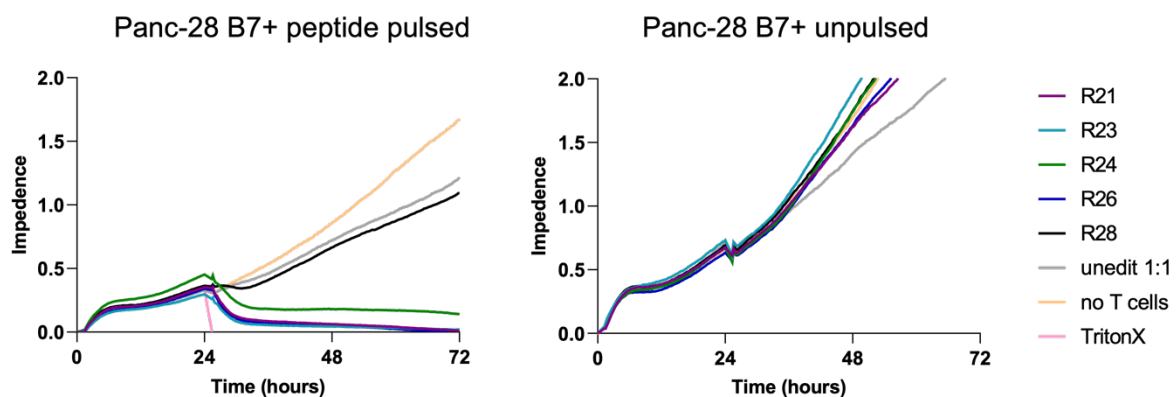


**Figure 24. TCRs targeting the VPSVWRSSL peptide show activation and killing effect in a peptide-pulsed setting.**

Engineered T cells expressing were co-cultured in an effector to target ratio 1:1. Media and triton X-100 (TRX) were added as controls. Panc-28 was pulsed with the VPSVWRSS peptide and the TCRs R21, R23, R25, R26 show a cytotoxic effect. In the unpulsed setting, no killing effect was observed. Cell index was normalized to the point of treatment addition.

As a control, the same conditions were applied in the Panc28 cell line without pulsing. In this case, there was no killing effect, thus suggesting that TCR R21, R23, R24 and R26 recognized the target peptide in a specific manner. However, additional tests need to be done in cells with endogenously expressed peptide to further characterize the TCRs.

## 4. Discussion

Among all cancer types, pancreatic cancer has the lowest 5-year survival rates. In recent years, the survival rate for this malignancy has increased from 8% to 11%, demonstrating a slight but insufficient improvement [1]. Low patient survival is attributed to several factors, including the absence of biomarkers for early detection, late diagnosis due to the late onset of illness symptoms, and lack of new therapeutical options. Therefore, efforts in basic research to unravel the essential molecules contributing to disease onset, progression, and therapy success are essential and have great potential for translational application.

RNF43 is an E3 ubiquitin ligase that was first identified as an oncoprotein upregulated in colon cancer [98]. Since then, research in the field has advanced rapidly, and *RNF43* has been found frequently mutated in various tumors, including gastric carcinomas, ovarian mucinous tumors, and endometrial carcinomas [97, 106, 108]. *RNF43* mutations in these cancers have been linked to tumor development, indicating a tumor suppressor function. Indeed, molecular studies proposed two mechanisms by which RNF43 acts as a tumor suppressor, depending on the cellular location of the protein. In the nucleus, RNF43 interacts with the T-cell factor 4 (TCF4), sequestering it to the nuclear membrane and inhibiting the transcription of Wnt target genes [95]. While in the cell membrane, RNF43 regulates Fz expression through ubiquitination, thus targeting the Wnt receptors for degradation [169]. However, more recent studies have found that RNF43 has a role in other signaling pathways. Thus, RNF43 knockdown in PC cell lines led to decreased activation of the DNA damage response (DDR) *in vitro* [170]. The link of RNF43 to the DDR was further demonstrated in the stomach. The depletion of RNF43 expression in gastric cancer cells conferred resistance to chemotherapy and gamma radiation by reducing the activation of the DDR through direct interaction between RNF43 and phosphorylated H2A histone family member X ( $\gamma$ H2AX) [107]. This new research indicates that there are still numerous unanswered questions regarding the precise molecular mechanisms by which RNF43 exerts its tumor suppressor function and its role in other signaling cascades.

As mentioned before, *RNF43* is frequently mutated in different tumor types of the GI tract, and previous studies indicated that 5-7% of pancreatic tumors carry mutated *RNF43* [99].

#### 4. Discussion

Here, we screened a panel of human PC cell lines for mutations. From all the lines assessed, 47% harbored mutations in the gene. Most of the mutations found were classified as frame-shift or nonsense mutations, resulting in a loss of protein function (LOF). To explore the effect of RNF43 LOF in pancreatic cells, its expression was lentivirally knocked down. This resulted in a higher proliferative capacity and survival rate of the RNF43 depleted cells, confirming the tumor suppressive nature of RNF43. These results align with previously published studies exploring the effects of RNF43 LOF. Thus, an increase in proliferation in RNF43 knockdown gastric and intestinal cells was observed [158] and in colorectal cancer cell lines after RNF43 silencing [171].

Previous research analyzing a panel of PDAC lines revealed that only cells with LOF mutations showed sensitivity to the porcupine inhibitor LGK974, linking RNF43 to the regulation of WNT signaling [172]. However, as mentioned before, other mechanisms could also explain the tumor suppressive nature of RNF43 in pancreatic cells and the contribution of LOF mutations to tumorigenesis. In a recent study in metastatic colorectal cancer, inactivating mutations in *RNF43* improved the responses to anti-BRAF/EGFR combinatory therapies in BRAF<sup>V600E</sup> tumors, indicating a crosstalk between the MAPK and WNT pathways. In another study in colorectal cancer, the *RNF43* mutation G659fs, which is the most frequent *RNF43* mutation [106], has been found to promote tumorigenic properties independently of Wnt signaling. Thus, the G659fs mutation was found to activate PI3K through the degradation of its regulatory subunit p85. Importantly, it was observed that PI3K/mTOR inhibitors had antitumor activity in patient-derived organoids as well as xenograft models carrying this mutation [173]. Together, *RNF43* mutations have good potential as a predictive biomarker for therapy selection cancer.

The knockdown effects of RNF43 in PC cells were also evaluated *in vivo*. Similarly to the results reported by Neumeyer et al in gastric cell lines, xenografts derived from shRNF43 tumors were significantly bigger, more differentiated, and cohesive, with infiltration of inflammatory cells at the margin of the tumors. On the other hand, shCtrl derived tumors showed a more undifferentiated growth, with high infiltration of polymorphonuclear (PMN) cells. This correlates with previous findings in pancreatic tumors, in which high PMN density is related to an overall poorly differentiated growth pattern [174]. However, the role of infiltrating PMN

#### 4. Discussion

cells in pancreatic tumors is controversial. Several studies have unraveled that the presence of these immune cells in pancreatic xenografts could be a sign of bad prognosis since certain subsets of chronically activated PMN cells can promote tumorigenesis [30]. However, other groups indicated that the presence of tumor-infiltrating neutrophils is associated with better prognosis in gastric cancer [175]. For pancreatic tumors derived from shRNF43 cells, low immune cell infiltration appears to correlate with a poorer prognosis, whereas the presence of PMN cells in shCtrl tumors correlated with less tumor progression, probably due to a more activated immune response. This could have a potential effect on immunotherapy approaches; however, the mechanisms of how RNF43 LOF could influence the recruitment of immune cells need to be further explored.

Knockdown of RNF43 *in vitro* was related to a more invasive capacity of pancreatic tumor cells. One possible explanation for this observation could be the activation of EMT in these cells. During tumor progression, EMT is significantly dysregulated; as a result, tumor epithelial cells lose cell-cell adhesion and polarity and acquire invasive and migratory capabilities, allowing solid tumors to become more malignant [176, 177]. Recent research in lung cancer has attributed RNF43 an important role in EMT. RNF43 was found to interact and degrade E-cadherin, a tumor suppressor protein with a role in epithelial cell-to-cell adhesion, thus regulating EMT [163]. In several cancer entities, including breast cancer, colorectal cancer, and oral squamous cell carcinomas, loss of E-cadherin expression is a hallmark of cancer progression and correlates with a worse prognosis [178-180]. *In vivo*, RNF43 knockdown increased E-cadherin expression, showing that EMT may not be involved in the differences in tumor pattern and growth observed between shCtrl and shRNF43 tumors. However, additional research is required to corroborate this finding.

To further investigate the effects of *RNF43* mutations in the pancreas, the mouse models RNF43<sup>H292R/H295R</sup>, bearing two point mutations in the RING domain of the gene and *Rnf43*<sup>ΔExon8</sup>, with a 57 base pair deletion leading to inactivation of *Rnf43*, were analyzed. The proliferative capabilities of organoids derived from *Rnf43* mutant mice were found to be higher than those of wt mice, thus corroborating previous findings in organoids derived from other organs. However, when the pancreas of *Rnf43* mutant animals was analyzed at different time points, it retained typical pancreatic characteristics, including low proliferation, scarce immune cell

#### 4. Discussion

infiltration, and normal fibrosis levels, indicating that *Rnf43* mutations alone do not induce changes in the pancreas under basal conditions. In contrast, prior research in other organs of these mouse models has revealed gastric mucosa thickening, hyperproliferation, and hyperplasia in the stomach [158], suggesting that *RNF43* mutations may have different effects and signaling pathway sensitivities in different organs. In the pancreas, *Rnf43* mutations play an important role in the progression of tumors from precursor lesions. Indeed, Wu et al reported that *RNF43* is frequently mutated in pancreatic precursor lesions, as inactivating mutations in the protein were found in around 20% of IPMNs and 50% of MCNs [99].

Another aspect to consider is that chronic inflammation significantly impacts most cancers of the GI tract, including PC. Continuous inflammation results in the persistent recruitment of inflammatory cells and the development of further damage [181]. Furthermore, inflammation promotes continuous proliferation, causing the accumulation of mutations, thereby driving tumorigenesis [182]. In addition, inflammation can alter the expression pattern of tumor suppressors or oncogenes. In this regard, *Rnf43* mutant mice infected with *Helicobacter pylori* exhibited worsened gastric pathology, with increased levels of nuclear  $\beta$ -catenin and phosphorylated STAT3 in the gastric mucosa [183]. Thus, the activation of these distinct signaling pathways appears to exacerbate pathology in the stomach, pointing to an important role for *RNF43* during chronic inflammation. In the pancreas, chronic inflammation causes fibrosis and atrophy of the organ and increases the risk for PC. To determine whether *RNF43* mutations in combination with chronic pancreatitis could influence the onset of pancreatic tumors the cerulein model was employed.

Cerulein is a cholecystokinin (CCK) analog that binds to the G-protein-coupled CCK receptor. This initiates the release of calcium from the endoplasmic reticulum into pancreatic acinar cells through the activation of phospholipase C and the induction of inositol 1,4,5-trisphosphate (IP3). Calcium then activates NADPH oxidase, leading to the production of reactive oxygen species (ROS). ROS induces I $\kappa$ B kinase that phosphorylates I $\kappa$ B in the cytosol and targets it for ubiquitination and proteasomal degradation. I $\kappa$ B is an inhibitory subunit bound to NF- $\kappa$ B. Consequently, NF- $\kappa$ B is released and translocated to the nucleus, inducing inflammatory cytokine expression in pancreatic acinar cells. Moreover, ROS can also disturb the cytoskeleton integrity and induce mitochondrial dysfunction in the cells [184, 185]. The

#### 4. Discussion

cerulein model is widely used since it presents some advantages. For instance, it is highly reproducible and does not require invasive procedures on rodents. Moreover, it mimics well some of the characteristics of pancreatitis observed in humans by progressive loss of the exocrine and endocrine compartments, resulting in atrophy or fibrotic tissue replacement [10, 30].

After successfully establishing the cerulein model, it was observed that the pancreata of cerulein-treated mice differed in color and consistency from that of PBS-treated mice. Cerulein treatment led to alterations in acinar structure, with an increase in collagen deposits, increased proliferation, and subtle immune infiltration. These findings are consistent with previous studies using the cerulein model, in which they observed atrophy of the pancreas, enlargement of the intra-acinar lumen, and increase in immune infiltrates, predominantly macrophages [186]. Notably, *Rnf43* mutant mice presented a more severe pancreatic pathology. *RNF43*<sup>H292R/H295R</sup> mice presented islet hyperplasia and an increase in vacuolization. This was exacerbated in the *Rnf43*<sup>ΔExon8</sup> model, exhibiting more severe pancreatitis, with completely disrupted acini, more ADM progression, an increase in fibrosis and proliferation. ADM is a process in which acinar cells differentiate into ductal-like progenitor cells and is classified as one of the earliest precursor lesions to PC development [187]. ADM progression is found to be influenced by oncogenic insults and/or environmental stress [55, 164]. Although ADM was observed in *Rnf43* mutant mice, progression to preneoplastic lesions as PanINs or cancer was not detected, even after long time treatment experiments. The cerulein model is commonly used to study acute pancreatitis; however, inflammation disappeared immediately after cessation of cerulein injections, and the pancreas of treated mice returned to normal, indicating that this model may not be ideal for the long-term induction of chronic pancreatitis. Nevertheless, previous mouse studies showed that Kras-driven carcinogenesis was accelerated when RNF43 was deleted by iCRISPR [111]. A similar result was observed in a *Kras*<sup>G12D/+</sup> *Rnf43*<sup>-/-</sup>, where RNF43 knock-out contributed to preneoplasia initiation [112]. These findings further suggest that mutations in *RNF43* alone cannot initiate PC; however, these mutations contribute to worsening of pathophysiology and malignant transformation.

#### 4. Discussion

As stated before, a key contributor to the bad prognosis of PC is the lack of good therapeutic options. The field of PC treatment has remained essentially unchanged over the past decade, clearly stating that there is a need for better and more targeted therapies for patients. Adoptive T cell transfer is a promising strategy that, despite being at its early stages, has already produced several FDA-approved clinical applications. Adoptive transfer of engineered T cells has overcome some of the CAR T cells flaws, such as the recognition of intracellular processed antigens; however, they are restricted by the MHC molecules. Until now, adoptive T cell transfer has shown good outcomes in hematological malignancies, but low clinical efficacy in solid tumors. PC exhibits a tumor microenvironment with high fibrosis, hypoxia, and immunosuppressive features; therefore, it is classified as an immunological cold tumor [188]. Research in the field has indicated that single-agent immunotherapies will not likely exhibit activity in PDAC, but combinatory treatments are needed [189]. An example of this, is the PRINCE phase II clinical trial, that combines nivolumab, a PD-1 checkpoint inhibitor, with sotigalimab, a CD40 agonistic antibody and classic chemotherapy drugs gemcitabine/nab-paclitaxel [190].

A critical factor for the success of ACT is the identification of high-quality targets that are safe and tumor specific. Previous studies in the field targeting TAA, such as MART-1 (Melan-A), the glycoprotein 100 (gp100), or colorectal cancer-associated carcinoembryonic antigen (CEA), revealed that these antigens were also expressed in normal tissues, causing “off-tumor, on-target’ toxicities [191-194]. Therefore, research in the field has moved to target neo-antigens, since they arise from somatic tumor mutations, and therefore their expression is tumor specific. For this reason, targeting neo-antigens can be more effective and lead to less toxicity risk than targeting TAAs [145]. However, most neo-antigens derive from unique somatic mutations, making these approaches highly patient-specific. To overcome this limitation, the use of neo-epitopes derived from frame-shift mutations represents an attractive alternative since multiple mutations can give rise to the same neo-ORF. Thus, these neo-antigens can be shared between patients. This strategy was employed in this project, where neo-epitopes derived from *RNF43* frame-shift mutations were used as targets in ACT. In recent studies, this approach has been implemented for several neo-antigen preclinical vaccine studies on mammary cancer and lynch syndrome in mouse model studies [150, 195, 196], indicating

#### 4. Discussion

that targeting neoantigens derived from frame-shift mutations have the potential to become “off-the-shelf” targeted therapy products.

Mutations in *RNF43* have been previously used in immunotherapy. Thus, attempts with RNF43 peptides in vaccine studies have shown that 50% of HLA-matched patients showed a positive CTL response in metastatic colorectal cancer [197]. In a related study, patients receiving vaccination showed higher plasma levels of RNF43 IgG, and increased CTL response; however, this did not correlate with better overall survival [198]. Altogether, efforts to target RNF43 demonstrated an increase in immunogenic response, making it a promising immunotherapy target.

To evaluate the potential use of *RNF43* frame-shift mutations in ACT, candidate neo-peptides were *in silico* predicted, and the peptides *SLLPTCWAL* (HLA-A\*02:01 restricted) and *VPSVWRSSL* (HLA-B\*07:02 restricted) were used in this study. Potential TCRs targeting the candidate peptides were isolated from the naïve repertoire of healthy donors. This represents certain advantages since the naïve repertoire is a vast source of TCR diversity that is easily accessible by apheresis. Moreover, T cells undergo positive and negative selection in the thymus prior to entering peripheral circulation. Therefore, using the naïve repertoire as a source of T cells represents a low risk of self-reactivity [199].

The naïve repertoire is composed of a vast range of TCR potencies. Thus, the functional avidity and cytotoxicity of engineered T-cells need to be assessed to evaluate their potential before performing preclinical assays. Several potential TCR ligands exhibited cytotoxic activity under peptide-pulsed conditions, whereas expression of the endogenous mutation was insufficient for T cell activation. There are many mechanisms that could explain these observations. One of them may involve the low potency of the T cells. Indeed, when the activation of engineered TCR 11 T cells was compared to other highly functional TCRs targeting SARSCoV2 peptides, cells showed activation at approximately two logarithmic orders magnitude lower than the functional T cells in response to peptide stimulation, indicating that the potency of the TCR R11 was low and possibly insufficient to elicit a cytotoxic response.

#### 4. Discussion

Another possible explanation could be weak peptide loading on the surface of mutated tumor cells. Here, peptide processing and MHC loading were only predicted *in silico*. To overcome this issue, further work needs to be done to characterize the cellular models, including immunopeptidome analysis by mass spectrometry to confirm the MHC-antigen association and to quantify the antigen density presented on the cell surface.

Induction of inhibitory signals by cancer cell lines is another possible reason for the low T cell activation observed. It is known that tumor cells evolve mechanisms to limit antigen processing and presentation to avoid T cell recognition [194]. One of these mechanisms is the PD-1/PDL-1 pathway that has a huge role in immune escape in cancer. Association between aberrant Wnt expression and PDL-1 has been investigated in mouse models for melanoma and breast cancer, where selective use of WNT inhibitors or activators were found to influence PDL-1, suggesting a functional crosstalk between the pathways [200-202]. Here, cells with mutations in *RNF43* expressed higher levels of PDL-1, suggesting that the use of checkpoint inhibitors in the project may improve the cytotoxic responses of the engineered T cells.

In summary, mutations in *RNF43* are associated with the proliferation and tumor development in PC. However, *RNF43* mutations alone do not lead to tumor development, even under inflammatory conditions. These mutations are potentially promising targets for the development of immunotherapy in combination with other treatments for PC patients.

## 5. Registers

### 5.1 List of abbreviations

ACT	Adoptive T cell therapy
ADM	Acinar to ductal metaplasia
APC	Adenomatous polyposis coli
APS	Ammonium persulfate
CAR	CD19-directed chimeric antigen receptor
Cas9	CRISPR associated protein 9
CCK	Cholecystokinin
CCK-8	Cell counting kit-8
CD3	Cluster of differentiation 3
CD40	Cluster of differentiation 40
CD8	Cluster of differentiation 8
CDKN2A	Cyclin-dependent kinase inhibitor 2A
cDNA	Complementary DNA
CEA	Carcinoembryonic antigen
CFTR	Cystic fibrosis transmembrane conductance regulator
CK19	Cytokeratin-19
CK19	Casein kinase 1
CO <sub>2</sub>	Carbon dioxide
CP	Chronic pancreatitis
CRD	cysteine-rich domain
CRISPR	Clustered Regularly Interspaced Short Palindromic Repeats
CT scan	Computed tomographic scan
CTL	Cytotoxic T lymphocyte
CTLA-4	Cytotoxic T-lymphocyte-associated protein 4
CTRC	Concerted actions of chymotrypsin C
DAMPS	Damage-associated molecular patterns
DAPI	4',6-diamidino-2-phenylindole
DDR	DNA damage response
dH <sub>2</sub> O	Distilled water
DMEM	Dulbecco's modified Eagle's medium
DMSO	Dimethyl sulfoxide
DN	Dominant-negative
dNTP	Deoxyribonucleotide triphosphates
Dvl	Dishevelled
E:T	Effector to target
EC <sub>50</sub>	Half maximal effective concentration
ECOG	Eastern Cooperative Oncology Group
EDTA	Ethylenediamine tetraacetic acid
EGF	Epidermal growth factor

## 5. Registers

EGFR	Epidermal growth factor receptor
ERCP	Endoscopic retrograde cholangiopancreatography
FACS	Fluorescence-activated cell sorting
FBS	Fetal bovine serum
FDA	Food and drug administration
fs	Frame-shift
Fzd	Frizzled receptor
GFP	Green fluorescent protein
GNAS	Guanine Nucleotide binding protein, Alpha Stimulating activity polypeptide
gp100	Glycoprotein 100
GSK3	Glycogen synthase kinase 3
Gy	Gray
H&E	Hematoxylin and eosin
HLA	Human leukocyte antigen
IBA1	Ionized calcium binding adaptor molecule 1
iCRISPR	Inducible CRISPR/Cas9
IF	Immunofluorescence
IF	Immunofluorescence
IFN- $\gamma$	Interferon gamma
IgG	Immunoglobulin G
IHC	Immunohistochemistry
IMDM	Iscove's Modified Dulbecco's Medium
IP3	Inositol 1,4,5-trisphosphate
IPMN	Intraductal papillary mucinous neoplasm
I $\kappa$ B	IkappaB
KRAS	Kirsten Rat Sarcoma
Lgr	Leucin-rich repeat containing G-protein-coupled
LOF	Loss of function
LRP5/6	LDL-receptor-related protein receptors 5/6
M	Molar
MAPK	mitogen-activated protein kinase
MAPK	Mitogen-activated protein kinase
MART-1	Melanoma antigen recognized by T cells 1
MCN	Mucinous cystic neoplasm
MHC	Major histocompatibility complex
MMP-7	Member of the matrix metalloproteinase 7
MRI	Magnetic resonance imaging
mRNA	Messenger ribonucleic acid
MSI	Microsatellite-instable tumors
mTOR	Mammalian target of rapamycin
MTT	3-(4,5-dimethylthiazol-2-yl)-2,5- diphenyltetrazolium bromide
n.d	Not determined

## 5. Registers

NADPH	Nicotinamide adenine dinucleotide phosphate
neo-ORF	New open reading frames
NF- $\kappa$ B	Nuclear factor kappa-light-chain-enhancer of activated B cells
NFAT	Nuclear factor of activated T-cells
OS	Overall survival
PA	Protease-associated
PanIN	Pancreatic intraepithelial neoplasia
PBS	Phosphate Buffer Saline
PC	Pancreatic cancer
PCP	Planar cell polarity
PD-L1	Programmed cell death ligand 1
PD1	Programmed cell death 1
PDAC	Pancreatic ductal adenocarcinoma
PFA	Paraformaldehyde
PI3K	Phosphoinositide 3-kinases
PMN	Polymorphonuclear
PP cells	Pancreatic polypeptide cells
PRSS1	Serine protease 1
Ptf1a	Pancreas transcription factor 1 subunit alpha
RNF43	RING finger protein
ROS	Reactive oxygen species
rpm	Revolutions per minute
RPMI	Roswell Park Memorial Institute medium
RSPO	R-spondins
RT-qPCR	Quantitative Realtime PCR
SARS-CoV-2	Severe acute respiratory syndrome coronavirus 2
SDS-PAGE	Sodium dodecyl sulfate–polyacrylamide gel electrophoresis
shRNA	Short hairpin RNA
SMAD4	SMAD family member 4
SPINK1	Serine protease inhibitor Kazal type 1
TAA	Tumor-associated antigens
TBS	Tris buffered saline
TCF/LEF	T cell factor/lymphoid enhancer factor family
TCF4	T-cell factor 4
TCR	T- cell receptor
TEMED	Tetramethylethylenediamine
TGF- $\beta$	Transforming growth factor beta
TILs	Tumor-infiltrating lymphocytes
TME	Tumor microenvironment
TP53	Tumor protein P53
TRAC	T-cell receptor $\alpha$ constant
VEGF	Vascular endothelial growth factor
WRE	Wnt response elements

## 5. Registers

wt	Wild type
ZNRF3	E3 ubiquitin ligase Zinc and Ring finger 3
$\beta$ -Trcp	Beta-transducin repeat containing protein
$\gamma$ H2AX	phosphorylated H2A histone family member X

## 5. Registers

### 5.2 List of figures

<b>Figure 1. Anatomy of the pancreas.</b> .....	8
<b>Figure 2. Precursor lesions of PDAC and frequently mutated genes.</b> .....	12
<b>Figure 3. Wnt/ <math>\beta</math>-catenin signaling pathway.</b> .....	16
<b>Figure 4. Targeted therapies in Wnt signaling.</b> .....	18
<b>Figure 5. Current treatments for pancreatic cancer patients.</b> .....	21
<b>Figure 6. RNF43 presents a high number of frame-shift mutations in pancreatic cancer.</b> ..	23
<b>Figure 7. RNF43 expression in pancreatic cancer cell lines.</b> .....	47
<b>Figure 8. Knockdown of RNF43 increases the tumorigenic potential of pancreatic cancer cell lines.</b> .....	48
<b>Figure 9. RNF43 knockdown potentiates tumor growth in vivo.</b> .....	50
<b>Figure 10. Xenografts derived from shRNF43 cells present low immune cell infiltration.</b> ..	51
<b>Figure 11. Tumors derived from shRNF43 pancreatic cancer cells are highly proliferative.</b> 52	
<b>Figure 12. Pancreatic organoids derived from <i>Rnf43</i> mutant mice increase proliferation in vitro.</b> .....	54
<b>Figure 13. <i>Rnf43</i> mutant mice display a normal pancreatic tissue architecture under basal conditions.</b> .....	56
<b>Figure 14. Cerulein-treated mice present morphological changes in the pancreas.</b> .....	57
<b>Figure 15. <i>Rnf43</i> mutant mice exhibit more severe cerulein-induced pancreatitis than the wt.</b> .....	59
<b>Figure 16. Long term pancreatitis in <i>Rnf43</i> mutant mice does not progress to PanIN lesions.</b> .....	62
<b>Figure 17. Graphical representation of the isolation of RNF43 neo-epitope specific TCRs from the naïve repertoire of a healthy donor.</b> .....	65
<b>Figure 18. VPSVWRSSL and SLLPTCWAL specific TCR repertoires contain functional TCRs.</b> 66	
<b>Figure 19. MZ1 and Capan2 cells carry mutations in RNF43 leading to the SLLPTCWAL peptide.</b> .....	68
<b>Figure 20. TCR R11 shows recognition in a peptide-pulsed setting.</b> .....	69
<b>Figure 21. TCRs targeting the SLLPTCWAL peptide show no cytotoxicity effect in cell lines expressing endogenous RNF43 fs-mutations.</b> .....	70
<b>Figure 22. RNF43 TCRs are activated at higher peptide concentrations than SarsCov-2 TCRs.</b> .....	71
<b>Figure 23. Cells with endogenous RNF43 fs-mutations show high expression of PDL-1.</b> ....	72
<b>Figure 24. TCRs targeting the VPSVWRSSL peptide show activation and killing effect in a peptide-pulsed setting.</b> .....	73

## 5. Registers

### 5.3 List of tables

<b>Table 1. Components for pancreatic organoid cell culture media. ....</b>	<b>37</b>
<b>Table 2. Cycling conditions for RT-qPCR.....</b>	<b>38</b>
<b>Table 3. SDS polyacrylamide gel preparation .....</b>	<b>42</b>
<b>Table 4. Characterization of pancreatic cancer cell lines.....</b>	<b>45</b>
<b>Table 5. Sequence variations of frequently mutated genes in pancreatic cancer cell lines.</b>	<b>46</b>
<b>Table 6. RNF43 candidate peptides for T cell therapy .....</b>	<b>64</b>
<b>Table 7. HLA-typing of pancreatic cancer cell lines. ....</b>	<b>67</b>

## 6. References

1. Siegel, R.L., et al., *Cancer statistics, 2022*. CA: A Cancer Journal for Clinicians, 2022. **72**(1): p. 7-33.
2. Bockman, D.E., *Anatomy of the Pancreas. Chapter 1*, in *The Pancreas: Biology, Pathobiology, and Disease (2nd Ed)*, V.L.W. Go and et al., Editors. 1993, Raven Press Ltd: New York. p. 1-8.
3. Yuan, Q., et al., *Anatomy and physiology of the pancreas*. Integrative Pancreatic Intervention Therapy, 2021: p. 3-21.
4. Longnecker, D.S., *Anatomy and Histology of the Pancreas*. Pancreapedia: The Exocrine Pancreas Knowledge Base, 2021.
5. Leung, P.S., *Overview of the pancreas*. Advances in Experimental Medicine and Biology, 2010. **690**: p. 3-12.
6. Rahier, J., et al., *The pancreatic polypeptide cells in the human pancreas: the effects of age and diabetes*. The Journal of clinical endocrinology and metabolism, 1983. **56**(3): p. 441-444.
7. Ishiguro, H., et al., *Physiology and pathophysiology of bicarbonate secretion by pancreatic duct epithelium*. Nagoya Journal of Medical Science, 2012. **74**(1-2): p. 1-1.
8. Frossard, J.L., M.L. Steer, and C.M. Pastor, *Acute pancreatitis*. Lancet (London, England), 2008. **371**(9607): p. 143-152.
9. Yadav, D. and A.B. Lowenfels, *The Epidemiology of Pancreatitis and Pancreatic Cancer*. Gastroenterology, 2013. **144**(6): p. 1252-1252.
10. Kleeff, J., et al., *Chronic pancreatitis*. Nature reviews. Disease primers, 2017. **3**.
11. Andersen, P.L., et al., *Quantification of parenchymal calcifications in chronic pancreatitis: relation to atrophy, ductal changes, fibrosis and clinical parameters*. Scandinavian journal of gastroenterology, 2018. **53**(2): p. 218-224.
12. Ouyang, G., et al., *The global, regional, and national burden of pancreatitis in 195 countries and territories, 1990–2017: a systematic analysis for the Global Burden of Disease Study 2017*. BMC Medicine, 2020. **18**(1): p. 1-13.
13. Hegyi, E. and M. Sahin-Tóth, *Genetic Risk in Chronic Pancreatitis: The Trypsin-Dependent Pathway*. Digestive Diseases and Sciences, 2017. **62**(7): p. 1692-1701.
14. Rakonczay, Z., et al., *The role of NF-kappaB activation in the pathogenesis of acute pancreatitis*. Gut, 2008. **57**(2): p. 259-267.
15. Singh, V.K., D. Yadav, and P.K. Garg, *Diagnosis and Management of Chronic Pancreatitis: A Review*. JAMA, 2019. **322**(24): p. 2422-2434.
16. Apte, M.V., R.C. Pirola, and J.S. Wilson, *Pancreatic stellate cells: a starring role in normal and diseased pancreas*. Frontiers in physiology, 2012. **3**.
17. Ammann, R.W., et al., *Progression of alcoholic acute to chronic pancreatitis*. Gut, 1994. **35**(4): p. 552-556.
18. Sidhu, S.S. and R.K. Tandon, *The pathogenesis of chronic pancreatitis*. Postgraduate medical journal, 1995. **71**(832): p. 67-70.
19. Bhanot, U.K. and P. Möller, *Mechanisms of parenchymal injury and signaling pathways in ectatic ducts of chronic pancreatitis: implications for pancreatic carcinogenesis*. Laboratory Investigation 2009 89:5, 2009. **89**(5): p. 489-497.
20. Overbeek, K.A., et al., *Surveillance for neoplasia in the pancreas*. Best practice & research. Clinical gastroenterology, 2016. **30**(6): p. 971-971.

## 6. References

21. Kichler, A. and S. Jang, *Chronic Pancreatitis: Epidemiology, Diagnosis, and Management Updates*. *Drugs* 2020 80:12, 2020. **80**(12): p. 1155-1168.
22. Löhr, J.M., et al., *United European Gastroenterology evidence-based guidelines for the diagnosis and therapy of chronic pancreatitis (HaPanEU)*. *United European gastroenterology journal*, 2017. **5**(2): p. 153-199.
23. Wilcox, C.M., et al., *Chronic pancreatitis pain pattern and severity are independent of abdominal imaging findings*. *Clinical Gastroenterology and Hepatology*, 2015. **13**(3): p. 552-560.
24. Martínez-Moneo, E., et al., *Deficiency of fat-soluble vitamins in chronic pancreatitis: A systematic review and meta-analysis*. *Pancreatology : official journal of the International Association of Pancreatology (IAP) ... [et al.]*, 2016. **16**(6): p. 988-994.
25. Sikkens, E.C.M., et al., *The prevalence of fat-soluble vitamin deficiencies and a decreased bone mass in patients with chronic pancreatitis*. *Pancreatology*, 2013. **13**(3): p. 238-242.
26. Li, B.R., et al., *Risk Factors for Steatorrhea in Chronic Pancreatitis: A Cohort of 2,153 Patients*. *Scientific Reports*, 2016. **6**.
27. Ewald, N. and P.D. Hardt, *Diagnosis and treatment of diabetes mellitus in chronic pancreatitis*. *World Journal of Gastroenterology : WJG*, 2013. **19**(42): p. 7276-7276.
28. Lerch, M.M. and F.S. Gorelick, *Models of acute and chronic pancreatitis*. *Gastroenterology*, 2013. **144**(6): p. 1180-1193.
29. Lampel, M. and H.F. Kern, *Acute interstitial pancreatitis in the rat induced by excessive doses of a pancreatic secretagogue*. *Virchows Archiv. A, Pathological anatomy and histology*, 1977. **373**(2): p. 97-117.
30. Aghdassi, A.A., et al., *Animal models for investigating chronic pancreatitis*. *Fibrogenesis & Tissue Repair*, 2011. **4**(1): p. 26-26.
31. Klaus, S., et al., *Genetically induced vs. classical animal models of chronic pancreatitis: A critical comparison*. *FASEB Journal*, 2018. **32**(11): p. 5778-5792.
32. *Global Cancer Observatory*. 2022; Available from: <https://gco.iarc.fr/>.
33. Rahib, L., et al., *Projecting cancer incidence and deaths to 2030: The unexpected burden of thyroid, liver, and pancreas cancers in the united states*. *Cancer Research*, 2014. **74**(11): p. 2913-2921.
34. Taherian, M., H. Wang, and H. Wang, *Pancreatic Ductal Adenocarcinoma: Molecular Pathology and Predictive Biomarkers*. *Cells*, 2022. **11**(19): p. 3068-3068.
35. Principe, D.R., et al., *The Current Treatment Paradigm for Pancreatic Ductal Adenocarcinoma and Barriers to Therapeutic Efficacy*. *Frontiers in Oncology*, 2021. **11**: p. 2773-2773.
36. Iodice, S., et al., *Tobacco and the risk of pancreatic cancer: a review and meta-analysis*. *Langenbeck's archives of surgery*, 2008. **393**(4): p. 535-545.
37. Arslan, A.A., et al., *Anthropometric measures, body mass index, and pancreatic cancer: a pooled analysis from the Pancreatic Cancer Cohort Consortium (PanScan)*. *Archives of internal medicine*, 2010. **170**(9): p. 791-802.
38. Huxley, R., et al., *Type-II diabetes and pancreatic cancer: a meta-analysis of 36 studies*. *British Journal of Cancer* 2005 92:11, 2005. **92**(11): p. 2076-2083.
39. Klein, A.P., et al., *Prospective risk of pancreatic cancer in familial pancreatic cancer kindreds*. *Cancer research*, 2004. **64**(7): p. 2634-2638.

## 6. References

40. Raimondi, S., et al., *Pancreatic cancer in chronic pancreatitis; aetiology, incidence, and early detection*. Best practice & research. Clinical gastroenterology, 2010. **24**(3): p. 349-358.
41. Mostafa, M.E., et al., *Pathologic classification of "pancreatic cancers": current concepts and challenges*. Chinese Clinical Oncology, 2018. **6**(6): p. 59-59.
42. Klöppel, G. and J. Lüttges, *WHO-classification 2000: exocrine pancreatic tumors*. Verhandlungen der Deutschen Gesellschaft für Pathologie, 2001. **85**: p. 219-228.
43. *Pathology Outlines - WHO classification*.
44. Grimont, A., S.D. Leach, and R. Chandwani, *Uncertain Beginnings: Acinar and Ductal Cell Plasticity in the Development of Pancreatic Cancer*. Cellular and molecular gastroenterology and hepatology, 2022. **13**(2): p. 369-382.
45. Bannoura, S.F., et al., *Targeting KRAS in pancreatic cancer: new drugs on the horizon*. Cancer metastasis reviews, 2021. **40**(3): p. 819-835.
46. Nagtegaal, I.D., et al., *The 2019 WHO classification of tumours of the digestive system*. Histopathology, 2020. **76**(2): p. 182-188.
47. Crippa, S., et al., *Mucin-producing neoplasms of the pancreas: an analysis of distinguishing clinical and epidemiologic characteristics*. Clinical gastroenterology and hepatology : the official clinical practice journal of the American Gastroenterological Association, 2010. **8**(2).
48. Thorel, F., et al., *Conversion of adult pancreatic alpha-cells to beta-cells after extreme beta-cell loss*. Nature, 2010. **464**(7292): p. 1149-1154.
49. Chera, S., et al., *Diabetes recovery by age-dependent conversion of pancreatic  $\delta$ -cells into insulin producers*. Nature, 2014. **514**(7523): p. 503-507.
50. Xu, X., et al., *Beta cells can be generated from endogenous progenitors in injured adult mouse pancreas*. Cell, 2008. **132**(2): p. 197-207.
51. Criscimanna, A., et al., *Duct cells contribute to regeneration of endocrine and acinar cells following pancreatic damage in adult mice*. Gastroenterology, 2011. **141**(4).
52. Pinho, A.V., et al., *Adult pancreatic acinar cells dedifferentiate to an embryonic progenitor phenotype with concomitant activation of a senescence programme that is present in chronic pancreatitis*. Gut, 2011. **60**(7): p. 958-966.
53. Stanger, B.Z. and M. Hebrok, *Control of Cell Identity in Pancreas Development and Regeneration*. Gastroenterology, 2013. **144**(6): p. 1170-1170.
54. Storz, P., *Acinar cell plasticity and development of pancreatic ductal adenocarcinoma*. Nature reviews. Gastroenterology & hepatology, 2017. **14**(5): p. 296-304.
55. Wang, L., D. Xie, and D. Wei, *Pancreatic acinar-to-ductal metaplasia and pancreatic cancer*. Methods in Molecular Biology, 2019. **1882**: p. 299-308.
56. Zhu, L., et al., *Acinar cells contribute to the molecular heterogeneity of pancreatic intraepithelial neoplasia*. The American journal of pathology, 2007. **171**(1): p. 263-273.
57. Shi, G., et al., *Maintenance of acinar cell organization is critical to preventing Kras-induced acinar-ductal metaplasia*. Oncogene, 2013. **32**(15): p. 1950-1958.
58. Kanda, M., et al., *Presence of Somatic Mutations in Most Early-Stage Pancreatic Intraepithelial Neoplasia*. Gastroenterology, 2012. **142**(4): p. 730-730.
59. Logsdon, C.D. and B. Ji, *Ras activity in acinar cells links chronic pancreatitis and pancreatic cancer*. Clinical gastroenterology and hepatology : the official clinical practice journal of the American Gastroenterological Association, 2009. **7**(11 Suppl).

## 6. References

60. Collins, M.A., et al., *Oncogenic Kras is required for both the initiation and maintenance of pancreatic cancer in mice*. The Journal of clinical investigation, 2012. **122**(2): p. 639-653.
61. Liou, G.Y., et al., *Mutant KRas-Induced Mitochondrial Oxidative Stress in Acinar Cells Upregulates EGFR Signaling to Drive Formation of Pancreatic Precancerous Lesions*. Cell reports, 2016. **14**(10): p. 2325-2336.
62. Liou, G.Y., et al., *Macrophage-secreted cytokines drive pancreatic acinar-to-ductal metaplasia through NF- $\kappa$ B and MMPs*. The Journal of cell biology, 2013. **202**(3): p. 563-577.
63. Hezel, A.F., et al., *Pancreatic LKB1 deletion leads to acinar polarity defects and cystic neoplasms*. Molecular and cellular biology, 2008. **28**(7): p. 2414-2425.
64. Polireddy, K. and Q. Chen, *Cancer of the Pancreas: Molecular Pathways and Current Advancement in Treatment*. Journal of Cancer, 2016. **7**(11): p. 1497-1497.
65. Jones, S., et al., *Core signaling pathways in human pancreatic cancers revealed by global genomic analyses*. Science, 2008. **321**(5897): p. 1801-1806.
66. Ram Makena, M., et al., *Wnt/ $\beta$ -Catenin Signaling: The Culprit in Pancreatic Carcinogenesis and Therapeutic Resistance*. International journal of molecular sciences, 2019. **20**(17): p. 4242-4242.
67. Reya, T. and H. Clevers, *Wnt signalling in stem cells and cancer*. Nature 2005 434:7035, 2005. **434**(7035): p. 843-850.
68. Rios-Esteves, J. and M.D. Resh, *Stearoyl CoA desaturase is required to produce active, lipid-modified Wnt proteins*. Cell reports, 2013. **4**(6): p. 1072-1081.
69. Gómez-Orte, E., et al., *Multiple functions of the noncanonical Wnt pathway*. Trends in genetics : TIG, 2013. **29**(9): p. 545-553.
70. Nusse, R. and H. Clevers, *Wnt/ $\beta$ -Catenin Signaling, Disease, and Emerging Therapeutic Modalities*. Cell, 2017. **169**(6): p. 985-999.
71. Rubinfeld, B., et al., *Association of the APC gene product with beta-catenin*. Science (New York, N.Y.), 1993. **262**(5140): p. 1731-1734.
72. Su, L.K., B. Vogelstein, and K.W. Kinzler, *Association of the APC tumor suppressor protein with catenins*. Science (New York, N.Y.), 1993. **262**(5140): p. 1734-1737.
73. Thompson, J.J. and C.S. Williams, *Protein Phosphatase 2A in the Regulation of Wnt Signaling, Stem Cells, and Cancer*. Genes 2018, Vol. 9, Page 121, 2018. **9**(3): p. 121-121.
74. Aberle, H., et al., *beta-catenin is a target for the ubiquitin-proteasome pathway*. The EMBO journal, 1997. **16**(13): p. 3797-3804.
75. MacDonald, B.T., K. Tamai, and X. He, *Wnt/beta-catenin signaling: components, mechanisms, and diseases*. Developmental cell, 2009. **17**(1): p. 9-26.
76. Bhanot, P., et al., *A new member of the frizzled family from Drosophila functions as a Wingless receptor*. Nature, 1996. **382**(6588): p. 225-231.
77. Tamai, K., et al., *LDL-receptor-related proteins in Wnt signal transduction*. Nature, 2000. **407**(6803): p. 530-535.
78. Pinson, K.I., et al., *An LDL-receptor-related protein mediates Wnt signalling in mice*. Nature, 2000. **407**(6803): p. 535-538.
79. Davidson, G., et al., *Casein kinase 1 gamma couples Wnt receptor activation to cytoplasmic signal transduction*. Nature, 2005. **438**(7069): p. 867-872.

## 6. References

80. Wallingford, J.B. and R. Habas, *The developmental biology of Dishevelled: an enigmatic protein governing cell fate and cell polarity*. Development (Cambridge, England), 2005. **132**(20): p. 4421-4436.
81. Stamos, J.L. and W.I. Weis, *The  $\beta$ -catenin destruction complex*. Cold Spring Harbor perspectives in biology, 2013. **5**(1).
82. Zeng, X., et al., *A dual-kinase mechanism for Wnt co-receptor phosphorylation and activation*. Nature, 2005. **438**(7069): p. 873-877.
83. Clevers, H., *Wnt/ $\beta$ -Catenin Signaling in Development and Disease*. Cell, 2006. **127**(3): p. 469-480.
84. Cavallo, R.A., et al., *Drosophila Tcf and Groucho interact to repress Wingless signalling activity*. Nature, 1998. **395**(6702): p. 604-608.
85. Daniels, D.L. and W.I. Weis, *Beta-catenin directly displaces Groucho/TLE repressors from Tcf/Lef in Wnt-mediated transcription activation*. Nature structural & molecular biology, 2005. **12**(4): p. 364-371.
86. Orsulic, S., et al., *E-cadherin binding prevents beta-catenin nuclear localization and beta-catenin/LEF-1-mediated transactivation*. Journal of cell science, 1999. **112 ( Pt 8)**(8): p. 1237-1245.
87. Hoffmans, R., R. Stadeli, and K. Basler, *Pygopus and legless provide essential transcriptional coactivator functions to Armadillo/ $\beta$ -catenin*. Current Biology, 2005. **15**(13): p. 1207-1211.
88. Zhan, T., N. Rindtorff, and M. Boutros, *Wnt signaling in cancer*. Oncogene, 2017. **36**(11): p. 1461-1473.
89. Clevers, H. and R. Nusse, *Wnt/ $\beta$ -Catenin Signaling and Disease*. Cell, 2012. **149**(6): p. 1192-1205.
90. Carmon, K.S., et al., *R-spondins function as ligands of the orphan receptors LGR4 and LGR5 to regulate Wnt/beta-catenin signaling*. Proceedings of the National Academy of Sciences of the United States of America, 2011. **108**(28): p. 11452-11457.
91. de Lau, W., et al., *The R-spondin/Lgr5/Rnf43 module: regulator of Wnt signal strength*. Genes & Development, 2014. **28**(4): p. 305-305.
92. Zebisch, M. and E.Y. Jones, *ZNRF3/RNF43 – A direct linkage of extracellular recognition and E3 ligase activity to modulate cell surface signalling*. Progress in Biophysics and Molecular Biology, 2015. **118**(3): p. 112-118.
93. Tsukiyama, T., et al., *A phospho-switch controls RNF43-mediated degradation of Wnt receptors to suppress tumorigenesis*. Nature Communications 2020 11:1, 2020. **11**(1): p. 1-16.
94. Jin, Y.R. and J.K. Yoon, *The R-spondin family of proteins: emerging regulators of WNT signaling*. The international journal of biochemistry & cell biology, 2012. **44**(12): p. 2278-2278.
95. Loregger, A., et al., *The E3 ligase RNF43 inhibits Wnt signaling downstream of mutated  $\beta$ -catenin by sequestering TCF4 to the nuclear membrane*. Science Signaling, 2015. **8**(393).
96. Groden, J., et al., *Identification and characterization of the familial adenomatous polyposis coli gene*. Cell, 1991. **66**(3): p. 589-600.
97. Ryland, G.L., et al., *RNF43 is a tumour suppressor gene mutated in mucinous tumours of the ovary*. The Journal of pathology, 2013. **229**(3): p. 469-476.
98. Yagyu, R., et al., *A novel oncoprotein RNF43 functions in an autocrine manner in colorectal cancer*. International journal of oncology, 2004. **25**(5): p. 1343-1348.

## 6. References

99. Wu, J., et al., *Whole-exome sequencing of neoplastic cysts of the pancreas reveals recurrent mutations in components of ubiquitin-dependent pathways*. Proceedings of the National Academy of Sciences of the United States of America, 2011. **108**(52): p. 21188-21193.
100. Gao, Z.H., et al., *Differential  $\beta$ -catenin expression levels are associated with morphological features and prognosis of colorectal cancer*. Oncology Letters, 2014. **8**(5): p. 2069-2076.
101. Chien, A.J., et al., *Activated Wnt/ $\beta$ -catenin signaling in melanoma is associated with decreased proliferation in patient tumors and a murine melanoma model*. Proceedings of the National Academy of Sciences of the United States of America, 2009. **106**(4): p. 1193-1193.
102. Zhang, Y. and X. Wang, *Targeting the Wnt/ $\beta$ -catenin signaling pathway in cancer*. Journal of Hematology & Oncology, 2020. **13**(1): p. 165-165.
103. Takahashi, N., et al., *Identification of two Wnt-responsive elements in the intron of RING finger protein 43 (RNF43) gene*. PloS one, 2014. **9**(1).
104. Serra, S. and R. Chetty, *Rnf43*. Journal of clinical pathology, 2018. **71**(1): p. 1-6.
105. Tsukiyama, T., B.K. Koo, and S. Hatakeyama, *Post-translational Wnt receptor regulation: Is the fog slowly clearing?: The molecular mechanism of RNF43/ZNRF3 ubiquitin ligases is not yet fully elucidated and still controversial*. BioEssays, 2021. **43**(4).
106. Giannakis, M., et al., *RNF43 is frequently mutated in colorectal and endometrial cancers*. Nature genetics, 2014. **46**(12): p. 1264-1266.
107. Neumeyer, V., et al., *Loss of RNF43 Function Contributes to Gastric Carcinogenesis by Impairing DNA Damage Response*. Cellular and molecular gastroenterology and hepatology, 2021. **11**(4): p. 1071-1094.
108. Bass, A.J., et al., *Comprehensive molecular characterization of gastric adenocarcinoma*. Nature, 2014. **513**(7517): p. 202-209.
109. Yu, J., et al., *The Functional Landscape of Patient-Derived RNF43 Mutations Predicts Sensitivity to Wnt Inhibition*. Cancer research, 2020. **80**(24): p. 5619-5632.
110. Aguilera, K.Y. and D.W. Dawson, *WNT Ligand Dependencies in Pancreatic Cancer*. Frontiers in Cell and Developmental Biology, 2021. **9**: p. 1027-1027.
111. Mishra, A., et al., *Generation of focal mutations and large genomic deletions in the pancreas using inducible in vivo genome editing*. Carcinogenesis, 2020. **41**(3): p. 334-334.
112. Zhou, X., Sun, Z., Zhang, M., Qu, X., Yang, S., Wang, L., Jing, Y., Li, L., Deng, W., Liu, F., Di, J., Chen, J., Wu, J., & Zhang, H., *Deficient Rnf43 potentiates hyperactive Kras-mediated pancreatic preneoplasia initiation and malignant transformation*. Animal models and experimental medicine, 2022. **5**(1): p. 61–71.
113. Witkowski, E.R., J.K. Smith, and J.F. Tseng, *Outcomes following resection of pancreatic cancer*. Journal of surgical oncology, 2013. **107**(1): p. 97-103.
114. Kamisawa, T., et al., *Hematogenous metastases of pancreatic ductal carcinoma*. Pancreas, 1995. **11**(4): p. 345-349.
115. Ferrone, C.R., et al., *Pancreatic ductal adenocarcinoma: long-term survival does not equal cure*. Surgery, 2012. **152**(3 Suppl 1).
116. Callery, M.P., et al., *Pretreatment Assessment of Resectable and Borderline Resectable Pancreatic Cancer: Expert Consensus Statement*. Annals of Surgical Oncology 2009 16:7, 2009. **16**(7): p. 1727-1733.

## 6. References

117. Kamisawa, T., et al., *Pancreatic cancer*. Lancet (London, England), 2016. **388**(10039): p. 73-85.
118. Ueno, H., et al., *A randomised phase III trial comparing gemcitabine with surgery-only in patients with resected pancreatic cancer: Japanese Study Group of Adjuvant Therapy for Pancreatic Cancer*. British journal of cancer, 2009. **101**(6): p. 908-915.
119. Regine, W.F., et al., *Fluorouracil vs gemcitabine chemotherapy before and after fluorouracil-based chemoradiation following resection of pancreatic adenocarcinoma: a randomized controlled trial*. JAMA, 2008. **299**(9): p. 1019-1026.
120. Neoptolemos, J.P., et al., *Adjuvant chemotherapy with fluorouracil plus folinic acid vs gemcitabine following pancreatic cancer resection: a randomized controlled trial*. JAMA, 2010. **304**(10): p. 1073-1081.
121. Neoptolemos, J.P., et al., *Therapeutic developments in pancreatic cancer: current and future perspectives*. Nature reviews. Gastroenterology & hepatology, 2018. **15**(6): p. 333-348.
122. Gillen, S., et al., *Preoperative/neoadjuvant therapy in pancreatic cancer: a systematic review and meta-analysis of response and resection percentages*. PLoS medicine, 2010. **7**(4).
123. Ye, M., et al., *Neoadjuvant chemotherapy for primary resectable pancreatic cancer: a systematic review and meta-analysis*. HPB, 2020. **22**(6): p. 821-832.
124. Wu, J. and J. Cai, *Dilemma and Challenge of Immunotherapy for Pancreatic Cancer*. Digestive Diseases and Sciences, 2021. **66**(2): p. 359-368.
125. Park, W., A. Chawla, and E.M. O'Reilly, *Pancreatic Cancer: A Review*. JAMA, 2021. **326**(9): p. 851-862.
126. Kawakubo, K., C.F.d. Castillo, and A.S. Liss, *Epigenetic regulation of pancreatic adenocarcinoma in the era of cancer immunotherapy*. Journal of gastroenterology, 2022. **57**(11): p. 819-826.
127. Royal, R.E., et al., *Phase 2 Trial of Single Agent Ipilimumab (Anti-CTLA-4) for Locally Advanced or Metastatic Pancreatic Adenocarcinoma*. Journal of immunotherapy (Hagerstown, Md. : 1997), 2010. **33**(8): p. 828-828.
128. Brahmer, J.R., et al., *Safety and Activity of Anti-PD-L1 Antibody in Patients with Advanced Cancer*. New England Journal of Medicine, 2012. **366**(26): p. 2455-2465.
129. O'Reilly, E.M., et al., *Durvalumab With or Without Tremelimumab for Patients With Metastatic Pancreatic Ductal Adenocarcinoma: A Phase 2 Randomized Clinical Trial*. JAMA Oncology, 2019. **5**(10): p. 1431-1438.
130. Narayanan, S., S. Vicent, and M. Ponz-Sarvisé, *PDAC as an Immune Evasive Disease: Can 3D Model Systems Aid to Tackle This Clinical Problem?* Frontiers in Cell and Developmental Biology, 2021. **9**: p. 3519-3519.
131. Karamitopoulou, E., *Tumour microenvironment of pancreatic cancer: immune landscape is dictated by molecular and histopathological features*. British Journal of Cancer 2019 121:1, 2019. **121**(1): p. 5-14.
132. Weiss, G.J., et al., *Phase Ib/II study of gemcitabine, nab-paclitaxel, and pembrolizumab in metastatic pancreatic adenocarcinoma*. Investigational New Drugs, 2018. **36**(1): p. 96-102.
133. Liang, C., et al., *Do anti-stroma therapies improve extrinsic resistance to increase the efficacy of gemcitabine in pancreatic cancer?* Cellular and Molecular Life Sciences, 2018. **75**(6): p. 1001-1012.

## 6. References

134. Schizas, D., et al., *Immunotherapy for pancreatic cancer: A 2020 update*. Cancer treatment reviews, 2020. **86**.
135. June, C.H., *Adoptive T cell therapy for cancer in the clinic*. The Journal of Clinical Investigation, 2007. **117**(6): p. 1466-1476.
136. Tang, R., et al., *Role of tumor mutation burden-related signatures in the prognosis and immune microenvironment of pancreatic ductal adenocarcinoma*. Cancer Cell International, 2021. **21**(1): p. 1-14.
137. Balachandran, V.P., G.L. Beatty, and S.K. Dougan, *Broadening the Impact of Immunotherapy to Pancreatic Cancer: Challenges and Opportunities*. Gastroenterology, 2019. **156**(7): p. 2056-2072.
138. Balachandran, V.P., et al., *Identification of unique neoantigen qualities in long-term survivors of pancreatic cancer*. Nature, 2017. **551**(7681): p. S12-S16.
139. Ino, Y., et al., *Immune cell infiltration as an indicator of the immune microenvironment of pancreatic cancer*. British journal of cancer, 2013. **108**(4): p. 914-923.
140. Miksch, R.C., et al., *Prognostic Impact of Tumor-Infiltrating Lymphocytes and Neutrophils on Survival of Patients with Upfront Resection of Pancreatic Cancer*. Cancers, 2019. **11**(1).
141. Sengsayadeth, S., et al., *Overview of approved CAR-T therapies, ongoing clinical trials, and its impact on clinical practice*. eJHaem, 2022. **3**(S1): p. 6-10.
142. Zhao, L. and Y.J. Cao, *Engineered T Cell Therapy for Cancer in the Clinic*. Frontiers in Immunology, 2019. **10**: p. 2250-2250.
143. Miliotou, A.N. and L.C. Papadopoulou, *CAR T-cell Therapy: A New Era in Cancer Immunotherapy*. Current pharmaceutical biotechnology, 2018. **19**(1): p. 5-18.
144. D'Ippolito, E., K.I. Wagner, and D.H. Busch, *Needle in a Haystack: The Naïve Repertoire as a Source of T Cell Receptors for Adoptive Therapy with Engineered T Cells*. Int J Mol Sci, 2020. **21**(21).
145. Yarchoan, M., et al., *Targeting neoantigens to augment antitumour immunity*. Nature Reviews Cancer 2017 17:4, 2017. **17**(4): p. 209-222.
146. Peng, M., et al., *Neoantigen vaccine: an emerging tumor immunotherapy*. Molecular Cancer 2019 18:1, 2019. **18**(1): p. 1-14.
147. Jiang, T., et al., *Tumor neoantigens: from basic research to clinical applications*. Journal of Hematology & Oncology 2019 12:1, 2019. **12**(1): p. 1-13.
148. Leidner, R., et al., *Neoantigen T-Cell Receptor Gene Therapy in Pancreatic Cancer*. New England Journal of Medicine, 2022. **386**(22): p. 2112-2119.
149. Raphael, B.J., et al., *Integrated Genomic Characterization of Pancreatic Ductal Adenocarcinoma*. Cancer cell, 2017. **32**(2): p. 185-203.e13.
150. Roudko, V., et al., *Shared Immunogenic Poly-Epitope Frameshift Mutations in Microsatellite Unstable Tumors*. Cell, 2020. **183**(6): p. 1634-1649.e17.
151. Ballhausen, A., et al., *The shared frameshift mutation landscape of microsatellite-unstable cancers suggests immunoediting during tumor evolution*. Nature Communications 2020 11:1, 2020. **11**(1): p. 1-13.
152. Vila, M.R., et al., *New pancreas cancers cell lines that represent distinct stages of ductal differentiation*. Laboratory investigation; a journal of technical methods and pathology, 1995. **72**(4): p. 395-404.

## 6. References

153. Heike, M., et al., *New cell lines of gastric and pancreatic cancer: distinct morphology, growth characteristics, expression of epithelial and immunoregulatory antigens*. *Virchows Archiv : an international journal of pathology*, 1995. **426**(4): p. 375-384.
154. Wölfel, T., et al., *Lysis of human pancreatic adenocarcinoma cells by autologous HLA-class I-restricted cytolytic T-lymphocyte (CTL) clones*. *International journal of cancer*, 1993. **54**(4): p. 636-644.
155. Moore, C.B., et al., *Short Hairpin RNA (shRNA): Design, Delivery, and Assessment of Gene Knockdown*. *Methods in molecular biology (Clifton, N.J.)*, 2010. **629**: p. 141-141.
156. Franken, N.A.P., et al., *Clonogenic assay of cells in vitro*. *Nature protocols*, 2006. **1**(5): p. 2315-2319.
157. Grada, A., et al., *Research Techniques Made Simple: Analysis of Collective Cell Migration Using the Wound Healing Assay*. *Journal of Investigative Dermatology*, 2017. **137**(2): p. e11-e16.
158. Neumeyer, V., et al., *Loss of endogenous RNF43 function enhances proliferation and tumour growth of intestinal and gastric cells*. *Carcinogenesis*, 2019. **40**(4): p. 551-559.
159. Neuschwander-Tetri, B.A., et al., *Repetitive self-limited acute pancreatitis induces pancreatic fibrogenesis in the mouse*. *Digestive Diseases and Sciences*, 2000. **45**(4): p. 665-674.
160. *Histopathology. Methods and Protocols*. Vol. 1180. 2014, New York, NY: Springer New York.
161. Zheng, S., et al., *Aberrant Cholesterol Metabolism and Wnt/ $\beta$ -Catenin Signaling Coalesce via Frizzled5 in Supporting Cancer Growth*. *Advanced Science*, 2022. **9**(28): p. 2200750-2200750.
162. Pavlovic, Z., et al., *A synthetic anti-Frizzled antibody engineered for broadened specificity exhibits enhanced anti-tumor properties*. *mAbs*, 2018. **10**(8): p. 1157-1157.
163. Zhang, Y., et al., *RNF43 ubiquitinates and degrades phosphorylated E-cadherin by c-Src to facilitate epithelial-mesenchymal transition in lung adenocarcinoma*. *BMC Cancer*, 2019. **19**(1): p. 1-18.
164. Baer, R., et al., *Pancreatic cell plasticity and cancer initiation induced by oncogenic Kras is completely dependent on wild-type PI 3-kinase p110a*.
165. Schober, K., et al., *Orthotopic replacement of T-cell receptor  $\alpha$ - and  $\beta$ -chains with preservation of near-physiological T-cell function*. *Nature Biomedical Engineering* 2019 3:12, 2019. **3**(12): p. 974-984.
166. Schober, K., T.R. Müller, and D.H. Busch, *Orthotopic T-Cell Receptor Replacement-An "Enabler" for TCR-Based Therapies*. *Cells*, 2020. **9**(6).
167. Nauerth, M., et al., *Flow cytometry-based TCR-ligand Koff -rate assay for fast avidity screening of even very small antigen-specific T cell populations ex vivo*. *Cytometry. Part A : the journal of the International Society for Analytical Cytology*, 2016. **89**(9): p. 816-825.
168. Liu, X., Y. Zhao, and H. Qi, *T-independent antigen induces humoral memory through germinal centers*. *Journal of Experimental Medicine*, 2022. **219**(3).
169. Koo, B.K., et al., *Tumour suppressor RNF43 is a stem-cell E3 ligase that induces endocytosis of Wnt receptors*. *Nature*, 2012. **488**(7413): p. 665-669.
170. Gala, M.K., et al., *Germline mutations in oncogene-induced senescence pathways are associated with multiple sessile serrated adenomas*. *Gastroenterology*, 2014. **146**(2).

## 6. References

171. Eto, T., et al., *Impact of loss-of-function mutations at the RNF43 locus on colorectal cancer development and progression*. The Journal of Pathology, 2018. **245**(4): p. 445-455.
172. Jiang, X., et al., *Inactivating mutations of RNF43 confer Wnt dependency in pancreatic ductal adenocarcinoma*. Proceedings of the National Academy of Sciences of the United States of America, 2013. **110**(31): p. 12649-12654.
173. Fang, L., et al., *RNF43 G659fs is an oncogenic colorectal cancer mutation and sensitizes tumor cells to PI3K/mTOR inhibition*. Nature Communications 2022 13:1, 2022. **13**(1): p. 1-12.
174. Mayer, P., et al., *Changes in the microarchitecture of the pancreatic cancer stroma are linked to neutrophil-dependent reprogramming of stellate cells and reflected by diffusion-weighted magnetic resonance imaging*. Theranostics, 2018. **8**(1): p. 13-13.
175. Zhang, H., et al., *Tumor-infiltrating Neutrophils is Prognostic and Predictive for Postoperative Adjuvant Chemotherapy Benefit in Patients with Gastric Cancer*. Annals of Surgery, 2018. **267**(2): p. 311-318.
176. Ribatti, D., R. Tamma, and T. Annese, *Epithelial-Mesenchymal Transition in Cancer: A Historical Overview*. Translational Oncology, 2020. **13**(6): p. 100773-100773.
177. Roche, J., *The Epithelial-to-Mesenchymal Transition in Cancer*. Cancers, 2018. **10**(2): p. 52-52.
178. López-Verdín, S., et al., *E-Cadherin gene expression in oral cancer: Clinical and prospective data*. Medicina Oral, Patología Oral y Cirugía Bucal, 2019. **24**(4): p. e444-e444.
179. Younis, L.K., H.E. Sakka, and I. Haque, *The Prognostic Value of E-cadherin Expression in Breast Cancer*. International Journal of Health Sciences, 2007. **1**(1): p. 43-43.
180. Christou, N., et al., *E-cadherin: A potential biomarker of colorectal cancer prognosis*. Oncology Letters, 2017. **13**(6): p. 4571-4576.
181. Bamford, K.B., *Chronic gastrointestinal inflammation*. FEMS Immunology & Medical Microbiology, 1999. **24**(2): p. 161-168.
182. Van Der Woude, C.J., et al., *Chronic inflammation, apoptosis and (pre-)malignant lesions in the gastro-intestinal tract*. Apoptosis : an international journal on programmed cell death, 2004. **9**(2): p. 123-130.
183. Neumeyer, V., et al., *Mutated Rnf43 Aggravates Helicobacter Pylori-Induced Gastric Pathology*. Cancers, 2019. **11**(3).
184. Kim, H., *Cerulein Pancreatitis: Oxidative Stress, Inflammation, and Apoptosis*. Gut and Liver, 2008. **2**(2): p. 74-74.
185. Yu, J.H., et al., *Suppression of Cerulein-Induced Cytokine Expression by Antioxidants in Pancreatic Acinar Cells*. Laboratory Investigation 2002 82:10, 2002. **82**(10): p. 1359-1368.
186. Folias, A.E., et al., *Aberrant innate immune activation following tissue injury impairs pancreatic regeneration*. PLoS ONE, 2014. **9**(7).
187. da Silva, L., et al., *Pharmacological inhibition and reversal of pancreatic acinar ductal metaplasia*. Cell Death Discovery 2022 8:1, 2022. **8**(1): p. 1-10.
188. Timmer, F.E.F., et al., *Pancreatic Cancer and Immunotherapy: A Clinical Overview*. Cancers 2021, Vol. 13, Page 4138, 2021. **13**(16): p. 4138-4138.
189. Bear, A.S., R.H. Vonderheide, and M.H. O'Hara, *Challenges and Opportunities for Pancreatic Cancer Immunotherapy*. Cancer cell, 2020. **38**(6): p. 788-802.

## 6. References

190. Padrón, L.J., et al., *Sotigalimab and/or nivolumab with chemotherapy in first-line metastatic pancreatic cancer: clinical and immunologic analyses from the randomized phase 2 PRINCE trial*. *Nature Medicine* 2022 28:6, 2022. **28**(6): p. 1167-1177.
191. Johnson, L.A., et al., *Gene therapy with human and mouse T-cell receptors mediates cancer regression and targets normal tissues expressing cognate antigen*. *Blood*, 2009. **114**(3): p. 535-535.
192. Parkhurst, M.R., et al., *T cells targeting carcinoembryonic antigen can mediate regression of metastatic colorectal cancer but induce severe transient colitis*. *Molecular therapy : the journal of the American Society of Gene Therapy*, 2011. **19**(3): p. 620-626.
193. Morgan, R.A., et al., *Cancer regression and neurological toxicity following anti-MAGE-A3 TCR gene therapy*. *Journal of immunotherapy (Hagerstown, Md. : 1997)*, 2013. **36**(2): p. 133-151.
194. Yamamoto, T.N., R.J. Kishton, and N.P. Restifo, *Developing neoantigen-targeted T cell-based treatments for solid tumors*. *Nature medicine*, 2019. **25**(10): p. 1488-1499.
195. Peterson, M., et al., *Comparison of personal and shared frameshift neoantigen vaccines in a mouse mammary cancer model*. *BMC Immunology*, 2020. **21**(1): p. 1-15.
196. Gebert, J., et al., *Recurrent Frameshift Neoantigen Vaccine Elicits Protective Immunity With Reduced Tumor Burden and Improved Overall Survival in a Lynch Syndrome Mouse Model*. *Gastroenterology*, 2021. **161**(4): p. 1288-1302.e13.
197. Kawamura, J., et al., *Cytotoxic T lymphocyte response to peptide vaccination predicts survival in stage III colorectal cancer*. *Cancer Science*, 2018. **109**(5): p. 1545-1551.
198. Kanekiyo, S., et al., *IgG response to MHC class I epitope peptides is a quantitative predictive biomarker in the early course of treatment of colorectal cancer using therapeutic peptides*. *Oncology reports*, 2018. **39**(5): p. 2385-2392.
199. de Greef, P.C., et al., *The naive T-cell receptor repertoire has an extremely broad distribution of clone sizes*. *eLife*, 2020. **9**.
200. Han, Y., D. Liu, and L. Li, *PD-1/PD-L1 pathway: current researches in cancer*. *American Journal of Cancer Research*, 2020. **10**(3): p. 727-727.
201. Castagnoli, L., et al., *WNT signaling modulates PD-L1 expression in the stem cell compartment of triple-negative breast cancer*. *Oncogene*, 2019. **38**(21): p. 4047-4060.
202. Taylor, A., D. Rothstein, and C.E. Rudd, *Small-Molecule Inhibition of PD-1 Transcription Is an Effective Alternative to Antibody Blockade in Cancer Therapy*. *Cancer research*, 2018. **78**(3): p. 706-717.

## 7. Publications

Neumeyer V, **Brutau-Abia A**, Allgäuer M, Pfarr N, Weichert W, Falkeis-Veits C, Kremmer E, Vieth M, Gerhard M, Mejías-Luque R. Loss of RNF43 Function Contributes to Gastric Carcinogenesis by Impairing DNA Damage Response. *Cell Mol Gastroenterol Hepatol*. 2021;11(4):1071-1094. doi: 10.1016/j.jcmgh.2020.11.005. Epub 2020 Nov 11. PMID: 33188943; PMCID: PMC7898035.

Neumeyer V, Grandl M, Dietl A, **Brutau-Abia A**, Allgäuer M, Kalali B, Zhang Y, Pan KF, Steiger K, Vieth M, Anton M, Mejías-Luque R, Gerhard M. Loss of endogenous RNF43 function enhances proliferation and tumour growth of intestinal and gastric cells. *Carcinogenesis*. 2019 Jun 10;40(4):551-559. doi: 10.1093/carcin/bgy152. PMID: 30380024.

### 8. Acknowledgments

First, I would like to thank my thesis supervisors Prof. Dr. Markus Gerhard and PD. Dr. Raquel Mejías Luque. To Markus, I really appreciate the opportunity to work on this project and for all the mentoring, ideas, and support during these past five years. To Raquel, thank you so much for your constant supervision, ideas, and encouragement during this work. But I would like to especially thank you for your continuous motivation, both at work and on a personal level. Moltíssimes gràcies!

I want to thank the AG Busch for their collaboration in this project within the CRC 1321. I am very grateful to my supervisor Prof. Dr. Dirk Busch, for his input and discussions throughout my Ph.D. To PD Dr. Killian Schober for his support at the beginning of the project and Dr. Elvira D'Ippolito for all the meetings, support, and feedback. To Dr. Karolin Wagner and Sarah Braun, for their collaboration and support in the project.

I would also like to thank my thesis supervisor Prof. Dr. Roland Rad, for his feedback and constructive discussions in the thesis committee meetings.

Many thanks to the TUM Institute of Pathology. Especially to PD.Dr. Katja Steiger, Olga Seelbach, and Thomas Metzler for their excellent support.

To all my colleagues in AG Gerhard/Mejías-Luque, thank you so much for providing such an excellent work environment. Special thanks to Karin Mink, Andreas Wanisch, and Martin Skerhut for their support with mice work. I would like to thank the "RNF43 team". To Dr. Victoria Neumeyer, who taught me everything I know in the lab during my Master's thesis and introduced me to RNF43. To Alisa for all the shared mice and discussions and Mona Wang, for all her ideas and help with the mice. To Ruth Itziar Urraca Arias, for being an excellent master's student and contributing so much to this project. To Ruolan, Xue, Anna, Veronika, Karin, Quyhn, Leonard, Teresa, Ahmed, Matt, and many others that had not only celebrated all the little accomplishments but always cheered me up when things did not go as planned. And to Dr. Youssef Hamway, who has always helped me in the lab, for all his corrections in this thesis and for being a great friend.

## 8. Acknowledgments

Special thanks to Pablo for all his support and patience during this time. To my family, especially my mother, for all her support and encouragement through the years. And to all my friends in Germany and Spain for always making everything better.

